INVESTIGATION ON SYNERGISTIC EFFECT OF BIOMINERALIZATION AND ASH-BASED SOIL STABILIZATION

Thesis

Submitted in partial fulfillment of the requirements for the degree of

DOCTOR OF PHILOSOPHY

by

KOTHURI MAHINDRA

(Roll. No. 187CV006)

DEPARTMENT OF CIVIL ENGINEERING

NATIONAL INSTITUTE OF TECHNOLOGY KARNATAKA,

SURATHKAL, MANGALORE-575025

DECEMBER, 2023

INVESTIGATION ON SYNERGISTIC EFFECT OF BIOMINERALIZATION AND ASH-BASED SOIL STABILIZATION

Thesis

Submitted in partial fulfillment of the requirements for the degree of

DOCTOR OF PHILOSOPHY

by

KOTHURI MAHINDRA

(Roll. No. 187CV006)

Under the guidance of

Prof. C. P. DEVATHA

DEPARTMENT OF CIVIL ENGINEERING

NATIONAL INSTITUTE OF TECHNOLOGY KARNATAKA,

SURATHKAL, MANGALORE-575025

DECEMBER, 2023

DECLARATION

I hereby *declare* that the Research Thesis entitled **"INVESTIGATION ON SYNERGISTIC EFFECT OF BIOMINERALIZATION AND ASH-BASED SOIL STABILIZATION"**, which is being submitted to the National Institute of Technology Karnataka, Surathkal, in partial fulfillment of the requirements for the award of the Degree of Doctor of Philosophy in the Department of Civil Engineering is *a bonafide report of the research work carried out by me*. The material in this report has not been submitted to any University or Institution for the award of any degree.

Place: NITK, Surathkal

Date: 12 December 2023

Kothuri Mahindra

(187CV006)

CERTIFICATE

This is to *certify* that the Research thesis entitled **"INVESTIGATION ON SYNERGISTIC EFFECT OF BIOMINERALIZATION AND ASH-BASED SOIL STABILIZATION"**, submitted by **Mr. Kothuri Mahindra (187CV006)** as the record of the research work carried out by him, is *accepted as the Research Thesis submission* in partial fulfillment of the requirements for the award of the degree of **Doctor of Philosophy**.

Prof. C. P. Devatha
Research Supervisor

Prof. Subhash C. Yaragal
Chairperson-DRPC

NATIONAL INSTITUTE OF TECHNOLOGY KARNATAKA, SURATHKAL ★
DEPT. OF CIVIL ENGG.

Chairman (DRPC)
Department of Civil Engineering
National Institute of Technology Karnataka
Surathkal, Mangalore - 575 025, Karnataka, INDIA

ACKNOWLEDGEMENT

I am immensely pleased to express my heartfelt gratitude to those who helped and motivated me to complete the Ph.D. dissertation.

I express my sincere gratitude to my Research Supervisor **Prof. C. P. Devatha**, Department of Civil Engineering, for the valuable guidance, suggestions, constructive criticism, and motivation, which played an inspiring role throughout the research work.

I would also like to sincerely thank **Prof. Subhash C. Yaragal**, the Head of the Department of Civil Engineering, and the previous Heads of the Department at NITK Surathkal.

I am deeply grateful to **Prof. A. C. Hegde** and **Prof. A. U. Ravi Shankar**, the RPAC committee members, for their unwavering support and encouragement throughout my Ph.D. journey.

I am also indebted to my friends and colleagues for their unrelenting encouragement, help, and support. Their presence and camaraderie have made this journey more enjoyable and memorable.

I am eternally grateful to my family members, whose endless encouragement and unwavering support have inspired me throughout this work. Their belief in me and their sacrifices have fueled my determination to complete this dissertation.

I am thankful to the Ministry of Education, Govt. of India, for providing the fellowship.

Once again, I express my deepest gratitude to everyone who has directly or indirectly contributed to completing my project on time. Your support has been invaluable, and I am truly grateful for it.

Finally, I would like to acknowledge the divine intervention and thank the almighty for bestowing me with blessings and guidance throughout my life.

NITK Surathkal **Kothuri Mahindra**

ABSTRACT

Waste management is an intricate and pressing global challenge that demands our immediate attention and concerted efforts to address the environmental impacts resulting in widespread pollution and adverse effects on human health. To combat these challenges, it is imperative to develop innovative and eco-friendly solutions that mitigate the negative consequences of waste and promote sustainable practices for a cleaner and healthier future.

Waste materials, including biomedical ash and ferrochrome ash, contain toxic heavy metals such as Pb, Ni, and Cr, which pose risks to the environment and human health. Hence, the present study aims to assess the effect of biomineralization to immobilize the heavy metals and allowing the safe application of biomedical ash (BMA) and ferrochrome ash (FCA) in enhancing the properties of black cotton soil (BCS). The research objectives encompass evaluating microbial growth in waste ashes, identifying the optimal protein source for bacterial urease production, optimizing nutrient medium composition for enhanced biomineralization, and analyzing the impact of biomineralization on the engineering properties of waste ashes as environmentally friendly soil stabilizers. To address these objectives, a three-stage methodology has been adopted.

In the first stage, the investigation focused on the presence of bacteria in waste ashes. Indigenous urease-positive bacteria were isolated using the serial dilution technique with Christensen's agar medium and identified through 16SrRNA analysis. The study identified *Bacillus cereus* and *Lysinibacillus sphaericus* as suitable urease-positive bacteria for biomineralization in BMA and ferrochrome ash FCA, respectively. The performance of different legumes as protein sources were compared by monitoring pH, optical density, and urease activity over time. Blackgram and soybean were identified as the most suitable protein sources for bacterial growth and urease activity.

The second stage of the research involved integrating biomineralization into biomedical ash for stabilizing black cotton soil. Response surface methodology (RSM) using a central composite design (CCD) was employed to model the role of protein, vitamin, and carbon sources in urease activity. The study determined the optimal combination

of 23.47 g/L black gram, 3.45 g/L yeast extract, and 0.03 g/L dextrose while also observing that the dosage of protein and vitamin sources significantly impacted bacterial growth and urease activity. The production of mineralized biomedical ash consisted of combining equimolar urea & calcium chloride (1 M) and the acquired bacteria with biomedical ash. Leachate extracted from mineralized biomedical ash demonstrated reduced concentrations of Hg (97 %), Cr (96 %), Zn (97 %), Pb (93 %), Fe (94 %), Cu (93 %), Cd (98 %), Ba (87 %), As (96 %), Ti (88 %), and Se (86 %), indicating the effectiveness of biomineralization in immobilizing heavy metals.

To assess the influence of mBMA on soil characteristics, black cotton soil (BCS) was subjected to different proportions (10 %, 20 %, 30 %, and 40 %) of mBMA. At 40 % soil replacement (m40) by mBMA, the soil's liquid limit (LL), plastic limit (PL), plasticity index (PI), and free swell index (FSI) were 47 %, 34 %, 13 %, and 14 %, respectively. The corresponding values in the same order are 53 %, 25 %, 27 %, and 114 % for BCS. The optimal moisture content (OMC) shifted from 22 % for BCS to 26 % for m40. The corresponding maximum dry density (MDD) reduced from 1.596 g/cm^3 for BCS to 1.458 g/cm^3 for m40. These values indicate improved soil consistency and reduced compressibility due to adding mBMA to BCS. Notably, the highest unconfined compressive strength (UCS) of 147 kPa was observed for m30 (30 % BCS replaced with mBMA). UCS of BCS was determined as 35 kPa.

Characterization studies (XRD, FEGSEM, FTIR, TGA) were conducted on mBMA. X-ray diffraction analysis detected significant amounts of calcite while scanning electron microscope images revealed the presence of dense matter connecting the ash particles, which was identified as calcite formed during biomineralization. Fourier transform infrared absorption bands corresponding to carbonates further supported the occurrence of biomineralization. A 10 % weight reduction in the characteristic thermal decomposition range for calcium carbonate also confirmed its presence due to biomineralization.

Calcite was identified in mBMA through XRD, with peaks observed at 23.03 °, 29.38 °, 25.47 °, 31.34 °, 35.98 °, 39.41 °, 43.15 °, 45.44 °, 48.48 °, and 57.40 °. Dense matter connecting the ash particles was observed in FESEM images of mBMA. It is believed to be the calcite formed during biomineralization. The carbonate presence was backed

by the FTIR absorption bands at 711.6 cm^{-1}, 873.6 cm^{-1}, and 1420.3 cm^{-1}. A 10% weight reduction in the characteristic thermal decomposition range (570 °C to 660 °C) for calcium carbonate confirmed its advent during biomineralization.

In the third stage of the present study, FCA was employed in conjunction with biomineralization to stabilize BCS. Through optimization of the quadratic model, an ideal combination of 20 g/L soybean, 3 g/L yeast extract, and 0.125 g/L dextrose was determined for maximum optical density (1.946) and urease activity (27 m.mol urease/min).

To stabilize the black cotton soil, soil bacteria were used with ferrochrome ash. The study involved assessing the extent to which ferrochrome ash could replace the black cotton soil and analyzing the impact of bacterial optical density, urea, and calcium chloride on enhancing the soil's unconfined compressive strength.

The soil composite with the highest UCS of 350 kPa (TC5) comprised 40 % FCA, a bacterial medium with an optical density of 1.12, 0.5 g urea, and 0.5 g calcium chloride. A quadratic model was employed to investigate the impact of ferrochrome ash, bacterial density, calcium chloride, and urea concentrations on the unconfined compressive strength. The model indicated FCA as the primary contributor for the UCS improvement.

The leachate of TC5 demonstrated reductions in heavy metal concentrations with efficiencies of 95% for Ni, 97% for Cu, 98% for Fe, 99% for Cr and Zn, and 100% for Pb, Cd, Ti, Hg, and As.

The XRD analysis of TC5 revealed peaks at 20.61 °, 26.39 °, 28.08 °, 29.20 °, 31.08 °, 36.29 °, 39.21 °, 42.20 °, 43.16 °, 49.92 °, and 55.17 °. Additionally, peaks of FCA were observed at 28.32°, 40.54 °, and 50.23 °, while peaks of BCS were observed at 20.96 °, 26.72 °, 36.63 °, 39.58 °, 40.41 °, 42.53 °, 45.92 °, and 50.24 °. SEM of TC5 contained rhombohedral crystals of calcium carbonate and spherical particles of FCA on the flaky surface of the clayey soil. The FTIR profile of TC5 contained a characteristic absorption band for carbonate at 1457 cm^{-1}, which was absent in the spectra of BCS and FCA. Other bands at 993 cm^{-1} and 1633 cm^{-1} indicate C-S-H formation. TGA analysis of TC5 exhibited an 18% weight loss in the temperature range

of 590 °C to 810 °C, indicating the decomposition of calcium carbonate formed during biomineralization.

These findings have important implications for waste management strategies, providing valuable insights into the potential of BMA and FCA with biomineralization in mitigating environmental risks and deriving value from waste.

Keywords: Bacterial urease production, Biomineralization, Biomedical ash, Black cotton soil, Ferrochrome ash, Heavy metals, Soil stabilization.

CONTENTS

LIST OF TABLES

LIST OF FIGURES

ABBREVIATIONS AND NOMENCLATURE

ANOVA	Analysis of variance
BCS	Black cotton soil
BMA	Biomedical ash
CCD	Central Composite Design
FCA	Ferrochrome ash
FEGSEM	Field Emission Gun Scanning Electron Microscopy
FTIR	Fourier Transform Infrared
FSI	Free swell index
LL	Liquid limit
m10	Mix with 10 % mineralized biomedical ash
m20	Mix with 20 % mineralized biomedical ash
m30	Mix with 30 % mineralized biomedical ash
m40	Mix with 40 % mineralized biomedical ash
mBMA	Mineralized biomedical ash
MDD	Maximum dry density
OMC	Optimum moisture content
PI	Plasticity index
PL	Plastic limit
RSM	Response Surface Methodology
SEM	Scanning Electron Microscopy
TC5	Target soil composite
TGA	Thermogravimetric Analysis
UCS	Unconfined compressive strength
XRD	X-Ray Diffraction

CHAPTER 1

INTRODUCTION

1.1 General

Waste management has become a critical issue faced by industries and governments worldwide. Governments strategically locate industries away from residential areas to protect the public from exposure to various types of waste generated by manufacturing and processing industries. However, with urbanization and population growth, many industries have been surrounded by households, making it increasingly challenging to find suitable space for waste disposal. As a result, waste disposal standards have been periodically updated, and extensive research has been conducted to explore innovative and eco-friendly technologies for waste treatment. The importance of effective waste management cannot be overstated, as it is essential for environmental protection, public health, resource conservation, climate change mitigation, sustainable development, regulatory compliance, and social responsibility. Waste management ensures the well-being of the environment and the public by minimizing pollution, preventing the release of hazardous substances, and safeguarding ecosystems.

One of the foremost challenges of waste management stems from the sheer volume of waste generated due to population growth and industrial activities. The continuous increase in waste production strains the existing waste management infrastructure, necessitating the development of innovative solutions to handle it effectively.

Furthermore, the diverse nature of waste materials poses another significant challenge. Municipal solid waste, hazardous waste, electronic waste, and agricultural waste, among others, all possess unique characteristics that require specific treatment methods. Managing such varied waste streams demands the implementation of specialized processes and techniques. Developing and implementing these practices on a large scale can be intricate and expensive, involving extensive research, technology, and expertise.

Moreover, the financial aspect of waste management presents a significant hurdle, particularly for developing countries with limited resources. Investing in waste treatment technologies, infrastructure development, and operational costs can be

financially burdensome. These costs can escalate depending on the scale of waste generated, the complexity of waste streams, and the environmental regulations that must be adhered to. As waste volumes increase, so do the costs associated with treatment and disposal. This financial strain makes it challenging for certain regions to establish and maintain effective waste management systems, hindering their ability to address the growing waste crisis.

1.2 Concept of waste valorization

The valorization of waste materials involves enhancing their value through the conversion into valuable products or materials rather than simply disposing of them. This approach aims to minimize the detrimental environmental impact of waste while simultaneously generating economic and social advantages (García-Díaz et al. 2016). Waste valorization has a rich historical background spanning thousands of years, although the terminology is more recent. In the 20th century, waste valorization gained increasing recognition as a viable alternative to conventional waste management practices. Recycling, for instance, emerged as a widely accepted method for resource conservation and waste reduction. Governments and businesses began to invest in novel technologies and processes, such as composting, anaerobic digestion, and waste-to-energy, to enable waste valorization. Embracing waste valorization is a significant step towards achieving a more sustainable and circular economy. Rather than perceiving waste as a burden necessitating disposal, it is acknowledged as a potential resource that can be utilized for economic and social benefit.

Waste valorization offers substantial environmental benefits by reducing waste, conserving resources, and mitigating greenhouse gas emissions. Waste is diverted from landfills through recycling, composting, and other valorization processes, mitigating environmental risks such as soil and water contamination. By recovering and reusing valuable materials from waste, valorization reduces the need for virgin resources like cement, conserves natural resources, and promotes resource efficiency. Waste valorization offers a multitude of benefits that extend beyond waste reduction. It presents a holistic solution to resource depletion, waste accumulation, and climate change challenges through environmental protection, economic opportunities, sustainable waste management, and promoting a circular economy. Two waste

materials, namely biomedical ash and ferrochrome ash, are being extensively researched for their potential utilization as construction materials. Instead of simply disposing of these materials, incorporating them into construction products provides a twofold advantage: reducing disposal costs and minimizing the demand for conventional materials.

1.3 Biomedical ash

Biomedical waste encompasses all waste generated from medical procedures in healthcare facilities, research centers, laboratories, and home healthcare (World Health Organization 2017). In India, the daily production of biomedical waste amounts to approximately 619 metric tons, while the incineration capacity is 814 tons (Central Pollution Control Board 2018). Incineration is the preferred method due to its efficiency in reducing the volume and weight of the waste. Biomedical ash (BMA) is the resulting residue from the incinerators treating biomedical waste.

The resulting ash contains various substances, including heavy metals and other potentially harmful compounds. The fate of BMA depends on multiple factors, including the type of ash, local regulations, and the specific disposal methods implemented. Sometimes, it may be treated as hazardous waste and undergo specialized treatment processes like stabilization, solidification, or encapsulation techniques to immobilize any hazardous components within the ash. Alternatively, depending on local regulations and the composition of the ash, it may be classified as non-hazardous waste and subjected to standard disposal practices like landfilling.

1.4 Ferrochrome ash

According to a United States Geological Survey report, Ferrochrome, a widely used alloy in stainless steel manufacturing, positions India as the fourth largest global producer. This ranking follows South Africa, Turkey, and Kazakhstan (Ruth F. Schulte 2020). In India, the main reserves of chromite ore are concentrated in Odisha and Karnataka, with smaller reserves found in Maharashtra and Andhra Pradesh. During ferrochrome production, a byproduct called Ferrochrome ash (FCA) is generated. FCA consists of fine dust particles formed during gas cleaning operations to eliminate harmful flue gases from smelting furnaces. Approximately 30 kg of FCA is produced

per ton of ferrochrome (Kumar et al. 2022). Traditionally, FCA is disposed of in open dump yards and landfills, posing significant environmental risks by potentially releasing heavy metals into water sources (Bulut et al. 2009).

1.5 Heavy metals

Heavy metals are a group of metallic elements that have high atomic weights and densities. They are also referred to as metals with atomic weight greater than sodium and some toxicity level (Adepoju-Bello 2012). They include lead, mercury, cadmium, arsenic, chromium, and many others. These metals have various industrial, commercial, and technological applications due to their unique properties, but they can also pose significant risks to human health and the environment. Heavy metals are non-biodegradable and can accumulate in the environment through natural or human activities such as mining, industrial emissions, and improper waste disposal.

They can enter the food chain through soil, water, and air, ultimately affecting humans and other organisms. Exposure to heavy metals can occur through inhalation, ingestion, or dermal contact. Once inside the body, these metals can interfere with various biological processes. It is important to note that heavy metals, in trace amounts, are naturally present in the environment and may not necessarily be harmful. Some heavy metals are essential and required by the human body in trace amounts. However, they become toxic and may cause damage to vital organs of the body like the heart, liver, kidneys, and brain when their concentrations increase (Akram et al. 2015; Tchounwou et al. 2012). Some common health problems associated with heavy metal exposure include neurological disorders, kidney damage, respiratory issues, cardiovascular problems, developmental issues in children, and certain types of cancers. According to Thakur et al. (2010), the movement of heavy metals in the form of sediments through inland waters poses a significant toxicity threat, extending to the coastal marine environment.

1.6 Biomineralization for heavy metal immobilization

Biomineralization is a natural process that can be used for heavy metal immobilization. It is an interdisciplinary field combining engineering, chemistry, and microbiology, widely applied for contamination containment or removal (Rajasekar et al. 2017). It

involves microbial metabolic processes to affect the species and mobility of metals. Biomineralization encompasses the controlled deposition of inorganic materials within organic matrices, enabling living organisms to create complex mineral structures with specific shapes, sizes, and compositions.

Coprecipitation is the simultaneous precipitation of heavy metal ions and other compounds or minerals, forming a solid phase that incorporates the metal ions. This process effectively immobilizes the heavy metals and reduces their mobility and potential toxicity. It offers advantages such as simplicity, cost-effectiveness, and scalability.

When microorganisms are exposed to contaminated environments containing heavy metals, they promote the coprecipitation of heavy metals with minerals. This process involves the transformation of soluble heavy metal ions into insoluble forms, which reduces their mobility and bioavailability in the environment. As a result, the heavy metals become immobilized and trapped within the solid precipitates formed during biomineralization.

The immobilization of heavy metals through biomineralization helps in the remediation of contaminated environments. By reducing the mobility and bioavailability of heavy metals, the risk of their uptake by plants, animals, and humans is minimized. This process is beneficial for restoring and protecting ecosystems affected by heavy metal contamination, as it can mitigate their harmful effects on organisms and the environment.

Urea hydrolysis is the best among several pathways of biomineralization (Ersan 2019). It is the most followed approach to precipitate calcite. The breakdown of urea by water in the presence of urease-producing bacteria releases alkaline ammonium, and carbonate ions (Yang et al. 2020). The pH of the environment elevates due to the ammonium and facilitates the precipitation of calcium carbonate minerals in the presence of calcium and carbonate ions (Torres-Aravena et al. 2018). Microorganisms capable of bioprecipitation induce the coprecipitation of heavy metals with minerals aiding in the immobilization and remediation of contaminated environments (Cuaxinque-Flores et al. 2020).

1.7 Black cotton soil stabilization

The black soil, known as "regur" in Telugu, is formed from volcanic rocks and lava, and it is commonly referred to as "Black Cotton soil" due to its suitability for cotton crops. It contains calcium carbonate, lime, potash, and magnesium carbonates. Found in South Asia, Middle Africa, and tropical regions, it covers about 20% of Indian land, including parts of the Deccan Plateau, western Madhya Pradesh, Rajasthan, Bundelkhand in Uttar Pradesh, Karnataka, and Andhra Pradesh.

The volume changes exhibited by the black cotton soil (BCS) pose significant challenges in construction, impacting residential buildings, pavements, and linings. This swell-shrink behavior renders it unsuitable for road construction due to its low strength and considerable expansion in moist conditions. Moreover, this soil type presents further difficulties, such as instability, shrinkage, and erosion, which can compromise foundations and cause structural damage (Randhawa et al. 2021). Proper soil preparation is essential to address these issues, including implementing stabilization techniques. Soil stabilization techniques are methods employed to improve the engineering properties of soil, enhancing its strength, durability, and load-bearing capacity. These techniques are commonly used in construction, road building, and other civil engineering projects. Here's an overview of some common soil stabilization techniques and their limitations:

Compaction: Compaction is mechanically densifying soil by applying pressure to reduce its voids and increase its shear strength. Compaction improves soil stability, reduces settlement, and increases bearing capacity. However, it may not be suitable for certain types of soils, such as highly organic or expansive clays.

Grouting: Grouting involves injecting a cementitious or chemical grout into the soil to fill voids and improve its strength and stability. Grouting is effective in stabilizing loose or granular soils. However, achieving uniform distribution of grout may be challenging, and the process can be time-consuming and expensive.

Chemical stabilization: Chemical stabilization involves adding chemicals, such as lime, cement, or fly ash, to the soil to alter its properties. Lime stabilization increases soil strength and reduces plasticity, while cement stabilization provides significant strength

improvement. However, chemical stabilization may be limited by the availability of suitable additives and the potential for long-term chemical reactions that can affect soil behavior.

Soil reinforcement: To improve soil strength and stability, soil reinforcement techniques involve adding materials like geosynthetics (e.g., geotextiles, geogrids) or steel elements. These materials enhance tensile strength, distribute loads, and control soil movement. However, soil reinforcement may require specialized expertise and careful design to ensure proper installation and long-term performance.

Soil exchange and replacement: This technique involves excavating poor-quality soil and replacing it with better-quality soil or aggregates. It is commonly used when the existing soil is unsuitable for construction. However, the cost and availability of suitable replacement materials can be limiting factors.

Soil encapsulation involves covering the soil with a geosynthetic layer or a concrete cap to prevent erosion, contamination, or settlement. It provides a barrier between the soil and the external environment. However, it may not address the underlying soil stability issues and can be costly.

Electrokinetic stabilization: Electrokinetic stabilization applies electric current to the soil, inducing various chemical and physical changes to improve its properties. This technique can be useful for fine-grained soils but is limited by the complexity of the process and the need for specialized equipment.

1.8 Research Objectives

The primary aim of this study is to systematically explore the potential utilization of FCA and BMA wastes for enhancing the geotechnical characteristics of BCS while ensuring safety. This approach seeks to add value to the waste materials as an alternative to traditional soil stabilizers. The biomineralization technique prevents heavy metal leaching from the wastes while concurrently improving soil properties. The following objectives were pursued to determine the synergistic effect of biomineralization and ash-based stabilization on BCS:

1. To assess the availability of urease-positive bacteria within the waste ashes.
2. To identify the best protein source among legumes such as Chickpea, Peanut, Black gram, Garbanzo bean, and Soybean for bacterial urease production.
3. To maximize the biomineralization potential of indigenous bacteria by optimizing the nutrient medium composition.
4. To evaluate the influence of biomineralization on the engineering properties of black cotton soil stabilized with waste ashes.

1.9 Thesis Organization

Chapter 1 is a general introduction and presents the objectives and outline of the thesis.

Chapter 2 provides a brief literature review on waste valorization, FCA and BMA in construction, biomineralization, and black cotton soil stabilization.

Chapter 3 presents the materials and methods used for the experimental studies.

Chapter 4 describes the experimental outcomes of the synergy between biomineralization and waste ashes in black cotton soil stabilization.

Chapter 5 outlines the key conclusions of this study.

CHAPTER 2

LITERATURE REVIEW

2.1 General

This chapter aims to explore the current state of knowledge on the usage of wastes in black cotton soil stabilization and the concept of biomineralization. It reports a brief summary of the outcomes of studies conducted by several researchers in the fields of BCS stabilization by using waste materials and biomineralization.

2.2 Partial replacement for stabilization of BCS

Soil stabilization is the process of enhancing the engineering properties of unstable soils by incorporating materials with inherent binder properties into the soil mixture (Yin et al., 2022). However, traditional stabilizers like cement and lime can compromise the sustainability of construction (Briga-Sá et al., 2022). Additionally, these traditional stabilizers may not effectively improve the properties of certain soil types, such as expansive soils, which can cause damage to infrastructure (Fondjo et al., 2021). Over the years, extensive research has explored various approaches for stabilizing BCS by replacing it with waste materials. Thus far, a number of studies have used a wide range of materials, additives, and their combinations to enhance soil properties and improve the effectiveness of stabilization.

Oza and Gundaliya (2013) reported that mixing cement dust reduced the plasticity index of the soil and resulted in the highest compressive strength compared to lime alone or a combination of cement dust and lime. Amadi (2014) focused on enhancing the durability of BCS by treating it with a combination of cement kiln dust and quarry fines, investigating its effectiveness in improving stability and strength. Goodarzi et al. (2016) aimed to reduce the binder content required for stabilization and decrease curing time by using silica fume and cement as additives. They found that incorporating silica fume into the cement-soil matrix developed new cementing compounds and provided a denser microstructure, offering valuable insights into optimizing soil stabilization composition and curing process.

Building on these advancements, Chethan and Ravi Shankar (2021) examined the combined effects of cement and fly ash on BCS stabilization. Calcium silicate hydrate gel was formed due to the hydration of cement and fly ash, significantly improving soil strength and freeze-thaw durability.

Apart from cement-based mixtures, researchers have also explored specific ash-lime combinations for soil stabilization. Mir (2015) investigated the effect of fly ash and lime on BCS's unconfined compressive strength (UCS), observing that even a slight 10% replacement with fly ash significantly increased soil strength over time due to pozzolanic reactions.

(Yi et al. 2015) investigated the use of carbide slag to activate ground granulated blast furnace slag for soft clay stabilization, comparing it to portland cement. The optimal slag content was 4%–6%, resulting in clay with more than twice the UCS compared to cement-stabilized clay. The main hydration products observed were calcium silicate hydrates, calcium aluminate hydrates, and alumino-ferrite monosulfate.

However, Mir and Sridharan (2017) demonstrated that excessively high fly ash content is not preferable as it can disturb the soil matrix, compensating for the strength increased by the pozzolanic activity.

Karatai et al. (2017) reported a 90% reduction in soil plasticity and a 70% reduction in free swell when replacing expansive soil with a combination of 20% rice husk ash and 2% lime. Ikeagwuani et al. (2019) made similar observations of pozzolanic reactions in soil stabilized with 16% sawdust ash and 4% lime. Along the same lines, Ramesh and Manjunatha (2020) stated similar behavior for soil treated with rice husk ash and carbide lime, justifying the decline in the soil's PI to the decrease in the diffuse double-layer thickness. Treating the soil with 1% sodium chloride and 1% sodium hydroxide improved the UCS due to the formation of alkali silicate and alkali aluminate hydrated gel, resulting in soil densification.

Darsi et al. (2021) identified that replacing soil with 6% lime and 10% ground-granulated blast furnace slag resulted in the flocculation of clay particles, leading to soil densification and an 85% increase in UCS. Gautam et al. (2021) studied municipal solid waste incinerator ash in combination with lime for soil stabilization. Adding 9%

lime decreased soil swelling by 75%, and when 24% incinerated municipal solid waste ash was added, it further reduced swelling by 100%. The soil's strength increased to 2.87 times that of the untreated soil.

Vijayan et al. (2023) treated expansive soils using palm kernel ash with lime. Adding 5% lime with 0.25% palm kernel ash increased the UCS of the soil. Lime was responsible for most changes observed in the soil, and the curing process did not affect the strength as the percentage of palm kernel ash increased.

In contrast to the use of cement and lime, Baloochi et al. (2020) conducted research on BCS stabilization without using these traditional stabilizers. Waste paper fly ash possesses cementitious properties due to its calcium, silica, and aluminum composition. Free lime and reactive phases in waste paper fly ash allow it to react and harden in water. However, it is essential to note that the expansion of free lime upon contact with water requires a delay time before utilizing waste paper fly ash for BCS stabilization.

While lime stabilization can enhance soil strength, Randhawa et al. (2021) emphasized the challenges and considerations associated with this technique. The calcium silicates and calcium aluminum hydrates formed during the reaction between lime and BCS can increase soil strength. However, the addition of excess lime adversely affects the soil due to inadequate water for the pozzolanic reactions, leading to adverse effects of strength loss.

Considering the limitations and drawbacks of cement and lime, Noolu et al. (2021) suggested an alternative approach using ground granulated blast furnace slag with sodium hydroxide to enhance soil properties. Adding ground granulated blast furnace slag with an 8-molar concentration of sodium hydroxide solution resulted in a significant five-fold increase in the UCS of the soil.

Singh (2020) introduced the concept of using bio enzymes in combination with cement kiln dust to enhance soil properties. This innovative approach aimed to improve the effectiveness of stabilization techniques and provide a sustainable solution for BCS stabilization. An optimal condition for UCS was achieved by replacing soil with 12.5% cement kiln dust and 2.5% terrazyme. In the presence of cement kiln dust, the bio enzyme played a role in early-stage reactions in the soils.

Pandey and Singh (2021) investigated the potential of construction and demolition waste, ground granulated blast furnace slag, and polypropylene fibers in enhancing soil properties. A four-fold increase in UCS was observed due to replacing fine clay with coarser additives. Also, a reduction in LL and PI was noted with increased additives in the soil. Dinesh et al. (2021) studied the effects of copper slag and sawdust ash on BCS. Optimum replacement percentages of 30% copper slag and 4% sawdust ash resulted in a UCS of 92 kPa, compared to 24 kPa for the untreated soil.

Singh and Kalita (2021) used bagasse ash and coconut fiber to improve BCS. Adding 10 % bagasse ash and 0.5 % coconut fiber doubled the soil strength. It reduced the soil swelling from 48 % to 25 %. Navagire et al. (2022) explored the utilization of coal bottom ash for soil stabilization. Mixing coal bottom ash with the soil-sealed cavities in the soil matrix makes it denser with reduced plasticity, resulting in increased UCS.

Biswas et al. (2021) aimed to enhance the durability of lime-treated sulfate-rich soil by adding a crystalline silica-based admixture. The results showed a significant reduction in ettringite-induced volumetric swelling, from 45% to 3%, and an improvement in retained UCS, from 5 to 40 kPa. This indicates that the addition of the crystalline silica-based admixture successfully mitigated the swelling effects and increased the strength of the treated soil.

These studies highlighted the potential of ash-lime combinations for effective stabilization and improving the stability and strength of BCS. They offered valuable insights into alternative materials and techniques, contributing to better understanding of BCS stabilization. Waste materials, such as ash, fiber, and slag, have been studied and found to be environmentally friendly and cost-effective for soil stabilization. They improve the engineering properties of BCS and reduce the swell-shrink tendency. These findings suggest the importance of considering alternative materials to overcome the challenges associated with BCS.

2.3 Utilization of BMA as construction material

The improper and unscientific handling of biomedical waste poses risks to individuals directly and indirectly involved in its management and presents challenges in preserving the quality of water, air, and soil. In their study, Manzoor and Sharma (2019)

highlighted these risks and emphasized the importance of research to explore innovative approaches for managing biomedical waste.

In their study, Kaur et al. (2019) proposed the utilization of BMA as a substitute for fine aggregate in concrete. By replacing 5% of the fine aggregate, the concrete significantly improved strength and enhanced pozzolanic activity. Moreover, the durability of the concrete surpassed that of conventional concrete, which is typically composed of ordinary portland cement and river sand. However, replacing sand with BMA beyond 10% reduced compressive strength, and beyond 20% compromised the heavy metal immobilization in the BMA by cement.

Exploring the applications of BMA further, Suresh Kumar et al. (2020) identified its potential as a suitable substitute for ground-granulated blast furnace slag in geopolymer concrete. However, it was observed that the use of BMA increased the initial setting time of the geopolymer concrete. Building upon this research, a geopolymer concrete was developed by partially replacing ground granulated blast furnace slag with BMA as the binder material and incorporating waste glass powder as a partial replacement for the fine aggregate (Suresh Kumar et al. 2022). Optimum results were achieved when BMA replaced 30% of ground granulated blast furnace slag, and 50% of waste glass powder was utilized. The geopolymer concrete demonstrated maximum compressive strength of 51.1 MPa, split tensile strength of 5.21 MPa, and flexural strength of 6.85 MPa under these conditions.

Katare et al. (2022) examined the viability of BMA as a partial replacement for cement in concrete. When 7.5% of the cement was replaced with BMA, the compressive strength increased by 20%. This gain in strength was attributed to several factors, including the pozzolanic action, densification, presence of calcium and silica in the ash, two-wall effect, and improved packing achieved through the micro-filling of BMA within the concrete matrix.

Girma and Asteray (2022) investigated the combined effect of biomedical waste incinerator ash and bagasse ash as supplementary cementitious materials in concrete. When 2.5% bagasse ash and 2.5% biomedical waste incinerator ash were used as replacements, the compressive strength of the concrete slightly decreased after 7 days

of curing. However, after 28 days of curing, the compressive strength of the control mix was lower (51.8 MPa) compared to the 5% replacement of cement (54.8 MPa) and 10% replacement of cement (52.5 MPa). Increasing the replacement percentage of ash increased slump, flowability, and compaction factor while decreasing the density of fresh concrete. Using ash resulted in a denser calcium silicate hydrate gel with fewer pores in the concrete, improving interlocking between the aggregate and cement paste and enhancing the mechanical properties of the high-strength concrete.

Bilal et al. (2022) reported a significant enhancement of concrete properties with increased content of BMA. They observed that the workability of concrete would be the limiting factor to restrict the replacement at 30 %. They also discussed the techno-economic features of utilizing biomedical waste and developed a theoretical model.

In their study, Nataraja et al. (2023) investigated using BMA as a partial substitute for cement in M30-grade self-compacting concrete. Increasing BMA content decreased the workability of the concrete due to higher water absorption. The optimal BMA substitution level was 5% for split and flexural tensile strengths. The presence of BMA improved pore refinement, resulting in reduced chloride permeability. Water absorption rates were slightly higher in BMA mixes, but Scanning electron microscopy (SEM) images showed overall microstructure densification.

Matalkah (2023) evaluated the effects of activating BMA for use in mortar and concrete. Dry milling increased the ash's reactivity, resulting in a more than 40 % increase in compressive strength compared to unmilled ash. Calcination of the ash further increased compressive strength by over 60 %. Ash activation improved concrete's resistance to hydrochloric acid exposure, minimizing strength loss. Activated ash paste reduced heavy metal leachate from hydrated matrices compared to untreated ash paste. The increase in ash surface area, efficient pozzolanic reactions, and formation of additional calcium-silicate hydrates contributed to this reduction.

2.4 Utilization of FCA in construction materials

FCA is reported as a suitable additive for improving the characteristics of building materials in the following studies:

Different percentages of FCA were substituted for cement along with 7% lime to examine their impact on various properties of concrete (Acharya and Patro 2015). These properties included compressive strength, splitting tensile strength, modulus of elasticity, ultrasonic pulse velocity, and water permeability. The researchers discovered that when 40 % FCA and 7 % lime were used to replace 47 % ordinary portland cement, the resulting concrete exhibited properties like conventional concrete after 28 days of curing.

Further, Acharya et al. (2016) investigated the flexural behavior of reinforced concrete beams containing 40% FCA and 7% lime, which replaced 47% ordinary portland cement. The results demonstrated that the FCA concrete beams exhibited a superior load-carrying capacity compared to the control concrete beams, with an increase of 8.33%. Additionally, the crack resistance ability of the FCA concrete was improved by 50%. Moreover, including FCA and lime did not negatively affect the bond between the concrete and reinforcement, and it improved the concrete's ductility.

In another study, Acharya and Patro (2016a) found that the replacement of cement with 40% FCA and 7% lime led to an enhancement in the 28-day compressive strength by 1.5% to 13.5%, flexural strength by 4.5% to 9%, bond strength by 15% to 29%, abrasion resistance by 10% to 23%, and a reduction in sorptivity by 25% to 43%. Acharya and Patro (2016b) demonstrated that adding FCA and lime enhanced the abrasion resistance of the concrete, indicating an improvement in durability, and reduced the total void content of the concrete.

Mohanty et al. (2019) investigated the combined influence of different percentages of fly ash and FCA as partial replacements for cement on the strength of concrete. The study showed that even a tiny amount of FCA significantly improved the concrete strength compared to the replacement by fly ash alone.

In another study, Mishra et al. (2020) investigated the behavior of a novel geopolymer binder utilizing FCA as the primary source material. Ground granulated blast furnace slag and lime were also used in combination. The mix with 80% FCA and 20% ground granulated blast furnace slag exhibited the highest compressive strength of 27 MPa, making it suitable for typical construction purposes. However, the workability of

geopolymer concrete mixes containing FCA was unsatisfactory, as zero slumps were observed. The authors recommended the addition of appropriate superplasticizers to improve workability.

Kumar B et al. (2020) utilized FCA combined with alkali-activated slag to develop an alternative alkali-activated mortar. The objective was to create a substitute for conventional ordinary portland cement mortar. The researchers successfully achieved the targeted compressive strength.

Saha et al. (2021) explored the behavior and feasibility of incorporating FCA as the base material in geopolymer concrete. The study reported that FCA is rich in iron and aluminum oxides and possesses the properties of a good binding material.

Mishra et al. (2022a) emphasized the importance of a high MgO content in FCA. High MgO content is crucial in reducing shrinkage cracks and porosity while promoting the acceleration of hydration and strength development in concrete. The researchers specifically investigated the effect of FCA on geopolymer concrete and concluded that a mixture of 60% FCA and 40% fly ash achieved a remarkable 28-day compressive strength of 29.3 MPa.

Mishra et al. (2022b) combined FCA and ground granulated blast furnace slag in different proportions to produce open-air cured geopolymer concrete. A mixture with 80 % FCA and 20 % ground granulated blast furnace slag achieved a compressive strength of 30.2 MPa. A significant reduction of 44.26 % in embodied energy and a decrease of 39.28 % in carbon dioxide emissions due to the geopolymer concrete compared to cement-based concrete with similar strength was reported.

Lime production contributes to significant carbon dioxide emissions and environmental impacts. Hence, Sharma et al. (2022) explored the utilization of FCA without lime and instead incorporated other industrial waste materials, such as silica fume and red mud, as partial cement replacements in concrete. Experimental results revealed that concrete mixtures consisting of 78% ordinary portland cement, 19% FCA, and 3% silica fume, and 80% ordinary portland cement, 10% FCA, and 10% red mud achieved comparable compressive strength to standard concrete.

Omur et al. (2023) examined the impact of FCA replacement on alkali-activated paste and alkali-activated mortar. The findings indicated that the inclusion of FCA resulted in a reduction of plastic viscosity and yield stress in the alkali-activated pastes. Additionally, there was a slight increase in water absorption and vacuum-pore property values with higher FCA content. The study also revealed decreased drying shrinkage with increased FCA content.

Acharya and Patro (2023) investigated the environmental impact and performance of concrete made with waste materials from the ferrochrome industry. A functional performance-based life cycle assessment evaluated various environmental disturbance indicators, including global warming, carcinogens, aquatic acidification, and terrestrial ecotoxicity. The study revealed that the environmental disturbance indicator associated with ferrochrome waste-based concrete was 14-46 % lower than standard concrete. Furthermore, the performance-linked functional unit of Ferro-waste concrete was approximately 9-62 % higher than that of traditional concrete. These results indicate that utilizing waste materials from the ferrochrome industry in concrete production can reduce the environmental impact and improve the material's overall performance compared to conventional concrete mixes. Therefore, the study suggests incorporating waste materials from the ferrochrome industry into concrete production. This approach can contribute to lower environmental impacts while enhancing the performance of concrete structures. It offers a sustainable and cost-effective alternative to traditional methods.

2.5 Methods and Technologies for Heavy metal stabilization in Ashes

2.5.1 Chemical stabilization

Chemical stabilization techniques aim to convert soluble and leachable heavy metals into insoluble and non-leachable forms using chemical agents.

Crannell et al. (2000) assessed the chemical stabilization of heavy metals in bottom ash from municipal solid waste incineration using soluble phosphates. The experimental dose of 0.38 mols of soluble phosphates per kg of residue reduced the leachable fraction of heavy metals, such as Ca, Cd, Cu, Pb, and Zn. pH-dependent leaching tests demonstrated a significant reduction in equilibrium concentrations for these heavy

metals. Spectroscopic analysis revealed the presence of stable mineral phases, including calcium phosphates, tertiary metal phosphates, and lead phosphates. The treatment effectively stabilized divalent metal cations in the bottom ash.

Sukandar et al. (2009) focused on chemically stabilizing heavy metals in medical waste fly ash using chelating agents (Ashnite S803), acidic phosphoric acid (Ashnite R303), and basic phosphoric acid (Ashnite R201). The leachability of heavy metals was evaluated using the Japanese Leaching Test, and ecotoxicity assessments were conducted using bioassays. The results showed a significant reduction in heavy metal concentration and toxicity in the leachate after adding the stabilizing agents.

Lv and Zhou (2016) explored the usage of meso-2,3-dimercaptosuccinic acid as a stabilizer to treat the incinerated municipal solid waste fly ash. It has shown superior performance in immobilizing mercury. It effectively converts heavy metals into insoluble and non-leachable forms, and its stabilization efficiency remains consistent regardless of pH changes.

In their study, Vavva et al. (2017) used phosphoric acid stabilization and water washing to improve the leachate quality of fly ash from a municipal solid waste incinerator. An optimized treatment with a 7 % w/w phosphoric acid ratio followed by water washing successfully stabilized the fly ash for non-hazardous waste landfilling. This method significantly reduced heavy metal pollution in the wastewater and provided insights into effective fly ash treatment. This concept was later applied to treat fly ash from medical waste incinerators (Vavva et al. 2020). The optimal acid-to-ash ratio was 10% w/w, and the liquid-to-solid ratio was 3 L/kg. The treatment effectively reduced lead leachate concentration and eliminated salts, ensuring compliance with regulatory guidelines. The modified treatment method effectively managed medical waste fly ash and ensured safe disposal.

Zhu et al. (2020) investigated the physicochemical characteristics of fly ash and tested various chemical reagent stabilization schemes for Cu, Zn, Pb, Cd, and Cr. Fly ash contained micro-sized particles and a range of toxic heavy metals. In single reagent schemes, 8 % sodium sulfide, 8 % sodium dihydrogen phosphate, 4.2 % ammonium dibutyl dithiophsphate, or 4.2 % 2,4,6-tri-mercapto-S-triazine trisodium salt reduced

leaching concentrations to meet regulatory limits, with 8 % sodium sulfide being the most cost-effective. However, a mixture of 1.2 % sodium sulfide, 1.2 % sodium dihydrogen phosphate, and 0.8 % ammonium dibutyl dithiophsphate was more effective and cheaper. The composite agent stabilization scheme showed promise for economically and effectively treating heavy metals in fly ash. This study reports the correlation between the particle size of fly ash and its level of toxicity, indicating that smaller particles may possess greater toxicity.

Several agents were tested for their effectiveness in removing specific heavy metals from raw paper incineration ash to render the ash recyclable (Kim et al. 2022). Ethylenediaminetetraacetic acid showed the highest efficiency in removing Pb, while oxalic acid exhibited the highest efficiencies for Cu, Cd, and As removal. Among the three advanced removal modes tested, the simultaneous use of a mixture of both solutions showed the best removal efficiencies for all the heavy metals, with significant percentages removed: Cd (11.9 %), Hg (10 %), As (28.42 %), Cu (31.29 %), and Pb (49.19 %). The application of the advanced removal method resulted in decreased elution of heavy metals and a higher content of CaO in the treated incineration ash. Additionally, the Cl content in the ash decreased.

2.5.2 Cement solidification/stabilization

Sobiecka et al. (2014) investigated the influence of pH on immobilizing heavy metals in hospital solid waste incinerator ash mixed with Portland cement using two solidification/stabilization processes: cement hydration and granulation. Cement hydration yielded more stable products than granulation. Higher ash content (60 %) with portland cement immobilized Pb^{2+} and Cu^{2+} the best, while lower ash content (10 %) reduced leachability of Zn^{2+}. Equal proportions (50 %) of ash and cement provided the highest encapsulation for Ni^{2+}, Cd^{2+}, and Cr^{3+}. Neutral to weakly alkaline pH (7–8) resulted in the lowest leachability of heavy metals.

Su et al. (2016) investigated using magnesium potassium phosphate cement mixed with municipal solid waste incineration fly ash to stabilize Cd and Pb. The study aimed to reduce stabilization costs while disposing of and reusing fly ash. The effects of fly ash on stabilizing Cd, Pb, and Cd-Pb mixtures were examined. Results showed that

increasing fly ash content gradually increased Cd leaching concentration during the stabilization. For Pb and Cd-Pb mixtures, Pb leaching concentration initially decreased and then increased with ash content. The compressive strength of cement pastes decreased with higher fly ash content after a 90-day curing period. Fly ash content below 40% was suitable for heavy metal stabilization, and less than 20% was recommended for construction material incorporation. Fly ash synergistically affected Pb stabilization with cement due to strong adsorption and chemical fixation, while its effect on Cd stabilization was relatively weaker.

Fan et al. (2018) conducted a comparative review analysis of solidification effects and leaching toxicity of municipal solid waste incineration fly ash treated with various types of cement. The study reports that phosphate cement and alkali-activated cement are more effective in immobilizing heavy metals present in fly ash. It also examines the interaction between cement hydration products and heavy metals. However, the immobilization mechanism of heavy metals through cement-based stabilization/solidification technology is controversial. These mechanisms can vary depending on external environmental factors and the structure of the matrix materials. Additionally, the hydrolysis of heavy metals can impact the pH values and cement hydration process, further complicating the study of immobilization mechanisms and the fixation effects of heavy metals.

Chen et al. (2021) proposed an approach using phosphate-modified calcium aluminate cement for the stabilization/solidification of municipal solid waste incineration fly ash. The study focused on mitigating the negative impact of Pb on the calcium aluminate cement reaction. The presence of Pb retarded the early-stage reaction of calcium aluminate cement, resulting in a prolonged setting time and a significant decrease in the compressive strength of calcium aluminate cement pastes. However, incorporating phosphate additives, particularly trisodium phosphate, in the calcium aluminate cement system effectively mitigated the negative impact of Pb and reduced its leachability. Elemental mapping results indicated that Pb^{2+} coordinated with phosphate to form insoluble precipitates, such as $Pb_3(PO_4)_2$.

Pateriya et al. (2022) explored the stabilization of marble waste with fly ash-based portland pozzolana cement. The modified matrix was further stabilized with cement

and reduced graphene oxide powder to enhance strength properties. The study demonstrated a significant 3 MPa increase in UCS compared to raw marble waste. The novel marble matrix showed potential for replacing weak subgrade soil and providing an effective waste management solution.

Wang et al. (2022a) studied the stabilization/solidification of municipal solid waste incineration fly ash using an innovative magnesium oxysulfate cement binder. The focus was on interactions between the binder, metallic cations Pb^{2+}, and oxyanions AsO_3^{3-}. Experimental findings showed that Pb and As had different effects on the reaction process of magnesium oxysulfate cement, inhibiting it slightly in the high-sulfate system and significantly suppressing it in the low-sulfate system. The high-sulfate binder system achieved excellent immobilization efficiencies, reaching 99.8% for Pb and As.

2.5.3 Thermal treatment

Yu et al. (2015) investigated a thermal treatment method to vaporize heavy metals and alkali/alkaline earth metals from fly ashes. Mixing two types of fly ash from fluidized bed incinerator and grate incinerator, and subjecting them to thermal treatment revealed that grate incinerator fly ash prevented melting and facilitated the vaporization of heavy metals. Increasing temperatures resulted in significant vaporization of chlorine, sodium, and potassium. Cadmium vaporized effectively, while the vaporization of lead was moderately enhanced. Copper vaporization was promoted by alkali/alkaline earth metals, while Zn vaporization was relatively low due to compound formation. Less than 20 % of Cr vaporized. The atmosphere influenced vaporization rates, but heavy metal leachate concentrations were below regulatory limits after treatment. This study demonstrates the efficacy of thermal treatment in vaporizing heavy metals and alkali/alkaline earth metals from fly ash, reducing their environmental impact.

Okada and Tomikawa (2016) investigated the effects of reducing atmospheres on metal separation and recovery during municipal solid waste ash-melting. They compared nitrogen (N_2) and carbon monoxide plus nitrogen ($CO + N_2$) atmospheres. The reducing ability of the atmosphere influenced metal separation efficiency, with some cases showing hindered separation and reduced metal recovery under the $CO + N_2$

atmosphere. High reducing ability inhibited the formation of water-soluble lead chlorides, affecting metal recovery through water leaching. To mitigate these effects, chlorine gas treatment at 1400 °C effectively achieved high metal separation and recovery efficiencies. These findings are valuable for optimizing metal recovery in different melting furnaces and improving ash-melting plant processes.

2.5.4 Alternative additives

Li et al. (2014) investigated the use of silica fume to stabilize heavy metals in municipal solid waste incineration fly ash. Adding 20 % silica fume reduced the leaching of toxic heavy metals, such as Cu, Pb, and Zn. Speciation analysis revealed the transformation of Pb and Cd into more stable forms. Adding 10% silica fume met the detoxification requirements for Cu and Zn, improved mechanical strength, and enhanced heavy metal immobilization through pozzolanic reactions. The researchers concluded that reduced leaching was achieved through physical entrapment and chemical incorporation.

The research conducted by (Mu et al. 2016, 2018) explores the use of fishbone to stabilize Pb in municipal solid waste incineration fly ash. Batch leaching tests were conducted with varying ratios of fishbone to fly ash and contact times. Higher fishbone doses and longer contact times resulted in better lead sequestration. The highest removal efficiency achieved was 24.76 % after a 72-hour leaching process using a 20 % fishbone dosage. Ignition of fishbone was studied to optimize the thermal treatment technique. Ignition removed the non-hydroxyapatite fraction and increased hydroxyapatite crystallinity. The optimal choice was fishbone ignited at 430 °C, providing more efficient metal stabilization than natural fishbone. The ignited fishbone had higher fishbone hydroxyapatite content and minimized the release of other elements. Higher fishbone doses were recommended instead of chemical adjustments, making the technique cost-effective and sustainable.

Benassi et al. (2019) proposed a novel method for immobilizing leachable heavy metals in municipal solid waste incineration fly ash using silica fume and flue gas desulfurization residues. Leaching tests show reduced Pb and Zn concentrations compared to fly ash leachate. The waste materials and by-products mixture promotes synergistic stabilization mechanisms, including pozzolanic reactions, phosphate

precipitation, and carbonation reactions. The method produced safe materials suitable for eco-composites without commercial chemicals.

2.5.5 Microbial methods

Heera et al. (2014) focused on mitigating the environmental risks associated with biomedical waste ash, which contains high levels of heavy metals (Al, Cr, Pb, Ag) and polycyclic aromatic hydrocarbons. A bacterial isolate *Bacillus sp.* was used as a biological tool to reduce the negative impact of the ash during landfilling. The isolate successfully decreased alkalinity, hardness, chloride, and heavy metal levels, minimizing groundwater, surface water, and soil contamination. This study highlights the potential of bacterial treatment to mitigate the toxicity of biomedical waste ash and emphasizes the need for effective strategies to address its environmental concerns.

Kaur et al. (2021) remediated incinerated biomedical waste ash using the alkaliphilic bacterium *Bacillus halodurans* strain. *Bacillus halodurans* showed optimal growth conditions at pH 8-11, 37 °C, and a 5% NaCl concentration. Treatment with *Bacillus halodurans* significantly reduced alkalinity (63.3%) and heavy metal (Al, As, Ag, Au, Bi, Ca, Cd, Cr, Cu, Fe, Mg, Mn) concentrations up to 95%. The method eliminated the need for hazardous chemicals, producing non-toxic materials suitable for construction and reducing landfill space and disposal costs. The bioremediation method aligned with the eco-friendly zero discharge concept, avoiding the generation of toxic effluents or by-products associated with chemical treatments.

2.5.6 Combined techniques

Hu et al. (2015) investigated the use of hydrothermal treatment for separating and stabilizing heavy metals in municipal solid waste incinerator fly ash. The hydrothermal treatment process, combined with ferric/ferrous additives, controlled Cu, Pb, and Cr leaching from the fly ash by forming iron oxides or hydroxides. Subsequent stabilization with soluble phosphate further reduced heavy metal leaching. Heavy metals underwent phase transformations and redistribution among new particles, aiding separation and stabilization. Special-shaped minerals were formed with high heavy metal content. Mild acid washing at pH 6.20 effectively removed soluble and integrated heavy metals.

Benassi et al. (2016) conducted a pilot-scale study focusing on the chemical stabilization of municipal solid waste incineration fly ash. The aim was to develop sustainable technology using waste materials to avoid landfilling. The pilot plant treated over 0.5 tons of fly ash daily using waste materials like coal fly ash, flue gas desulfurization residues, and rice husk ash. The stability of the treated material was evaluated by examining metal leaching six months later. The study demonstrated a stabilized product with significantly lower concentrations of leachable metals (K, Ca, Mn, Fe, Co, Ni, Cu, Zn, As, Br, Rb, Sr, Ba, Pb) than untreated fly ash at different pH.

Ma et al. (2017) investigated the effects of water-wash extraction and wrapping pretreatment on fly ash's heavy metal volatilization and leaching behavior. Thermal arc plasma treatment significantly reduced the volume (68.7-82.2 %) and weight (23.8-56.7 %) of fly ash. Water-washing and wrapping methods reduced heavy metal volatilization, with glass bottle wrapping being the most effective. Successful melting of fly ash required specific CaO-Al_2O_3-SiO_2 ratios. The leaching of heavy metals (Cr, Ni, Cd, Pb, Cu, Zn) in the slag was below standard limits.

Chen et al. (2017a) examined methods to reduce heavy metal leaching and stabilize municipal solid waste incineration fly ash. Water washing, electrodialytic separation, and thermal treatment at 1000 °C were tested. Combining these methods minimized heavy metal leaching and met specified limits for As, Cr, Pb, and Zn. Cr levels were notably lower with this combination compared to other treatments. Electrodialytic separation increased Cd and Zn leaching but reduced Cr leaching. Water washing alone had minimal metal extraction. However, arsenic and chromium leaching remained problematic after thermal treatment, limiting recycling for construction. Re-alkalization during thermal treatment stabilized most heavy elements, but arsenic and chromium leaching persisted. Calcium removal during electrodialytic separation affected leaching patterns after thermal treatment.Municipal solid waste incineration fly ash is challenging to handle due to heavy metal leaching and thermal treatment emits air pollutants while producing residue with high Cr leaching. The combined approach of water washing, electrodialytic separation, and thermal treatment effectively stabilized municipal solid waste incineration fly ash, reducing evaporation levels and improving its recyclability.

Chen et al. (2022a) used a calcium carbonate polymer coupled with thermal treatment for immobilizing heavy metals (Zn, Pb, Cd, Cr, Cu) in municipal solid waste incineration fly ash. Different curing pathways and thermal treatment temperatures were investigated to assess their impact on leaching. Results showed high solidification efficiencies for Pb and Zn using the wet carbonation pathway. At the same time, lower leaching concentrations of Cd and Cr were achieved through fly ash mixing with calcium carbonate polymer. Increasing the thermal treatment temperature to 500 ^{o}C improved solidification, but acidic leaching agents weakened the immobilization effect.

Xu et al. (2023) investigated microwave hydrothermal treatment with additives to stabilize heavy metals in municipal solid waste incineration fly ash. Four common additives (Na_2S, Na_2SiO_3, $Na_2B_4O_7$, and H_3BO_3) were tested at varying conditions. The study found that Na_2S was the most effective additive, forming zeolites, aiding adsorption and precipitation, and converting heavy metals into a stable state. Treatment conditions of 125 °C, 10 minutes, 3 mol/L Na_2S concentration, and 2 mL/g L/S ratio met regulatory limitations for heavy metal leaching concentration. The treated fly ash exhibited higher residual and reducible fractions, indicating heavy metal stability. Microwave hydrothermal treatment with Na_2S shows promise as an efficient and scalable method for treating hazardous waste.

2.5.7 Other techniques

To control heavy metal pollution, Tzanakos et al. (2014) used incinerated medical waste ash in geopolymers. The waste ash was combined with sodium hydroxide, sodium silicate solution, and metakaolin to create geopolymers. By incorporating fly ash and calcium compounds, the strength of the geopolymer specimens was improved, and heavy metal leaching was significantly reduced.

Sohal et al. (2021) utilized vermicomposting to stabilize biomedical waste ash and extract essential minerals. Combining BMA with organic waste and using *Eisenia fetida* worms reduced the heavy metal content in the vermicompost. The highest earthworm growth and reproduction were observed with a 10:90 ratio of BMA to organic waste. Vermicomposting process converted BMA into nutrient-rich manure

while minimizing heavy metal content. This approach demonstrates safe detoxification and nutrient recovery, offering a valuable solution for solid waste management.

Nag et al. (2022) evaluated the use of mordenite, a natural zeolite, as an affordable adsorbent for stabilizing Pb and Zn in municipal solid waste incineration fly ash. Batch experiments demonstrated that higher dosages of mordenite resulted in increased removal efficiency of heavy metals. Mordenite exhibited a higher affinity for Pb compared to Zn. The Freundlich isotherm model provided a better fit for the adsorption data. The study concluded that mordenite has the potential to be a cost-effective material for treating fly ash and removing heavy metals. Further research is needed to enhance the efficiency of heavy metal stabilization and explore the detailed mechanisms.

Chen et al. (2022) focused on the sustainable treatment of hazardous wastes using carbon-negative rice husk biochar and yard waste biochar as green additives in solidifying municipal solid waste incineration fly ash. Adding biochars improved cement hydration reactions, increased the content and connectivity of calcium-silicate-hydrate gel, and enhanced the immobilization of toxic elements in fly ash.

Sun et al. (2023) developed a low-carbon and high-efficiency binder for stabilizing/solidifying municipal solid waste incineration fly ash. They used CaO or MgO to activate ground granulated blast furnace slag and form calcium silicate hydrate or magnesium silica hydrate gel to stabilize the hazardous municipal solid waste incineration fly ash. The presence of potentially toxic elements like Pb and Zn inhibited the formation of reaction products in the CaO-based system but had a negligible effect on the MgO-based system. The MgO-based system showed lower leachabilities and higher mechanical strengths than the CaO-based system. Stabilization/solidification experiments successfully recycled 70 % municipal solid waste incineration fly ash using a 30 % MgO-ground granulated blast furnace slag binder, producing blocks with desirable compressive strength (3.9 MPa) and high immobilization efficiencies of 99.8 % for Zn and 99.7 % for Pb.

Ajorloo et al. (2022) reviewed fly ash treatment, focusing on the technology used to remove and stabilize heavy metals. Various methods were discussed, including physical

separation, leaching, thermal treatment, and chemical stabilization. The review emphasized the importance of considering economic and environmental factors when selecting a treatment method. Strategies such as chemical stabilization, water washing, acid extraction, and thermal treatment were mentioned as approaches to reduce heavy metal leachability. Combinations of different methods were proposed for efficient heavy metal removal and stabilization. The review suggested further research to explore more combinations of methods and conduct detailed economic analyses for industrial-scale implementation.

2.6 Biomineralization for heavy metal immobilization

The following research papers discuss the application of microbial-induced carbonate precipitation (MICP) technology for the immobilization of heavy metals, such as Pb, Cu, Ni, and Cd, in various environmental contexts. MICP involves microorganisms capable of precipitating carbonates, such as calcium carbonate ($CaCO_3$), in the presence of certain metal ions, forming mineral phases that immobilize the metals.

Nam et al. (2016) examined the ability of crude extracts of *Canavalia ensiformis* to catalyze the precipitation of calcium carbonate in heavy metal-contaminated mine waste. The study investigated the effect of $CaCO_3$ precipitates on the leaching of heavy metals from the waste. The results showed that the crude extracts, containing urease, catalyzed urea hydrolysis and formed $CaCO_3$ precipitates, which immobilized heavy metals within the mine waste. Column experiments demonstrated reductions in the leaching of heavy metals such as As, Mn, Zn, Pb, Cr, and Cu when treated with *C. ensiformis* crude extract. The study also compared the microbial communities in treated and untreated mine waste, revealing a greater diversity of microorganisms in the treated columns. The findings suggest that crude extracts of *C. ensiformis* could be used to stabilize and immobilize heavy metals in contaminated mine waste.

Kang and So (2016) investigated the interplay between heavy metals and antibiotic resistance in ureolytic bacteria. They found a close association between the isolates' heavy metal resistance and antibiotic resistance patterns. The study also examined the immobilization of heavy metals using MICP and observed a significant increase in the

compressive strength of treated samples. The isolates effectively immobilized heavy metals in the treated samples.

Zhu et al. (2016) used a urease-positive bacterial isolate, *Bacillus cereus* NS4, for the large-scale remediation of Ni-contaminated soil. The bacterial isolate induced carbonate precipitation, reducing the bioavailability of nickel and stabilizing it as calcite, vaterite, aragonite, and nickelous carbonate minerals. The study highlighted the role of microbial carbonate precipitation in transforming mobile nickel species into stable biominerals, thus facilitating the remediation of metal-contaminated soil.

Yang et al. (2016) focused on the bioimmobilization of copper, lead, and cadmium in contaminated mine tailing soils using MICP. They isolated an indigenous calcifying urease-producing bacterial strain (identified as *Bacillus firmus*) from copper mine tailing soil. The study employed a five-stage sequential soil extraction procedure to analyze metal distribution patterns. After bioremediation, the mobility of toxic metals was significantly reduced in the exchangeable fraction, while their concentrations increased in the carbonated fraction. Scanning electron microscopy revealed the precipitation of calcite associated with the bacterial cells. X-ray diffraction identified calcium carbonate minerals such as calcite, gwihabaite, and aragonite in the bioremediated tailings soils. The researchers concluded that MICP shows promise for the remediation of mine tailing soils by efficiently immobilizing toxic metals like copper, lead, and cadmium.

Qian et al. (2017) focused on using a ureolytic fungal strain, *Penicillium chrysogenum*, on biomineralizing chromate and lead from aqueous solutions and contaminated soil. The fungal strain effectively immobilized Pb and Cr(VI), reducing their concentrations in the solution. The biomineralization process involved the precipitation of carbonate crystals, and the resulting biominerals were identified as calcite, vaterite, calcium chromium oxide carbonate, and hydrocerussite. In soil remediation experiments, the fungal strain increased the carbonate-bound fraction of metals, decreasing the exchangeable Pb and Cr(VI) fraction in contaminated soil.

In a study by Mwandira et al. (2017), the bacterium *Pararhodobacter sp.* was investigated for its potential in bioremediating Pb-contaminated soil using MICP. The

bacterium effectively removed Pb from the solution, and subsequent characterization studies confirmed calcium carbonate and lead coprecipitation. Continuing the research, Mwandira et al. (2019a) further explored the application of MICP in reducing the mobility of hazardous contaminants in mine wastes. The study revealed that biocemented materials exhibited reduced leachate Pb concentrations, resistance to slaking, and improved physicochemical properties.

Chen et al. (2017b) used *Sporosarcina pasteurii* to simultaneously immobilize heavy metals and cement soil particles in tailings containing high levels of arsenic and molybdenum. The results demonstrated a reduction of approximately 98 % in molybdenum content after the bacterial treatment, while the arsenic content only slightly decreased compared to the reference group.

Bhattacharya et al. (2018) used urease-positive *Serratia marcescens* and *Enterobacter cloacae* to remediate Cd. The cultures efficiently removed cadmium from the media by co-precipitating Cd (II) and Ca (II). *S. marcescens* and *E. cloacae* exhibited 96 % and 98 % removal of initial 5.0 mg/L soluble Cd (II) after 96 hours of incubation, respectively. At higher Cd (II) concentrations of 10 and 15 mg/L, *E. cloacae* showed higher cadmium removal efficiency than *S. marcescens*. In vitro remediation studies using cell-free culture supernatant of *S. marcescens* and *E. cloacae* with urease activity resulted in 98 % and 53 % removal of initial 50 mg/L Cd (II) in the presence of Ca (II). However, in the sole presence of Cd (II), only 16 % and 8 % removal of Cd (II) were observed for *S. marcescens* and *E. cloacae*, respectively. This study presents coprecipitation as a sustainable bioremediation approach for effectively addressing Cd (II) pollution.

Wang et al. (2019) converted microbial-induced calcite to hydroxyapatite to enhance Cd removal efficiency and reduce Cd release. The results showed that the conversion of calcite to hydroxyapatite significantly improved Cd removal compared to the MICP process and adsorption by calcite. The study suggests that the conversion of calcite to hydroxyapatite can control the environmental behavior of Cd and be applied for soil remediation.

Chen and Achal (2019) investigated the use of biostimulation in MICP for Cu immobilization in soil. Unlike previous studies that focused on bioaugmentation, this study aimed to enhance MICP through biostimulation. After biostimulation, the researchers assessed the bacterial community's abundance, composition, and diversity and evaluated Cu immobilization in soil. The results showed that biostimulation induced calcite precipitation, resulting in Cu immobilization mainly in the carbonated fraction of the soil. The soluble-exchangeable fraction of Cu decreased significantly from 45.54 mg/kg to 1.55 mg/kg.

Zhang et al. (2019a) investigated the effect of biochar on the remediation of Ni using MICP. The addition of biochar inhibited calcite production and suppressed Ni remediation. Biochar weakened the adsorption bonds responsible for carbonate formation, which dissociated the carbonate structure produced by *Bacillus cereus*.

He et al. (2019) applied MICP for the remediation of divalent Pb and hexavalent Cr in solution using ureolytic *Staphylococcus epidermidis*. The removal efficiency of Pb(II) and Cr(VI) reached up to 86 % and 76.8 %, respectively, with an initial metal concentration of 25 mg/L. The study demonstrated the significant difference in terms of Cr(VI) and Pb(II) immobilization, highlighting the clear efficacy or preference of MICP in immobilizing divalent over multivalent metal ions.

Peng et al. (2020) isolated a Cd-resistant ureolytic bacterium, identified as *Enterobacter sp.*, and investigated its performance in immobilizing Cd in solution and soil under different treatment conditions. The results showed that the Cd removal rate reached a maximum of 99.50 % within 7 days in solution by MICP. Characterization of the precipitates revealed the presence of biominerals such as calcite and vaterite, which absorbed Cd^{2+} ions. In soil, the highest Cd immobilization rate achieved was 56.10%. The study also evaluated the impact of different treatments on soil properties and microbial communities. The combination of *Enterobacter sp.* and oyster shell wastes showed excellent ability and potential reuse value for remediating Cd-contaminated environments.

Do et al. (2020) focus on the role of psychrotolerant bacteria in the remediation of heavy metal contamination at low temperatures. A psychrotolerant Ni-resistant bacterial

strain, *Bacillus cereus*, was isolated from a nickel mining area. The strain exhibits urease activity and the ability to induce carbonate precipitation, resulting in the removal of Ni ions (73.47 %) from the culture solution and contaminated soil at low temperatures.

Cuaxinque-Flores et al. (2020) investigated the capacity of two strains (UB3 and UB5) of *Sporosarcina luteola* to induce metal sequestration through carbonate precipitation. The strains exhibited high urease activity and carried the ureC gene. They were also highly resistant to metals and capable of producing metallophores and arsenophores. In vitro experiments revealed that the two strains induced the precipitation of various carbonates such as calcite, vaterite, magnesian calcite, and several $(M^{2+})CO_3$ compounds including hydromagnesite (Mg^{2+}), rhodochrosite (Mn^{2+}), cerussite (Pb^{2+}), otavite (Cd^{2+}), strontianite (Sr^{2+}), witherite (Ba^{2+}), and hydrozincite (Zn^{2+}). Inoculating a mixed culture of UB3 and UB5 in tailings resulted in increased pH and vaterite, calcite, and smithsonite precipitation. This enhanced biocementation, reduced pore size and permeability and slowed the oxidation of residual sulfides.

Jalilvand et al. (2020) investigated the bioprecipitation of heavy metals using ureolytic bacteria. The study aimed to isolate urease-producing bacteria from contaminated soils and assess their potential for biomineralizing heavy metals. Four isolates exhibiting high urease production, calcite precipitation, and endurance to heavy metals were selected from contaminated areas. These isolates, along with *Sporosarcina pasteurii*, were used to bioprecipitate Zn, Pb, and Cd from solutions with varying concentrations of these metal ions. Among the isolates, *Stenotrophomonas rhizophila* and *Variovorax boronicumulans* demonstrated the highest carbonate mineral production of heavy metals. *S. rhizophila* removed 96.25 %, 71.3 %, and 63.91 % of Pb, Cd, and Zn, respectively, after 72 hours of incubation. *V. boronicumulans* removed 95.93 % of Pb, 73.45 % of Cd, and 73.81 % of Zn within the same incubation period. *S. pasteurii* exhibited removal efficiencies of 98.71 % for Pb, 97.15 % for Cd, and 94.83 % for Zn.

Eltarahony et al. (2021) aimed to employ the $CaCO_3$ bioprecipitation technique using the ureolytic fungal strain *Metschnikowia pulcherrima* and bacterial strain *Raoultella planticola* for the removal of Pb and Hg. They were selected based on their high ureolytic activity and minimum inhibitory concentration against Pb^{2+} and Hg^{2+}. The

maximum urease activity reached 884 and 639 U/mL for *Metschnikowia pulcherrima* and *Raoultella planticola*, respectively. Complete removal of Pb^{2+} was achieved at 42 h (*Metschnikowia pulcherrima*) and 90 h (*Raoultella planticola*), while Hg^{2+} was entirely removed at 60 h (*Metschnikowia pulcherrima*) and 102 h (*Raoultella planticola*).

Zeng et al. (2021) examined the potential of microbially induced phosphate precipitation to immobilize cadmium. The study focused on the role of an indigenous bacterium, *Burkholderia ambifaria,* in Cd removal. The addition of Ca^{2+} significantly increased the removal ratio of Cd. The researchers found that Cd was removed by Cd-containing hydroxyapatite.

Liu et al. (2021a) established an immobilized biofilm reactor to remove Ca^{2+}, F^-, Ni^{2+}, and nitrate $NO_3^{2-}N$ through MICP. The study discusses the reactor's operating parameters and the target contaminants' removal efficiencies. The results showed that the reactor achieved stable removal performances for Ca^{2+}, F^-, Ni^{2+}, and $NO_3^{2-}N$ under specific operating conditions. The study also provided insights into the bio-crystal morphology, precipitate components, gas production, and bacterial community associated with the reactor. The findings suggest the potential application of MICP-based bioremediation for simultaneous remediation of these contaminants in water bodies.

Liu et al. (2021b) used *Sporosarcina pasteurii* to bioremediate Pb, Zn, and Cd-contaminated soils. Adding *S. pasteurii* reduced the leaching concentrations of heavy metals and immobilized them through carbonate precipitation. The study demonstrated that *S. pasteurii* bioremediation effectively reduced the bioavailability and toxicity of heavy metals in contaminated soil.

Wang et al. (2021a) investigated the behavior of carbonate-bound As during the conversion of calcium carbonate to hydroxylapatite. The study prepared bio-induced $CaCO_3$ in an As solution and converted it to hydroxylapatite to understand the stability and immobilization of As. The results showed that a high arsenate concentration promoted the conversion of $CaCO_3$ to hydroxylapatite. The dissolution data verified the

low solubility of As in hydroxylapatite, whereas the As-bearing $CaCO_3$ precursor released a significant amount of As during the conversion.

Liang and Hu (2021) isolated a novel bacterium, *Achromobacter sp.*, with capabilities for sulfamethoxazole degradation and Cd^{2+} immobilization. Microbial degradation and sediment adsorption played important roles in Cd^{2+} immobilization, while microbial degradation played a decisive role in sulfamethoxazole degradation. The study also proposed a relationship between aerobic denitrification, sulfamethoxazole degradation, and Cd^{2+} immobilization.

Qiao et al. (2021) investigated the efficiency of MICP for Cu, Zn, Ni, and Cd in mining areas. *Sporosarcina* bacteria was selected based on their urease activity and precipitation ability. The study found that Cd removal was mainly based on forming cadmium carbonate induced by bacterial activity, while Cu removal depended on the pH increase generated by the same process. Precipitation contributed to Zn and Ni removal through the MICP process. The study demonstrated that urease-producing bacteria could co-precipitate multiple heavy metals even without the ability to tolerate them, suggesting the potential of MICP for immobilizing multiple heavy metals in ecological restoration.

Bai et al. (2021) described a halophilic ureolytic bacterium, *Exiguobacterium sp*., and its ability to immobilize heavy metals, focusing on Pb as a model heavy metal. The strain precipitated calcite and vaterite under non-growth conditions and efficiently removed Pb by incorporating it within microbially induced calcium carbonates. The removal efficiency of Pb^{2+} was affected by solution salinity, with higher salinity promoting vaterite formation but reducing removal efficiency.

Li et al. (2021) focused on immobilizing potentially toxic elements using ureolytic bacteria and MICP in the context of electronic waste environments. Bacterial strains were isolated from an E-waste area and a strain of *Lysinibacillus sp.* shows great persistence in immobilizing heavy metals (Cu and Pb). The study reveals a novel heavy metal resistance metabolic system (S-layer protein).

Wang et al. (2022b) studied the immobilization of carbonate-bound uranium through the conversion process from microbial-induced calcite to hydroxylapatite. The

researchers investigated the phase and morphology evolution of minerals and the efficiency, distribution, and stability of uranium immobilization. The results showed that most calcite converted to hydroxylapatite, leading to enhanced uranium removal efficiencies compared to calcite precipitation. The stability test confirmed that uranium -bearing hydroxylapatite significantly decreased uranium solubility compared to calcite.

Li et al. (2022) investigated using corncob powder as a replacement for biochar in microbial carbonate precipitation process. Ureolytic bacterial strain *Bacillus sp.* was isolated and, it was well attached to the surfaces of corncob powder, indicating the carrier's role as a durable shelter for bacterial cells. The study examined the multi-directional benefits of the biochemical composite material for cadmium (Cd) remediation in soil. The composite material showed superior performance in terms of urease activity, bacterial propagation, surface functional groups, calcite precipitation, and Cd immobilization (68.54 %).

Disi et al. (2022) studied the potential of MICP for removing and immobilizing heavy metals (Cd, Cr, Cu, Ni, and Zn), in crude oil-contaminated environments. Bacterial strains *Pseudomonas aeruginosa* and *Providencia rettgeri* were discovered with ureolytic activity and heavy metal tolerance. These strains effectively immobilized heavy metals through biomineralization. The study demonstrated the capability of hydrocarbon-degrading ureolytic bacteria to tolerate heavy metal toxicity and co-precipitate heavy metals.

Sheng et al. (2022) investigated the micro-dynamic process of MICP for the immobilization of heavy metals, focusing on Cd^{2+} removal. They used a novel Cd-tolerant ureolytic bacterium *Pseudochrobactrum sp*. and optimized the conditions using response surface methodology. The Cd^{2+} removal efficiency reached 99.89 %. Five synergistic effects contributing to Cd^{2+} removal were discovered, including co-precipitation, adsorption by precipitation, crystal precipitation on the cell surface, intracellular accumulation, and extracellular chemisorption. This study provided valuable insights into the mechanism of heavy metal removal by MICP and offered a more straightforward method to study the dynamic process related to biomineralization.

Xue et al. (2022) focused on the remediation of Cu-rich water bodies using MICP technology. They investigate the factors influencing Cu immobilization efficiencies, such as the degree of urea hydrolysis, pH conditions, culture medium, bacterial suspension dosage, and $CaCl_2$ addition. The study reveals that the immobilization efficiency of Cu is influenced by the degree of urea hydrolysis and pH conditions. The addition of yeast extract and $CaCl_2$ improved the degree of urea hydrolysis and enhanced the Cu immobilization efficiency.

Zhao et al. (2022) explored the potential of *Fusarium cerealis*, *Phoma herbarum*, and *Mucor hiemalis*, in biomineralizing $CaCO_3$ for concrete protection and metal immobilization. They demonstrate that these fungi exhibit significant urease activity and can produce carbonate biominerals, primarily calcite when cultured in media containing $CaCl_2$. The fungi also show the ability to mediate the formation of strontium carbonate, with *F. cerealis* exhibiting the highest removal efficiency for strontium.

Tan et al. (2022) used a microalgal strain *Chlorella sorokiniana* for Pb(II) biomineralization in the presence of montmorillonite in soil. The addition of montmorillonite facilitated the formation of $Pb_3(CO_3)_2(OH)_2$ on the surface of the *Chlorella*-montmorillonite composite, increasing the algal cells' tolerance to Pb(II) poisoning. The results showed that Pb(II) adsorption and biomineralization were significantly enhanced in the *Chlorella*- montmorillonite composite compared to *Chlorella* alone. Montmorillonite promoted photosynthesis and urea hydrolysis, leading to increased biomineralization.

Zhang et al. (2022a) introduced MICP to immobilize chromium (Cr) in stainless steel pickling sludge. Both bacteria lysis liquor-based MICP and bacteria-based MICP effectively entrapped Cr into mineral lattices, reducing the potential environmental risk of stainless steel pickling sludge. Bacteria lysis liquor-based MICP exhibited better immobilization performance while adding calcium enhanced the immobilization performance of bacteria-based MICP. The leaching of Cr followed an amphoteric pattern, while the leaching of Ni and Ca followed the cation pattern. Geochemical modeling revealed that the leaching of Cr from bio-mineralized products was solubility-controlled by $Cr(OH)_3$ and Cr_2O_3.

Zhang et al. (2022c) explored the use of environmentally friendly bio-$CaCO_3$ precipitation induced by carbonate-precipitating bacteria to improve the performance of coal gangue aggregates. Bio-$CaCO_3$ formation on/in the surface/pores of gangue aggregates reduced water penetration and decreased water absorption. The process also improved the immobilization rate of heavy metals (Cr, Cd, Cu, Ni, Pb) present in coal gangue aggregates.

Song et al. (2022a) focused on using MICP to block the migration of cadmium (Cd) in soil irrigated with Cd-containing wastewater. MICP effectively increased Cd^{2+} adsorption capacity in the soil and trapped Cd^{2+} more effectively than soil alone. Cd^{2+} retention time in the MICP-treated soil column increased with urea content and pH but decreased with flow rate. The MICP process altered soil physicochemical properties and resulted in the formation of $CdCO_3$.

Song et al. (2022b) investigated the use of MICP to solidify and stabilize municipal solid waste incineration fly ash. They explore the effect of blending metakaolin as a protective carrier for bacteria in the fly ash. The MICP treatment effectively immobilized Pb, Cd, and Zn in fly ash. The researchers also investigated the impact of MICP activities on the mechanical and chemical properties of fly ash-based materials.

Xiang et al. (2022) investigated the use of MICP technology to treat municipal solid waste incineration bottom ash. They demonstrated that the biotreatment of ash reduces the leaching of heavy metals, such as Cr, Cu, Zn, Cd, and Pb. The heavy metals become immobilized in a carbonate-bound state, enhancing the binder properties of the treated ash.

Zeng et al. (2022) investigated the immobilization of Cd using MICP technology. The ureolytic bacterium *Sporosarcina ureilytica* effectively removed Cd, and Cd mineralization products are identified. The three Cd^{2+} mineralization products generated by MICP were attributed to surface precipitation ($Cd^{2+} \rightarrow Cd(OH)_2$), direct binding with the CO_3^{2-}/substitution calcium site of calcite ($Cd^{2+} \rightarrow CdCO_3$, otavite), and calcite lattice vacancy anchors ($Cd^{2+} \rightarrow (Ca_xCd_{1-x})CO3$). The study provides insights into the mechanisms by which MICP achieves in situ stabilization of Cd.

Niu et al. (2022) focused on the reinforcement and immobilization of uranium and radon in uranium mill tailings. They incorporated metakaolin and *Bacillus subtilis* \ into the MICP solidification process. The results showed enhancement in the triaxial compressive strength and improved the immobilization capacity of U and Rn in uranium mill tailings. The study highlights the reduction of pore volume, the formation of more crystals, and the enhancement of coprecipitation and encapsulation capacity as contributing factors.

Hu et al. (2023) proposed a novel approach to enhance the stability of immobilized Pb^{2+} by combining biochar and MICP technology. A $CaCO_3$ layer was created as a surface barrier on biochar after Pb^{2+} immobilization, significantly increasing the stable fraction of immobilized Pb^{2+} on biochar. The formation of the $CaCO_3$ layer on biochar acts as a physical and chemical barrier, blocking the contact between acids and Pb^{2+} and buffering against acidic attacks from the environment.

Xie et al. (2023) investigated the relationships between Cu immobilization efficiency and pH conditions. Narrowing the pH range to around 7 with appropriate bacterial inoculation proportion improved Cu immobilization efficiency. The study also performed one-dimensional soil column tests and analyzed Cu immobilization efficiency with depth. Alkaline environments encouraged coordination adsorption of Cu, different from the test tube experiments where Cu^{2+} was encapsulated by carbonate precipitates to prevent migration. The findings suggest the potential of MICP technology for Cu remediation in water bodies and Cu-contaminated sites.

Min et al. (2023) constructed a bioreactor containing *Pseudomonas sp.*, polyester fiber wrapped with shell powder, and iron-carbon spheres to achieve simultaneous ammonia nitrogen (NH^{4+}-N) removal, phosphate (PO_4^{3-}-P) recovery, and nickel immobilization. The bioreactor achieved high removal efficiencies of NH^{4+}-N, PO_4^{3-}-P, Ca^{2+}, and Ni^{2+} through biomineralization, co-precipitation, adsorption, and lattice substitution. The study also analyzed the microbial community and found that *Pseudomonas* was the predominant genus with tolerance to Ni^{2+} toxicity. This study presents an effective method for synchronously removing NH^{4+}-N, recovering PO_4^{3-}-P, and fixing heavy metals using MICP and heterotrophic nitrification and aerobic denitrification technology.

Xue et al. (2023) explored the application of MICP technology for remediating Pb-rich water bodies and Pb-contaminated loess soil sites. They achieved a high Pb immobilization efficiency in test tube experiments using $PbCO_3$ and $Pb(CO_3)_2(OH)_2$ precipitation. However, in loess soil column tests, the Pb immobilization efficiency decreased with depth due to the limited availability of hydroxyl groups. The study highlighted the need to address the size issue of ureolytic bacteria for deeper penetration into the ground in future applications.

Cai et al. (2023) focused on the immobilization of Cd in paddy soil using MICP coupled with the application of rice straw and *Sporosarcina pasteurii*. The study demonstrated that the treatment reduced Cd bioavailability and increased Cd immobilization efficiency through co-precipitation with $CaCO_3$. Furthermore, applying rice straw and *S. pasteurii* enhanced soil fertility and ecological functions, improving various soil parameters and bacterial community composition.

Liao et al. (2023) investigated the long-term stability of Cd immobilization through MICP in farmland soils contaminated with different Cd compounds. They found that MICP treatment effectively immobilized exchangeable Cd but mobilized carbonate and Fe/Mn oxide-bound Cd. The addition of diammonium phosphate had varying effects on Cd immobilization depending on the P/Ca molar ratio. The study emphasized the importance of evaluating the long-term stability of heavy metals in remediated sites, particularly in agricultural areas with phosphate and nitrogen fertilizer input.

The study by Castillo et al. (2023) evaluates a passive treatment system called BDAS for acid mine drainage remediation. They find that bacterial communities in the system shift from chemoautotrophs to chemoheterotrophs, some of which have the potential to immobilize metals. MICP and biofilm formation aid in removing metals (Ca^{2+}, Fe^{3+}, Al^{3+}, and Mn^{2+}) from the water.

Tan et al. (2023) focused on the remediation of heavy metal-contaminated tailings from non-ferrous metal mining activities. They found that the interaction between *Chlorella* microalgae and montmorillonite clay enhances the immobilization of heavy metals, such as Pb and Cu. Montmorillonite aids in transforming the metals into residual and

carbonate-binding states, reduces their leaching, and provides a favorable environment for rebuilding microbial communities and plant growth.

Zeng et al. (2023) examined MICP treatment in a sewage sludge anaerobic digestion-land application process. The study demonstrates that MICP treatment effectively immobilizes heavy metals, such as Cd and Pb, in sewage sludge, preventing their transfer to the supernatant and reducing their soluble exchangeable fractions. The analysis confirmed the excellent performance of the ureolytic bacterium *Sporosarcina ureilytica* ML-2 in the sludge system. The study suggests that MICP technology is feasible for permanently stabilizing heavy metals in sewage sludge before land disposal.

These studies collectively demonstrate the potential of MICP, utilizing bacteria, fungi, or microalgae, in immobilizing and reducing the mobility of heavy metals, such as Cu, Pb, Cd, Mo, Cr, and Hg.

2.7 Biomineralization for strength improvement

In addition to its role in immobilizing heavy metals, biomineralization is renowned for its ability to enhance the strength characteristics of materials.

2.7.1 Crack Healing in Concrete

Achal et al. (2013) focused on the role of *Bacillus sp.* bacteria in the durability and crack remediation of cementitious structures. The study demonstrated that the "biocement" induced by *Bacillus sp.* significantly reduced mortar specimens' porosity and chloride permeability. The bacteria successfully healed simulated cracks in cement mortars, increasing compressive strength by up to 40% compared to the control. The results showcased the potential of microbially induced calcium carbonate precipitation for crack remediation and durability enhancement in various building materials.

Choi et al. (2017) repaired cracked mortar samples using MICP and evaluated water permeability, splitting tensile strength, and the amount and morphology of precipitated calcium carbonate ($CaCO_3$). The results showed that MICP reduced water permeability and increased tensile strength. A positive relationship was observed between tensile strength and the amount of calcite and vaterite precipitated in the samples.

Li et al. (2019) aimed to consolidate cementitious materials using MICP. Bacteria capable of precipitating calcium carbonate were isolated and identified as *Acinetobacter sp*. It was used for crack consolidation in masonry cement mortars. The bio-consolidation significantly improved compressive strength and reduced water absorption. The formation of calcite was confirmed through various analytical techniques. This study provided valuable insights into *Acinetobacter sp*.-induced carbonate precipitation in MICP.

Kaur et al. (2020) emphasized the importance of efficient crack healing methods and reliable monitoring techniques for concrete structures. The study presented an experimental demonstration of bacterial-based healing of fine cracks (0.6 mm) and investigated the efficiency of bacterial healing using advanced monitoring techniques. Ultrasonic signals were used to monitor the healing progression, and water-tightness tests validated the effectiveness of the bacterial technique. The study highlighted the capability of the ultrasonic technique in monitoring crack healing.

Fahimizadeh et al. (2020) investigated using calcium alginate capsules containing biological self-healing agents for cementitious materials. The study examined the survivability and retention of the healing agents, material stability, biomineralization, and in situ self-healing in pre-cracked cement paste and mortar specimens. The encapsulated *Bacillus pseudofirmus* bacteria survived the encapsulation process and precipitated $CaCO_3$ when exposed to water, oxygen, and calcium under alkaline conditions. After 56 days of wet-dry cycles, the capsules regained significant flexural strength and observed full crack closure. The self-healing system acted as a biological CO_3^{2-} pump, retaining and activating the bio-agents for up to 56 days. The study highlights the potential of this self-healing strategy while acknowledging the need for further research and optimization.

In their study, Brasileiro et al. (2020) focused on utilizing *Bacillus cereus* bacteria and calcium lactate in combination with portland cement to produce $CaCO_3$ crystals to reduce the risk of concrete ruptures. The study evaluated the production of $CaCO_3$ crystals under different conditions using the bacterium *Bacillus cereus* and analyzed the crystals' composition. Promising results were obtained, with crystals appearing within 17 hours.

Intarasoontron et al. (2021) studied crack healing through MICP in biological self-healing concretes. The performance of two methods cell/nutrient dropping and immobilization, were compared. *Bacillus sphaericus* was used as vegetative cells and microencapsulated bacterial spores. Pre-cracked mortar specimens were repaired under wet-dry cycles for 7 days after 7 and 28 days of curing. The results showed that the vegetative cell dropping method was more effective in closing cracks and restoring the ultimate load than the immobilized microencapsulated bacterial spores method. Additionally, specimens with microencapsulated bacterial spores exhibited lower ultimate loads than control specimens.

Zhang et al. (2022b) focused on the self-healing efficiency of alkali-activated slag-based composites using bacteria immobilized in expanded glass granules. The study investigated the effect of different calcium sources on reaction kinetics, mechanical properties, capillary water absorption, and self-healing compounds. The bio-based specimens exhibited an enhanced crack healing ratio and reduced sorptivity coefficient. Calcite was identified as the dominant self-healing product.

Nasser et al. (2022) developed bio-based self-healing concrete using MICP as an eco-friendly approach to improve durability. *Bacillus pasteurii* and *Bacillus sphaericus* were added to mortar mixtures with varying cement content. Treated samples showed reduced water uptake, capillary permeability, and volume of permeable voids compared to the control. After 28 days, all treated samples exhibited a significant increase in compressive strength by 28–50 %. At 120 days, flexural strength increased by 19.29–65.94 % in the treated samples. Mortar became denser with fewer voids due to MICP. Bacterial-treated samples had improved calcite and crystallinity. Load deflection tests showed that bacterial reinforced laminates had less deformation than the control. Moreover, reloaded bacterial reinforced laminates demonstrated excellent restoration of physicomechanical properties, highlighting the healing process.

Sohail et al. (2022) investigated the self-healing process in concrete using MICP with an adapted indigenous strain of *Bacillus cereus* isolated from soils in Qatar. The strain could withstand and perform MICP in hot and humid conditions. This strain's performance was compared to that of *Sporosarcina pasteurii*. The strains were encapsulated in sodium alginate beads and incorporated into the cement-sand mortar.

The local *Bacillus cereus* strain exhibited the capability to fill cracks with widths ranging from 162 µm to 670 µm, while *Sporosarcina pasteurii* filled cracks with widths ranging from 200 µm to 4700 µm. The bacterial cells survived in the mortar and developed calcium carbonate in the cracks. The *Bacillus cereus* strain showed high urease activity, suggesting its viability and cost-effectiveness for bio-self-healing concrete through MICP in hot and humid climates.

Sarkar et al. (2023) investigated the healing capabilities of alkaliphilic spore-forming *Bacillus cohnii* in cement concrete. The healing process was evaluated based on mechanical strength, durability properties, and crack sealing. Bio-mineralized calcium carbonate effectively sealed many nanopores, reducing total voids. Microbes precipitated healing agents without affecting the concrete's structure. Statistical analysis showed that calcite deposition significantly influenced compressive strength, enhancing it compared to reference concrete. Visual inspection confirmed the sealing of cracks of different widths. The study demonstrated that microbes seal cracks and improve mechanical strength and durability, providing evidence of self-healing in bio-concrete.

Anand et al. (2023) developed a ready-to-use fly ash-based bacterial inoculum to practically implement MICP in field-scale concrete repair. The bio-grouts, tested for various properties, were used to repair cracks in concrete structures of different orientations. The performance of the repaired surface was evaluated in terms of flexural strength recovery and water tightness. The mineral analysis confirmed the presence of calcite crystals, and calcium carbonate precipitation was quantified using electromechanical impedance. The study concluded that the fly ash-based inoculum effectively promoted MICP, sealing cracks in existing concrete structures.

Lu et al. (2023) proposed a novel approach, the combined injection and diffusion method, for repairing vertical cracks in concrete using MICP. The combined injection and diffusion method overcomes the issue of incomplete crack repair by employing the ureolytic bacterium *Sporosarcina Pasteurii* and a sponge with a saturated cementation solution of urea and calcium acetate. The effectiveness of this method was compared to the traditional injection method through various tests. The results showed that this

method was more effective, producing denser calcium carbonate clusters and higher waterproof performance improvement coefficients.

2.7.2 Strength Enhancer in Concrete

Abo-El-Enein et al. (2013) used MICP to improve cement-sand mortar strength and water absorption. The researchers incorporated *Sporosarcina pasteurii* at varying cell concentrations with the mixing water. The results showed a significant 33 % increase in compressive strength of the cement mortar after 28 days, achieved by adding bacterial cells of 1 OD_{600}. The improvement in strength and water absorption is attributed to the growth of calcite crystals within the pores of the cement-sand matrix.

Li et al. (2017) used the MICP concept in metakaolin-modified cement mortars to enhance their compressive strength. Despite replacing cement with metakaolin up to 50%, MICP with *Bacillus cereus* improves mortar strength by 27%, comparable to conventional cement mortars. Biocementation effectively reduced the cement content without compromising compressive strength, offering a sustainable solution for enhancing strength in concrete.

Charpe and Latkar (2020) investigated the use of MICP to enhance the mechanical properties of cement and concrete. Bacterial solutions derived from soil were employed, with cost reduction achieved by using lentil seeds and sugar as substitutes for nutrient sources. The study found a 23 % increase in compressive strength for bio-cement specimens and a 25% increase for bio-concrete specimens after 28 days of curing. Additionally, the experimental specimens exhibited significantly reduced water absorption compared to the control specimens.

2.7.3 Improvement of sandy soils

Cheshomi et al. (2018) investigated the application of MICP as a method for ground improvement in urban areas. The researchers focused on loose quartz sand with varying densities stabilized using bacteria. They found that MICP effectively produced calcium carbonate cement in the sand, enhancing its shear strength. The highest cement content was observed in the sample with the lowest density. Increasing the injection time and bacterial treatment period further improved shear strength.

Liu et al. (2018) proposed calcareous sand as an alternative calcium source in MICP. Comparative tests were conducted between MICP treatments using soluble calcium from calcareous sand and calcium chloride at the same calcium concentration. The results showed that increasing the cementation solution improved strength, stiffness, and reduced permeability in the treated calcareous sand.

Sharaky et al. (2018) compared the methods of application of biocementation for stabilizing loosely packed soils using *Sporosarcina pasteurii* bacteria. Different treatment methods were employed, including injection with and without fixation and mixing. The results showed that the injection method with fixation solution was most effective in improving the mechanical properties of the sand. Gradual solution addition and non-sterilized growth media enhanced siliceous sandy soil's strength and stiffness.

Yu et al. (2019) explored a novel method of cementing loose desert sand grains through microbially-induced magnesium ammonium phosphate sedimentation, forming bio-sandstone. *Sporosarcina Pasteurii* bacteria hydrolyze urea to produce ammonia and ammonium, which react with hydrogen phosphate ions to create environmentally friendly magnesium ammonium phosphate.

Mwandira et al. (2019b) used Pb-resistant *Oceanobacillus profundus* KBZ 1-3 and KBZ 2-5 strains to biocement the sand cover, preventing dust generation and reducing contaminant mobility. The biocemented sand exhibits significant compressive strength (3.2 MPa for KBZ 1-3 and 5.5 MPa for KBZ 2-5) and reduced water permeability, limiting water and oxygen infiltration and minimizing heavy metal leaching.

Sharma et al. (2021) investigated the effects of different gram-positive bacteria (*Sporosarcina pasteurii*, *Bacillus subtilis*, and *Bacillus sphaericus*) on calcite formation in poorly graded, liquefiable sand using various microbial and cementation media. The results suggest that *Bacillus subtilis* and *Bacillus sphaericus* can effectively induce calcite precipitation and have the potential for sand stabilization, similar to *Sporosarcina pasteurii*.

2.7.4 Strength Improvement in clayey soils

Xiao et al. (2020) found MICP to be effective in enhancing the strength of soft clay. Directly mixing bacteria, nutrient salts, and clay improved their spatial distribution and simplified sample preparation. MICP-treated specimens showed a significant increase in strength, up to 2.42 times, compared to control specimens. The process involved urea hydration consuming water and calcite formation within the clay's pores. MICP also increased calcite abundance, and the optimal nutrient concentration was determined to be 0.5 mol/L.

Kulanthaivel et al. (2020) explored the effectiveness of MICP in enhancing the UCS of clayey soils. Two types of bacteria (*L. fusiformis* and *S. pasteurii*), different soil types (Low and intermediate compressible clay), externally supplied calcium solutions, molarities of cementing solution (0.25, 0.50, 0.75, and 1.00 M), and curing periods (1, 3, 5, and 7 days) were considered in the experimental design. The results showed significant improvement in UCS for both soils, with variations depending on bacterial types, soil types, calcium solutions, molarities, and curing period. *S. pasteurii* exhibited higher strength enhancement due to its high urease activity. Low-compressible soil showed more remarkable improvement than intermediate-compressible soil. The optimal calcium solution and molarity were identified as the eggshell solution and 0.50 M, respectively.

Arpajirakul et al. (2021) determined the optimal urea-Ca^{2+} input rate for promoting calcite precipitation by bacteria. The stiffness and shear strength of the soil samples increased with the amount of precipitated calcite. However, the degree of improvement varied depending on the natural characteristics of the clay. Clayey soils with high plasticity showed less observable MICP activity and limited enhancement in soil properties due to inefficient nutrient permeation. The research emphasizes the importance of controlling chemical conditions and considering soil characteristics when applying MICP for soft soil improvement.

Teng et al. (2021) developed an injection method to apply MICP to silty clays with low permeability and small pore size. The injection of bacterial and cementation solutions resulted in a 200% increase in soil strength. The strength profile showed peak strength

at the top portion of the samples, indicating bacterial migration and MICP occurrence. Approximately 70-90% of the soil volume was improved through MICP. Analysis of drainage solutions confirmed ongoing urease activity. These findings demonstrate the feasibility of using MICP to enhance the strength of silty clays with similar properties.

Tiwari et al. (2021) used native bacteria to improve the mechanical properties of expansive soil. They employed biostimulation through MICP to control swelling behavior and enhance shear strength. The study developed a procedure for culturing indigenous bacteria and effectively applied MICP to clayey soil, considering its low permeability. The results showed increased calcite content by up to 205 %, improving compressive and tensile strength and reducing swelling pressure and swell strain.

2.8 Need for optimal nutrition in biomineralization

Many organisms form precipitates when provided with suitable environmental conditions due to their metabolic activities. Organisms related to *Bacillus sp* were historically used by several researchers in their studies (Chaurasia et al. 2019; Joshi et al. 2019; Khaleghi and Rowshanzamir 2019; Mujah et al. 2019; Schwantes-Cezario et al. 2019; Tayebani and Mostofinejad 2019; Wilkinson and Rajasekar 2019; Zhang et al. 2019b). *Sporosarcina Pasteurii* is another widely used microorganism for biomineralization studies (Cheshomi et al. 2018; Grabiec et al. 2017; Jiang et al. 2019; Kalantary and Kahani 2018; Liang et al. 2019; Montoya et al. 2019; Tayebani and Mostofinejad 2019; Yu et al. 2019). Instead of foreign organisms, some authors incorporated indigenous organisms for biomineralization (Amini Kiasari et al. 2019; Kim and Lee 2019; Maity et al. 2019; Mwandira et al. 2019a; Zhang et al. 2019b). Using non-axenic cultures without isolation is effective and economical due to their robust nature and self-protection capabilities (De Belie and Wang 2015; Charpe et al. 2017; Chetty et al. 2021; Ersan 2019; Ersan et al. 2015; da Silva et al. 2015).

Omoregie et al. (2019) conducted a study emphasizing the significance of reducing costs in cultivating bacteria for biomineralization. A low-cost food-grade yeast medium was investigated as an alternative to expensive laboratory-grade media. In this study, cultivating *Sporosarcina pasteurii* in a low-cost food-grade yeast medium at a

concentration of 15 g/L and an initial pH of 8.5 resulted in the highest biomass concentration and urease activity when supplemented with 4% urea.

According to Fang et al. (2019), the expense associated with microbial growth accounts for approximately 60% of the total operational cost. However, this cost can be effectively managed by utilizing more economical alternatives to standard nutrient media. To address this concern, Charpe and Latkar (2020) proposed the utilization of lentil seeds, meat extract, and sugar to fulfill the bacteria's protein, vitamin, and carbon requirements, thereby facilitating cost control. Supporting this notion, Maleki-Kakelar et al. (2022) assert that the cultivation of bacteria represents the most expensive and crucial phase in biomineralization. When food is present, bacteria grow faster and duplicate all their proteins quickly (Koch 1988; Maitra and Dill 2015). In balanced growth conditions, bacteria are as simple as any free-living organism. The efficiency with which they use the ribosomal machinery increases as the environment provides more favorable conditions for balanced growth (Koch, 1988). Substrate concentrations and enzymes control fluxes of intracellular reactions (Dourado et al. 2021). Hence, providing the right combination of food for the bacteria is crucial.

Researchers investigated different media for consideration as a nutritional source for the microorganisms involved in biomineralization. Achal et al. (2009) used lactose mother liquor, an industrial effluent from the dairy industry, as a growth medium for microbiologically induced calcite precipitation using Sporosarcina pasteurii. Lactose mother liquor proved effective, with calcite constituting 24.0 % of the sand sample weight and urease production of 353 U/ml. The presence of *S. pasteurii* in lactose mother liquor increased the compressive strength of cement mortar, indicating its potential as a nutritional source for the bacteria.

Yoosathaporn et al. (2016) explored effluent from a chicken manure bio-gas plant as a cost-effective alternative growth medium for carbonate precipitation by *Bacillus pasteurii*. The urease activity of *B. pasteurii* cultured in the chicken manure effluent medium was compared to three standard media, and the highest urease production was observed in the chicken manure effluent medium. The cost per liter of this medium was significantly lower than that of the traditional media. The most effective cultivation medium was used for carbonate precipitation in cement cubes.

Joshi et al. (2018) focused on replacing expensive laboratory nutrient broth with corn steep liquor, an industrial by-product, as a nutritional source in MICP for concrete improvement. The influence of corn steep liquor and nutrient broth on concrete's chemical and structural properties was investigated. The findings showed that corn steep liquor did not affect cement-setting properties, while nutrient broth did. Corn steep liquor-treated specimens exhibited lower carbon and nitrogen content than nutrient broth-treated specimens. Additionally, corn steep liquor replacement led to decreased permeability and increased compressive strength in bacteria-treated specimens.

Fang et al. (2019) explored the use of tofu wastewater as a nutritional source for biocementation, a sustainable and eco-friendly process in construction. *Bacillus cereus* was grown in tofu wastewater and compared with growth characteristics in commercial nutrient broth. Results showed no significant difference in bacterial growth, with tofu wastewater identified as a preferred medium supporting growth and urease activity crucial for biocementation. Moreover, tofu wastewater demonstrated the ability to enhance the compressive strength of sandstone and mortars, highlighting its potential as a viable and cost-effective source for biocementation.

Kahani et al. (2020) optimized the culture media for producing *Sporosarcina pasteurii*. Inexpensive nutrients and water resources are utilized, and sanitized media are explored as an alternative to sterilized ones. A central composite design (CCD) is employed to investigate the effects of yeast extract, whey, heating temperature, and Caspian Sea water on the process. The study finds that the maximum specific urease activity can be achieved under specific conditions of 12.31 g/L yeast extract, 23.43 g/L whey, and 0% seawater sanitized by heating at 100.0 °C. The study also highlights whey as a nutrient source, addressing environmental and economic concerns.

Nikseresht et al. (2020) studied the use of sugar cane molasse and vinasse as nutritional sources for MICP to mitigate wind erosion in arid regions. Results showed that both substances significantly increased soil stability and reduced soil loss.

Behzadipour and Sadrekarimi (2021) investigated using different carbon and nutrient sources, including yeast extract, molasses, and biochar, to stimulate native ureolytic

microorganisms in microbially induced calcite precipitation. Biochar, derived from a mixture of wheat straw and sugarcane bagasse, is enriched with sugarcane molasses to provide a stable energy source for the native microorganisms.

Amini et al. (2022) utilized a low-cost microbial solution derived from ureolytic bacteria cultured in a cost-effective corn-steep liquor medium as a nutritional source in MICP. The microbial solution was used instead of water in cement-sand mortar production. The results demonstrated a significant improvement in the 28-day compressive strength of the mortar samples, with a 65% increase compared to the control samples. Additionally, water absorption was reduced through this method when curing the samples with a 1/3 M equimolar urea and calcium chloride solution. Using the low-cost corn steep liquor medium highlights the potential of the microbial technique in enhancing the compressive strength and durability of mortar and concrete at a reduced cost.

Comadran-Casas et al. (2022) explored the potential of cow urine as a nutritional source for MICP. Both fresh and sterilized cow urine showed suitable urea concentrations and stability for MICP. The soil response to cow urine treatments at different pH levels was comparable to the chemical-based solution. Higher solution pH resulted in faster activation of ureolytic microorganisms and increased carbonate content.

2.9 Research gap

Numerous studies and research show that BMA and FCA have been extensively investigated and used as cement and concrete additives. However, their potential application in soil stabilization remains largely unexplored. One significant knowledge gap in this area pertains to the effect of biomineralization on the immobilization of heavy metals present in these waste materials. As BMA and FCA are known to disperse heavy metals into the environment, understanding the capability of biomineralization to restrict heavy metal mobility within these wastes remains undiscovered.

This research aims to address the existing research gap by examining the impact of biomineralization on the immobilization of heavy metals within BMA and FCA. By exploring the potential synergistic effects of biomineralization and ash-based stabilization, this study seeks to enhance the material properties of BCS.

CHAPTER 3

EXPERIMENTAL INVESTIGATION

This chapter provides a comprehensive overview of the materials used in the study, including the sources of biological specimens, chemicals, laboratory equipment, and software tools. Additionally, it outlines the methodology adopted to address the research questions, describing the experimental design and analytical techniques employed.

3.1 Materials

3.1.1 BCS

This study utilized BCS sourced from the Chikmagalur district in Karnataka, India. Table 3.1 provides the chemical oxide composition of the soil. Based on the classification standard IS 1498: 2016, the soil falls under high plastic clay (CH). This type of soil is prone to considerable expansion and contraction in response to changes in moisture content. Proper stabilization measures are necessary to make it suitable for construction purposes. The particle size distribution is depicted in Figure 3.1, and additional soil properties can be found in Table 3.2. Figure 3.2 (a) is the photograph of BCS and Figure 3.2 (b) is the SEM image of BCS.

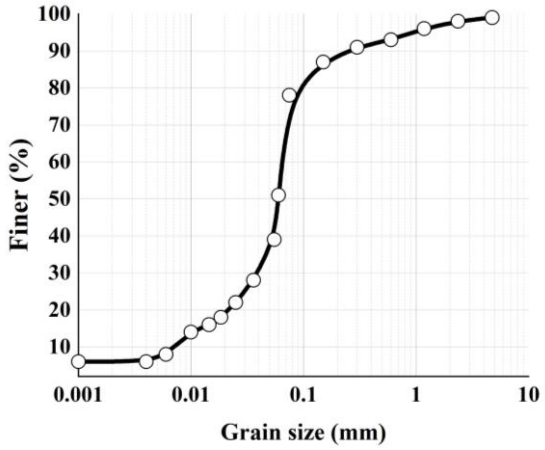

Figure 3.1 Grain size distribution of BCS

Table 3.1 Chemical oxide composition of BCS

Element	SiO_2	Al_2O_3	Fe_2O_3	CaO	MgO	Na_2O	K_2O	P_2O_5	Cl	SO_3	Cr_2O_3	ZnO
(%)	63.1	18.9	7.67	3.93	3.12	0.51	0.79	0.11	0.03	0.17	0.1	0.07

Table 3.2 Index properties of BCS

Soil property	Value
Specific gravity	2.58
Liquid limit	54 %
Plastic limit	26 %
Shrinkage limit	22 %
Free swell index	114 %
Maximum dry density (Standard Proctor)	1.596 g/cm^3
Optimum moisture content	21.7 %
Unconfined compressive strength	35 kPa

Figure 3.2 (a) Photographic image of BCS

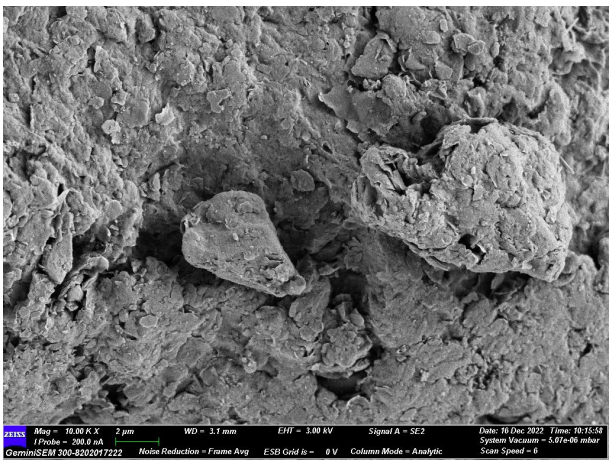

Figure 3.2 (b) SEM image of BCS

3.1.2 BMA

BMA was collected from Biomedical Waste Management Services, located near Mangalore. It exhibited a strong odor and contained sharp objects, specifically the needles from syringes. The ash underwent sieving using a 2.36 mm IS sieve to eliminate these sharps. The sieved ash was then stored in airtight containers. The predominant components found in the ash were calcium, sodium, and silica oxides (Table 3.3). Notably, the BMA displayed a considerable amount of chloride content. Figure 3.3 (a) and Figure 3.3 (b) presents the physical appearance and analytical characteristics of BMA.

Figure 3.3 (a) Photographic image of BMA

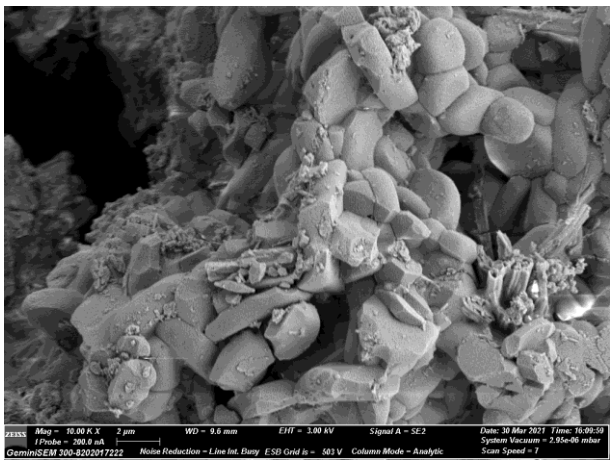

Figure 3.3 (b) SEM image of BMA

Table 3.3 Chemical oxide composition of BMA

Element	SiO_2	Al_2O_3	Fe_2O_3	CaO	MgO	Na_2O	K_2O	P_2O_5	Cl	SO_3	Cr_2O_3	ZnO
(%)	10.6	2.08	0.58	37.2	1.9	23.9	0.71	0.77	12.6	6.5	0.07	0.82

3.1.3 FCA

The FCA used in the study was sourced from M/s Balasore alloys Ltd., located in Balasore, Odissa, India. It is a grey-colored fine powder with a smooth texture (Figure 3.4 (a)). The smooth texture is evident in the microstructure of the FCA, mainly containing spherical particles of diverse sizes (Figure 3.4 (b)). Its chemical oxide composition has silica, aluminum, magnesium, potassium, chromium, and iron (Table 3.4).

Figure 3.4 (a) Photographic image of FCA

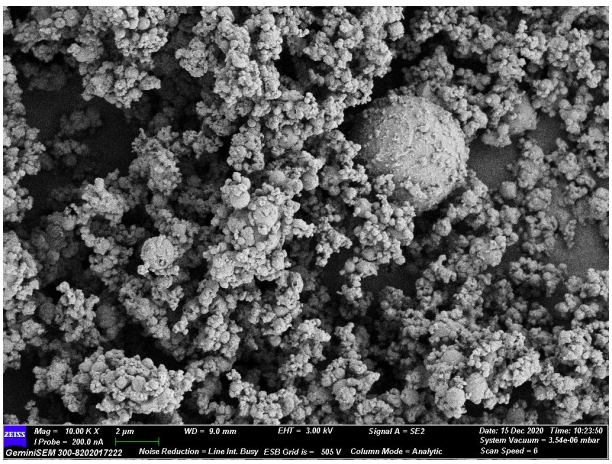

Figure 3.4 (b) SEM image of FCA

Table 3.4 Chemical oxide composition of FCA

Element	SiO_2	Al_2O_3	Fe_2O_3	CaO	MgO	Na_2O	K_2O	P_2O_5	Cl	SO_3	Cr_2O_3	ZnO
(%)	16.4	7.69	3.83	2.14	22.5	2.19	14.2	0.06	7.75	3.12	6.65	1.75

Urea and calcium chloride used in this study were laboratory-grade manufactured by LOBA Chemie. The legumes (Chickpea, Peanut, Black gram, Garbanzo bean, and Soybean) were purchased from the local market.

3.2 Methodology and Scheme of Experiments

3.2.1 General

The overall methodology of this study is pictorially presented in Figure 3.5. This investigation began with examining the availability of indigenous urease-positive bacteria in the waste ashes so that the bacteria required for the biomineralization do not require to acclimatize in a new environment. Indigenous bacteria offer several advantages over pure foreign cultures. One advantage is their adaptation to the specific conditions of their natural habitat. Since they have evolved and established themselves in their native environments, they are well-suited to thrive and perform efficiently under local conditions. Their adaptability enables them to withstand environmental challenges like temperature variations and pH fluctuations.

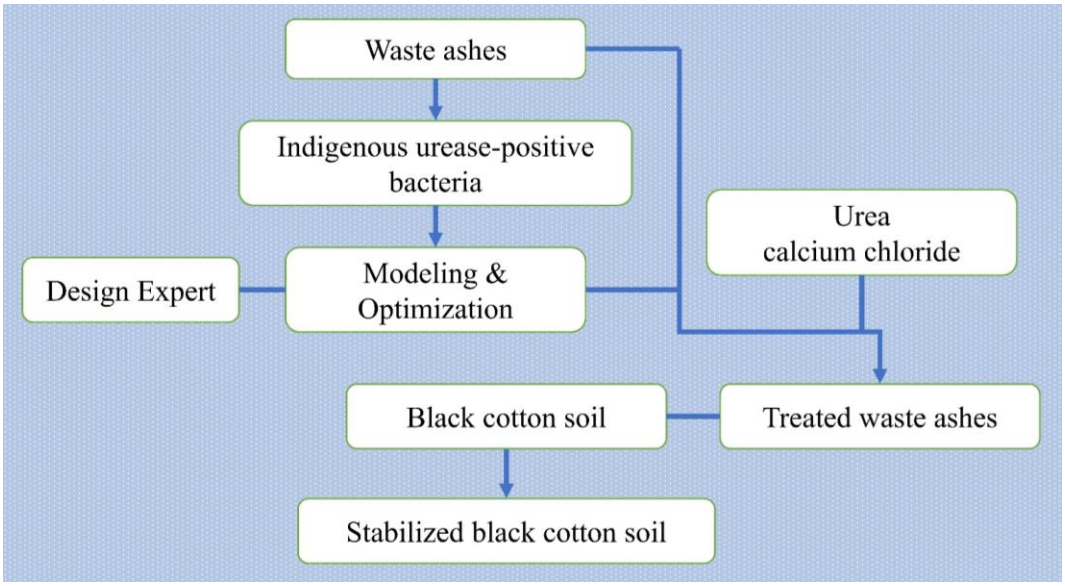

Figure 3.5 Overall methodology

Indigenous bacteria also offer practical advantages in terms of cost-effectiveness and sustainability. Additionally, their natural presence implies that they are already adapted to local conditions, minimizing the need for extensive environmental modifications or additions.

3.2.2 Isolation and Identification of indigenous bacteria

Ash samples were collected into a clean, sterile container. A series of dilutions were prepared by mixing 500 mg of the sample with a sterile diluent. 100 µL from each dilution was spread evenly onto the surface of solid nutrient agar plates. The agar plates were incubated upside down at 37 ^{o}C temperature. After incubation, the plates were observed with the grown bacterial colonies. Distinct and well-separated colonies were selected for further analysis. Each selected bacterial colony was transferred to a fresh Christensen's agar plate using a sterile inoculation loop or needle. The urease-positive bacteria changed the color of the medium to pink indicating the ability to secrete urease enzyme. The selected petri plate was submitted for 16SrRNA analysis to identify the bacteria.

3.2.3 Selection of protein source

In order to assess and compare the performance of the bacteria in different nutrient media and determine the most suitable option for further investigation, inocula obtained from BMA and FCA were introduced into various media containing different legumes (Chickpea, Peanut, Black gram, Garbanzo bean, and Soybean) as the protein source.

The performance evaluation involved measurements of optical density, pH, and urease activity, following standardized procedures. These parameters were utilized to evaluate the effectiveness of the bacteria in different nutrient media and select the most promising medium for subsequent studies.

(i) pH:

The electrode and the pH meter were ensured to be clean and in proper working condition. The pH meter was calibrated using standard pH calibration buffers of pH 4, pH 7, and pH 10 to establish accurate measurements. The pH electrode was then rinsed with distilled water to remove any residue before immersion in the sample. The pH reading on the meter was allowed to stabilize, and the pH value was recorded once it became steady. The electrode was rinsed again with distilled water between measurements of different samples to prevent cross-contamination.

(ii) Optical density:

The methodology employed in this study involved the determination of OD_{600} (Optical Density at 600 nm) as a measure of bacterial cell density. The aliquots of the cultures were transferred to cuvettes and inserted into a UV-visible spectrophotometer. Prior to measuring the absorbance, a calibration step was performed using a blank sample. The absorbance of the samples was then read at 600 nm as the mean of three readings to ensure accuracy.

(iii) Urease activity:

The rate of urea hydrolysis was determined by measuring the change in electrical conductivity. 1 ml of bacterial suspension was added to 9 ml of 1.11 M urea solution, and the electrical conductivity was measured at room temperature over a 5-minute duration, expressed as mS/min. A bacterial activity of 1 mS/min (electrical conductivity rate) was found to correspond to the hydrolysis of 11 mM urea within 1 minute.

3.2.4 Integration of BMA in BCS stabilization

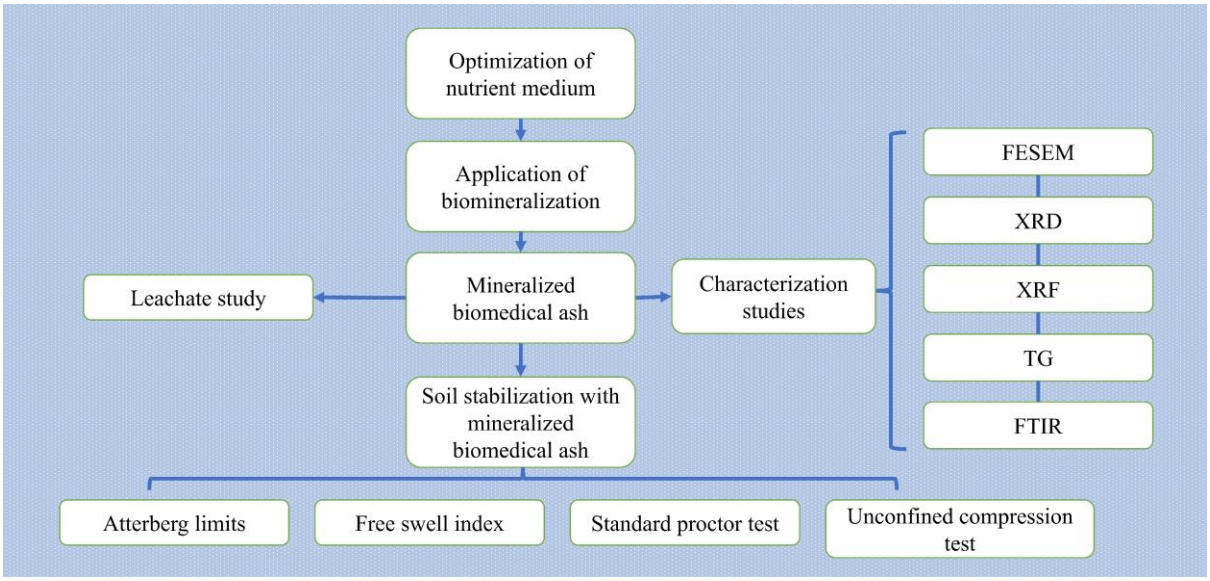

Figure 3.6 Flow chart of using BMA with biomineralization for stabilizing BCS

Figure 3.6 is a pictorial representation of the methodology for testing the applicability of BMA.

3.2.4.1 Optimization of feed composition

The optimization process for the feed composition of bacteria considered both the performance of the bacteria and the cost economics associated with the production of essential nutrients for the bacteria. Hence, experiments were planned using a CCD to evaluate the combined effects of black gram (protein source), yeast extract (vitamin source), and dextrose (carbon source) on the urease activity of the medium. The CCD resulted in 20 experiments (Table 3.5).

After collecting the data, it was fit into the linear, 2-factorial, and quadratic models as the fit into cubic and higher order models were found aliased. The influence of the factors on urease activity was determined using the ANOVA analysis, and the statistical significance of each relation was determined.

Table 3.5 CCD for optimization of urease activity

Experiment	Factor 1 A: Protein (g/L)	Factor 2 B: Vitamin (g/L)	Factor 3 C: Carbon (g/L)
1	12.5	1.875	0.313
2	20	3	0.125
3	20	0.75	0.5
4	5	3	0.125
5	12.5	1.875	0.313
6	5	3	0.5
7	12.5	3.767	0.313
8	20	0.75	0.125
9	20	3	0.5
10	0	1.875	0.313
11	12.5	1.875	0.313
12	25.114	1.875	0.313
13	5	0.75	0.125
14	12.5	1.875	0.313
15	12.5	1.875	0.313
16	5	0.75	0.5
17	12.5	1.875	0.313
18	12.5	1.875	0
19	12.5	0	0.313
20	12.5	1.875	0.628

3.2.4.2 Mineralized biomedical ash

The optimal combination with the highest urease activity was selected to produce bacteria for the study utilizing BMA. The BMA was incorporated into a nutrient medium containing 1M urea and calcium chloride, and the mixture was left undisturbed for 24 hours. The liquid portion was drained, and the remaining solid fraction underwent air-drying until all moisture was eliminated. This dried solid fraction was subsequently called mineralized biomedical ash (mBMA).

3.2.4.3 Analytical techniques

The composition analysis of the mBMA was carried out using X-ray fluorescence (XRF) analysis, providing insights into the elemental makeup of the material. X-ray diffraction (XRD) was also conducted to identify the specific minerals formed within mBMA, enhancing our understanding of its crystalline structure. SEM images were captured to visualize the microstructural changes, comparing the BMA before and after the mineralization treatment. Further confirmation of the presence of carbonates in the mBMA was achieved through Fourier Transform Infrared Spectroscopy (FTIR) and Thermogravimetric (TG) studies. These systematic investigations utilizing various analytical techniques contributed to a comprehensive characterization of the mBMA, shedding light on its composition, crystalline structure, microstructural changes, and specific functional groups or compounds.

(i) X-ray fluorescence

The elemental composition analysis of the mBMA was carried out using X-ray fluorescence analysis with the Bruker S8 Tiger instrument. Analysis was performed on pressed pellets to determine trace elements, while fusion glass disks were utilized for analyzing major elements.

(ii) X-ray diffraction

Prior to analysis on the EMPYREAN PAN analytical instrument, the samples underwent thorough drying to ensure optimal conditions for the X-ray diffraction analysis. The analysis was conducted under specific test conditions, including a tube current of 30 mA and a voltage of 45 kV, with a CuKα wavelength of 1.540598 Å. The scan angle (2θ) ranged from 15° to 60°, with a step size of 0.026°. The obtained diffraction patterns were evaluated using the X'pert Highscore plus software.

(iii) Scanning electron microscopy

A field emission gun scanning electron microscope (ZEISS GeminiSEM300) was utilized to examine the surface morphology of both mBMA and BMA. The ash samples underwent vacuum drying in a desiccator to eliminate any moisture content. Prior to analysis, a thin layer of gold was sputtered onto the samples to enhance conductivity. The scanning electron microscope analysis was conducted at a working distance of 9.6

mm, with an electron high tension of 3 kV. Selective regions of interest were further analyzed using energy-dispersive X-ray spectroscopy (EDS) to gather elemental composition information.

(iv) Fourier Transform Infrared Spectroscopy

To prepare the mBMA sample for infrared spectrum (IR) analysis, pelletization was performed using potassium bromide as a carrier. The pelletized samples were then analyzed in the infrared spectrum, covering a range of 400 cm^{-1} to 4000 cm^{-1}, utilizing the FTIR instrument (JASCO FT/IR-4200). This systematic approach ensured the characterization of the sample's IR absorption patterns across a broad frequency range, enabling the identification of specific functional groups and chemical bonds present in the mBMA.

(v) Thermogravimetric analysis

To investigate the thermal behavior of the mBMA sample, thermogravimetric analysis was conducted. The analysis was performed using a TG analyzer (Seiko Exstar TG-DTA 6300) under a nitrogen atmosphere. The samples were heated at a constant rate of 5 °C per minute until the cell temperature reached 825 °C. Throughout the heating process, the sample weight was recorded at five-second intervals. Plots were then generated to visualize the changes in weight and the differential weight as a function of the cell temperature.

3.2.4.4 Leachate extraction and analysis

The leachates derived from the BMA and mBMA were obtained following the shake extraction method as per ASTM D 3987 guidelines. Containers containing 50 grams of ash were filled with distilled water as the extraction fluid, ensuring a liquid-to-solid ratio of 20. The containers were then subjected to agitation on a rotary shaker, operating at a speed of 30 rotations per minute for a duration of 18 hours. The resulting filtrates, passing through a 0.45-micron glass fiber filter, were carefully collected, and stored in airtight PVC containers at a temperature of 4 °C. Subsequently, the concentrations of various elements including mercury, chromium, zinc, lead, iron, copper, cadmium, barium, arsenic, titanium, and selenium present in both the BMA and mBMA were

determined using inductively coupled plasma optical emission spectroscopy (7500cx, Agilent Technologies).

3.2.4.5 Soil Testing

mBMA was mixed with the BCS in 10 %, 20 %, 30 %, and 40 % replacements by weight. For each soil composite, the following geotechnical properties were determined: Atterberg limits, free swell index (FSI), maximum dry density (MDD), optimum moisture content (OMC), and UCS.

(i) Atterberg Limits

The determination of the plastic limit and liquid limit of the soil followed the guidelines specified in IS 2720 (Part 5): 1985, as prescribed by the Bureau of Indian Standards in 1985. To conduct the liquid limit test, 120 grams of soil was collected in an evaporating dish. Water was gradually added and thoroughly mixed until a consistent paste was obtained. The sample was then loaded onto the cup of the Casagrande apparatus. A clean and sharp groove of the appropriate dimensions was formed using a grooving tool. The cup was fitted and dropped by turning the crank at a rate of two revolutions per second until the two halves of the soil cake met the bottom of the groove, spanning approximately 12 mm. The number of drops required to close the groove over 12 mm length was recorded. The soil was collected and remixed by adding a small amount of additional water, and the procedure was repeated until the required number of blows was less than 15. The number of blows was recorded in each case, and the moisture content was determined. A flow curve was then plotted on a semi-logarithmic graph, with water content represented on the arithmetical scale and the number of drops on the logarithmic scale. The moisture content corresponding to 25 drops, as read from the curve and rounded off to the nearest whole number, was reported as the liquid limit of the soil.

For the plastic limit, the soil sample was mixed thoroughly with distilled water on a flat glass plate until the soil mass became sufficiently plastic to be easily molded with fingers. An 8-gram portion of this plastic soil mass was rolled between the fingers and the glass plate, applying just enough pressure to form a thread of consistent diameter throughout its length, measuring 3 mm. The soil was then kneaded to create a uniform

mass and rolled again. This alternating rolling and kneading process continued until the thread crumbled under the required rolling pressure, and no further threading was possible. The crumbled soil thread pieces were carefully collected in an airtight container, and the moisture content was determined. The plasticity index was calculated as the difference between the liquid and plastic limits. It plays a significant role in determining the behavior of the soil in the presence of water.

(ii) Free swell Index

FSI was determined following the guidelines outlined in IS 2720 (Part 40): 1977, as specified by the Bureau of Indian Standards in 1977. Two graduated cylinders, each with a capacity of 100 ml, were filled with 10 grams of soil in each cylinder. One cylinder was filled with water, while the other was filled with kerosene up to the 100 ml mark. To eliminate any trapped air, the soil in both cylinders was stirred using a glass rod and then allowed to settle undisturbed for at least 24 hours. The final volumes of the soil in both cylinders were recorded. The FSI was calculated as per Equation 3.1.

$$FSI, \% = \frac{V_w - V_k}{V_k} \times 100 \qquad \text{(Equation 3.1)}$$

V_w is the volume of the soil read from the cylinder containing water, and V_k is the soil volume in the cylinder containing kerosene.

(iii) Standard Proctor test

The Standard Proctor compaction test was conducted following the procedure outlined in IS: 2720 (Part 7) - 1980, as specified by the Bureau of Indian Standards in 1980. The test aimed to determine the MDD and OMC of the soil. Before the experiment, the weight of the empty compaction mold was recorded. The soil was compacted in three layers, with each layer subjected to 25 blows using a rammer weighing 2.5 kg. The weight of the mold, including the compacted soil, was measured to calculate the soil density.

The moisture content of the soil was determined as the mean average of samples taken from the compacted soil's top, center, and bottom faces. After extracting the soil from the mold, a small amount of water was added, and the compaction process was repeated. This process was repeated for different moisture contents, and the corresponding

densities were recorded. A plot was created depicting the relationship between density and moisture content. By connecting all the points with a smooth curve, the peak point on the curve represented OMC and MDD. At this point, the horizontal axis represented the MDD of the soil, and the vertical axis represented the OMC.

(iv) Unconfined compression test

To prepare the UCS specimens, a steel mold with a diameter of 38 mm and a height of 76 mm was used. The specimens were carefully extracted from the mold, and precise measurements were recorded. They were positioned on the bottom plate of the loading device, and the upper plate was adjusted to make contact with the specimen. A proving ring with a capacity of 1kN was attached to the loading device, and the dial gauge was set to zero. Force was applied to the specimen, causing axial compression at 1.25 mm per minute. Readings from the proving ring were recorded after every 25-dial gauge reading.

The compression of the specimens continued until a failure surface was observed. The failure angle of each specimen was determined by examining the characteristics of the failed specimen. The UCS was defined as the maximum stress developed in the sample during the test. The procedure followed for the UCS test adhered to the guidelines provided in IS 2720 (Part 10): 1991, as specified by the Bureau of Indian Standards in 1991.

3.2.5 Integration of FCA in BCS stabilization

Figure 3.7 is a pictorial representation of the methodology for testing the applicability of FCA. Soybean was selected as the protein source for the bacteria based on the findings from section 4.1.2.

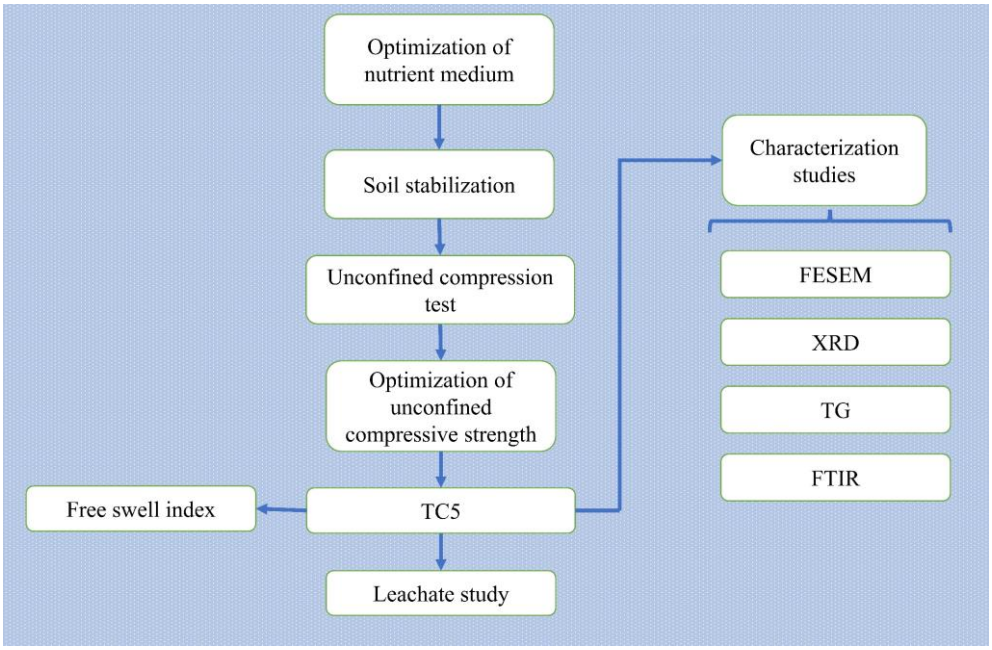

Figure 3.7 Flow chart of using FCA with biomineralization for stabilizing BCS

3.2.5.1 Medium Optimization for indigenous bacteria in FCA

A CCD was employed to optimize urease activity and optical density simultaneously. The CCD incorporated the adjustment of soybean, yeast extract, and dextrose concentrations in the nutrient medium (Table 3.6). By systematically varying these variables, the study aimed to determine the optimal combination to maximize urease activity while achieving the desired optical density.

Following the conduction of tests, the experimental data were subjected to fitting into different models, including the linear, 2-factorial, and quadratic models. The cubic and higher-order models were not considered due to aliasing. The next step involved determining the factors' influence on urease activity and optical density. This analysis used ANOVA (variance analysis) to assess each relation's statistical significance.

Table 3.6 CCD for optimization of urease activity and optical density

Experiment	Factor 1 A: Protein (g/L)	Factor 2 B: Vitamin (g/L)	Factor 3 C: Carbon (g/L)
1	12.5	1.875	0.3125
2	20	3	0.5
3	5	3	0.5
4	12.5	3.767	0.3125
5	0	1.875	0.3125
6	12.5	1.875	0.3125
7	5	0.75	0.125
8	12.5	1.875	0.628
9	5	0.75	0.5
10	12.5	1.875	0.3125
11	20	0.75	0.5
12	20	0.75	0.125
13	12.5	0	0.3125
14	5	3	0.125
15	12.5	1.875	0
16	25.113	1.875	0.3125
17	12.5	1.875	0.3125
18	12.5	1.875	0.3125
19	12.5	1.875	0.3125
20	20	3	0.125

3.2.5.2 Soil preparation and scheme of experiments

Experiments were designed using a CCD with FCA %, bacterial optical density, urea, and calcium chloride as the independent factors in determining their influence on strengthening the BCS (Table 3.7). UCS was considered the representative response to understand the effects of FCA and biomineralization on soil characteristics.

Table 3.7 CCD for UCS of soil composite

Experiment	Factor 1 A: FCA (%)	Factor 2 B: Bacteria OD_{600}	Factor 3 C: Calcium chloride (g)	Factor 4 D: urea (g)
1	20	1.156	0.5	0.5
2	40	0.649	0.5	0.5
3	50	0.902	0.75	1
4	20	0.649	1	1.5
5	40	1.156	0.5	0.5
6	40	1.156	1	0.5
7	30	0.902	0.75	1
8	30	0.902	0.75	1
9	30	0.902	0.25	1
10	20	0.649	0.5	0.5
11	40	1.156	1	1.5
12	40	0.649	1	1.5
13	30	1.409	0.75	1
14	40	1.156	0.5	1.5
15	30	0.902	0.75	1
16	30	0.902	0.75	2
17	40	0.649	1	0.5
18	30	0.902	0.75	1
19	10	0.902	0.75	1
20	20	0.649	1	0.5
21	30	0.902	0.75	0
22	30	0.902	0.75	1
23	20	1.156	1	1.5
24	20	1.156	1	0.5
25	30	0.395	0.75	1
26	40	0.649	0.5	1.5
27	20	1.156	0.5	1.5
28	30	0.902	0.75	1
29	20	0.649	0.5	1.5
30	30	0.902	1.25	1

After conducting the tests, the experimental data underwent fitting into various models, such as the linear, 2-factorial, and quadratic models. However, the aliasing issue excluded the cubic and higher-order models from consideration. The subsequent step involved investigating factors' influence on UCS. Analysis of variance (ANOVA) was employed to evaluate the statistical significance of each relation. The composite material that exhibited the highest UCS was denoted TC5.

3.2.5.3 Leachate extraction and heavy metal analysis

Batch tests were conducted to assess the leaching behavior of heavy metals from FCA and TC5. 50 grams of the samples were digested in volumetric flasks containing 1 N sulfuric acid, with a liquid-to-solid ratio of 20. The flasks were then agitated on a rotary shaker for 18 hours at a speed of 30 rotations per minute. This procedure was repeated using double-distilled water, following the guidelines outlined in ASTM-D-3987. After the agitation, all samples were centrifuged at 4000 rpm for 10 minutes to separate the liquid phase. Subsequently, 49 mL aliquots of the separated liquid were taken and stored in a refrigerator at 4 °C, adding 1 mL of concentrated nitric acid to preserve the samples. The aliquots were filtered through 0.45-micron filters. The filtered samples were then analyzed using an inductively coupled plasma-mass spectrometer (ICP-MS) instrument (NexION 2000, Perkin Elmer). This analytical technique enabled the measurement and quantification of various elements, including chromium, iron, zinc, lead, nickel, cadmium, copper, titanium, mercury, and arsenic.

3.2.5.4 Characterization studies

Several systematic investigations were conducted using various analytical techniques to comprehensively understand the TC5 soil composite. XRD analysis was performed to identify the specific minerals formed within the composite, providing insights into its crystalline structure. SEM was utilized to capture images and visualize the microstructural changes. The impact of stabilization on the composite's microstructure could be observed by comparing the stabilized soil sample with the untreated BCS and FCA. Fourier Transform Infrared Spectroscopy and Thermogravimetric studies were conducted to detect the presence of carbonates in TC5 soil composite.

(i) X-ray diffraction

The samples were analyzed using a diffractometer instrument (EMPYREAN PAN analytical) to obtain diffraction patterns. The analysis covered a range of diffraction angles from 20° to 60° with a resolution of 0.026°. The XRD measurements were conducted using a CuKα radiation source with a wavelength of 1.540598 Å.

(ii) Field emission gun scanning electron microscopy

The microstructural changes were systematically visualized by capturing FEGSEM images. A thin layer of gold was uniformly sputtered onto the samples to enhance the conductivity and quality of the images. The images were captured using the Field emission gun scanning electron microscope (ZEISS GeminiSEM300) with an accelerating voltage of 3 kV. Surface morphology was captured by utilizing the secondary electron signals emitted from the surfaces of the BCS, FCA, and TC5 samples. The images were taken at a specific working distance of 3.2 mm for the BCS and TC5 samples and 9 mm for the FCA sample. A consistent magnification of 10000x was employed for all the captured images.

(iii) Fourier Transform Infrared Spectroscopy

The FTIR analysis was conducted using a Bruker instrument (Alpha II) within a wavenumber range of 4000 to 500 cm^{-1}, with a resolution of 2 cm^{-1}. The specific compounds present in the stabilized soil due to the biomineralization activity were accurately identified by comparing the patterns of TC5 with those of BCS and FCA.

(iv) Thermogravimetric analysis

Thermogravimetric analysis was conducted to investigate the thermal behavior of the stabilized soil. The samples were heated up to 950 °C using a Q500 Hi-Res Thermogravimetric analyzer with a temperature gradient of 20 °C/min. It also provided insight into the calcium carbonate bioprecipitate in the stabilized soil sample.

CHAPTER 4

RESULTS AND DISCUSSION

This section explains the findings of the current investigation and provides a detailed analysis and interpretation of the collected data. It effectively communicates the main findings of the research by presenting the raw data, statistical analyses, and other relevant information that support the research objectives. This section discusses how the findings relate to the research objectives while critically analyzing the data. This section is broadly categorized into three sections. The first section details the outcomes of the indigenous bacteria present in the waste ash and identifies the best-suited protein source. The second section contains the detailed results and the discussion related to incorporating biomineralization in BMA followed by blending mBMA in BCS. Finally, the third section contains the experimental results and discussion related to integrating FCA and biomineralization in BCS and analyzing their effect on the UCS of the soil composite.

4.1 Bacterial analysis

4.1.1 Isolation and Identification of indigenous bacteria

This section focused on investigating the native bacteria present in two different types of ash: BMA and FCA. The specific objective was to determine if these bacteria can secrete urease enzymes. The bacteria obtained from the respective ash samples were grown on a Christensen's agar medium. The change of the color of the medium to pink confirmed the presence of urease-secreting bacteria. This identification was likely based on morphological characteristics, such as colony appearance and microscopic observations. Their genome sequences were obtained and compared to the 16S ribosomal RNA sequence database. This comparison was done using the Basic Local Alignment Search Tool (BLAST) provided by the National Center for Biotechnology Information (NCBI). The results revealed that the bacterial colonies derived from the BMA were identified as *Bacillus cereus,* while those from the FCA were identified as *Lysinibacillus sphaericus*.

The growth characteristics of the bacterial cultures derived from the two types of ash were observed. The doubling time, which represents the time required for the bacterial

population to double in size, was determined. The culture from the FCA exhibited a doubling time of 44 minutes, while the culture from the BMA had a slightly longer doubling period of 49.5 minutes (Figure 4.1). These growth rates provide insights into bacterial physiology and their adaptation to the respective ash environments.

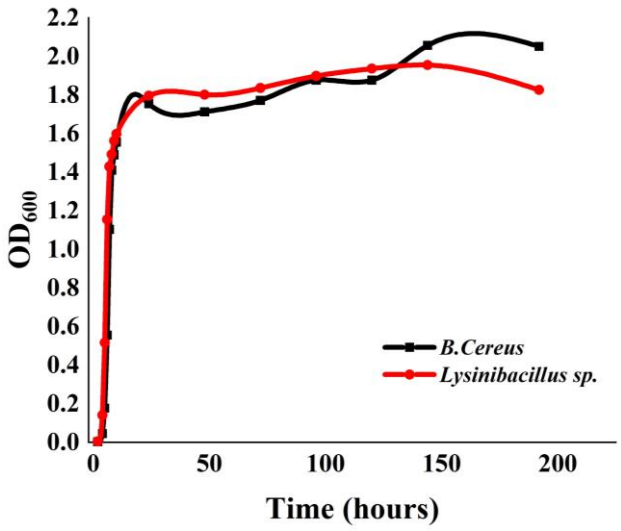

Figure 4.1 Growth profile of the indigenous urease-positive bacteria from BMA and FCA

A phylogenetic tree was constructed to visualize the evolutionary relationships between the bacteria using Molecular Evolutionary Genetics Analysis (MEGA) software, employing the neighbor-joining method with 1000 bootstrap replicates. The MUSCLE program was used for multiple sequence alignment, which helps to align and compare the gene sequences accurately. To share and preserve the obtained gene sequences, they were deposited in the NCBI database, resulting in accession numbers OM345234 (Figure 4.2) for *Bacillus cereus* and OM346720 (Figure 4.3) for *Lysinibacillus sphaericus*.

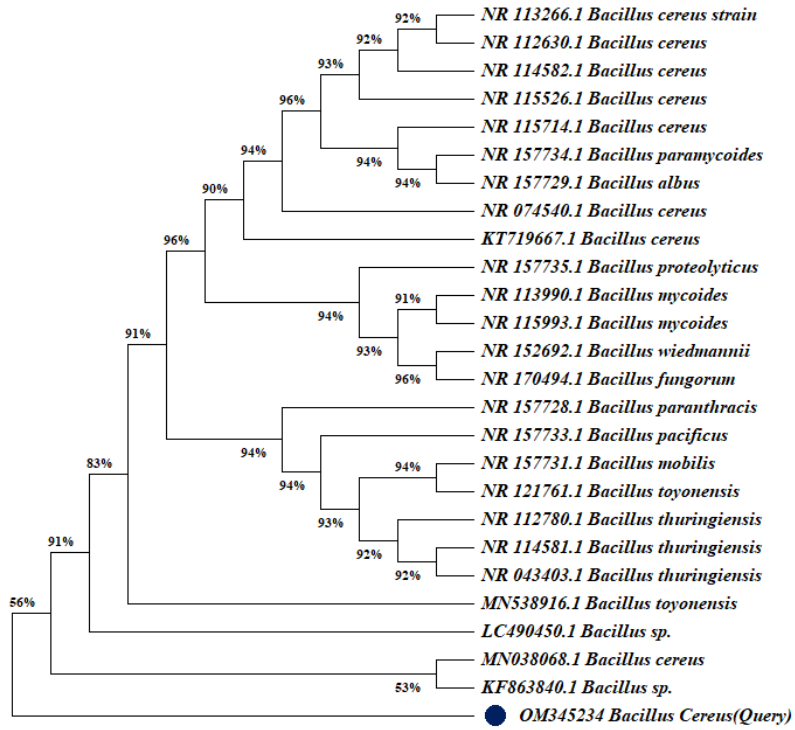

Figure 4.2 Phylogenetic tree of *Bacillus cereus* from BMA

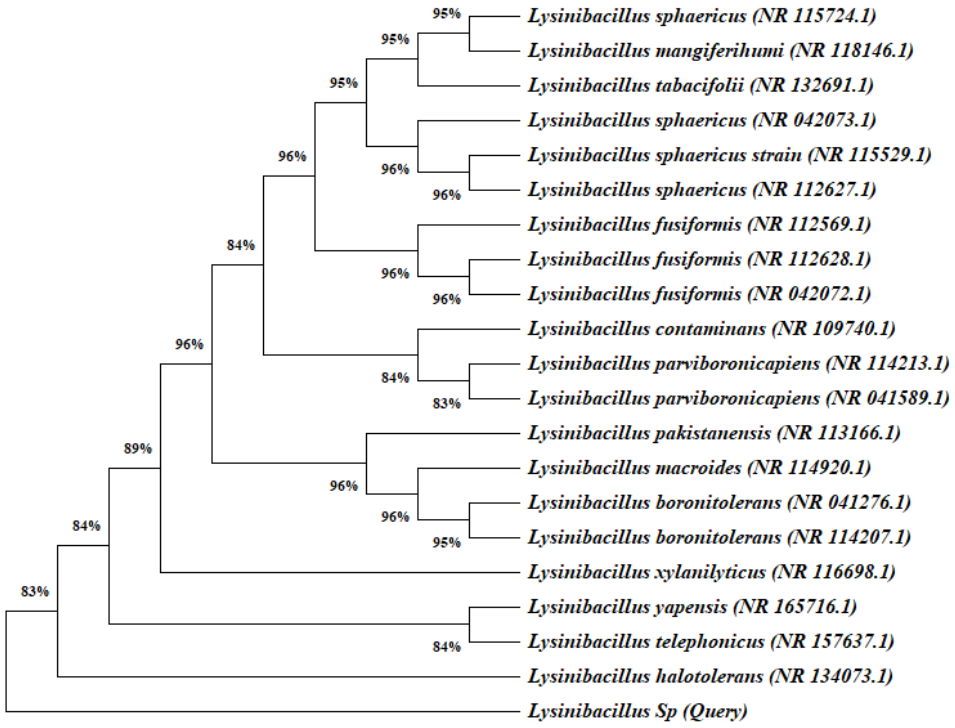

Figure 4.3 Phylogenetic tree of *Lysinibacillus sphaericus* from FCA

4.1.2 Selection of protein source

An experiment was conducted where bacterial growth was monitored in different media aimed to determine the influence of different protein sources on bacterial growth. The results of this experiment are presented in Figure 4.4. Among the various media tested, the medium that utilized black gram as a protein source exhibited the highest bacterial growth within the first 48 hours after inoculation (Figure 4.4 (a)). This indicates that black gram provides a favorable bacterial growth environment and is an efficient protein source for the bacteria under study. The pH profile of the black gram medium was also investigated, and it was observed to range between 7.4 and 8.2, which falls within the slightly alkaline range (Figure 4.4 (b)).

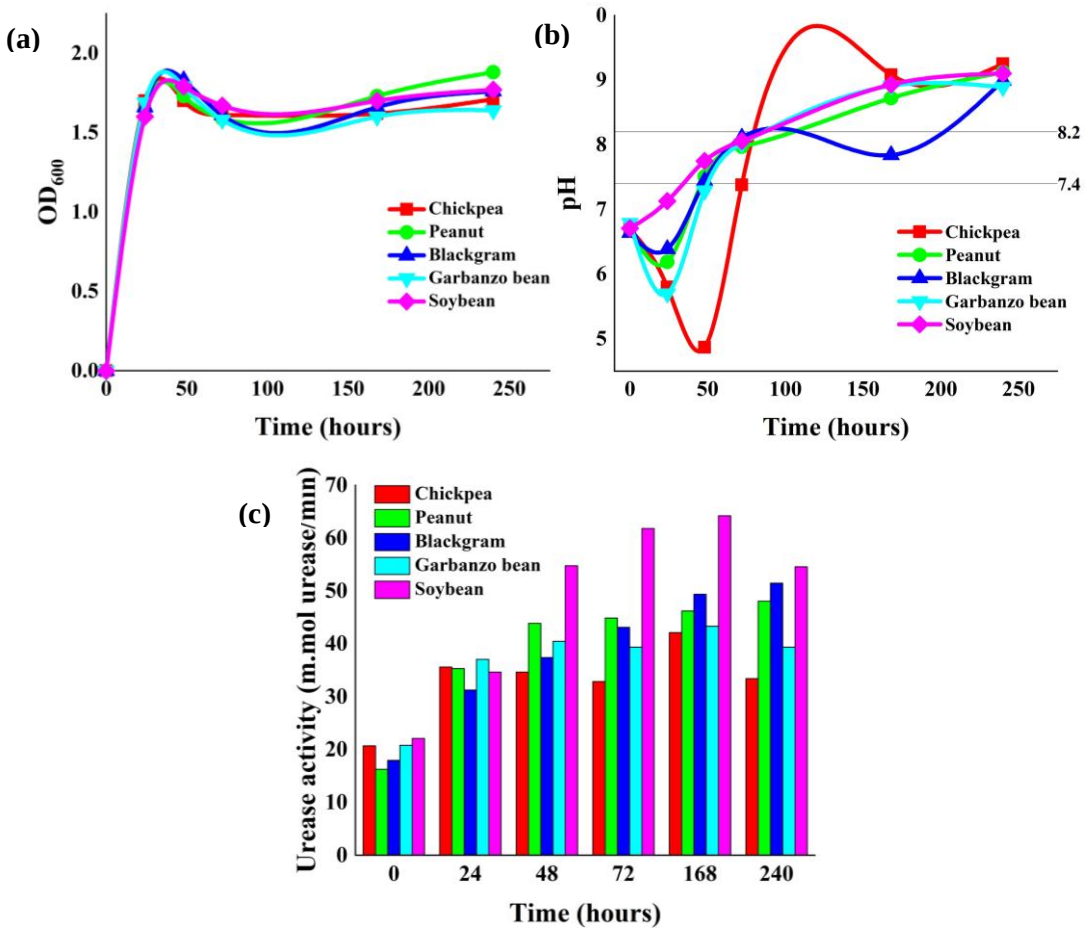

Figure 4.4 Comparison of legumes as the protein source

Alkaline media are preferred in the biomineralization process because an alkaline environment facilitates the formation of carbonates during the hydrolysis of urea, which is an essential step in the biomineralization process. The pH range of 7.4 to 8.2 in the

selected media was conducive to good urease activity. Cuzman et al. (2015) reported a positive correlation between urease activity and the pH range of 7.4 to 8.2. From Figure 4.4 (c), on comparing the urease activity of the different media, it was observed that the soybean medium consistently exhibited the highest activity (22 m.mol urease/min at the beginning of the experiment, 35 m.mol urease/min @ 24 hours from inoculation, 55 m.mol urease/min @ 48 hours from inoculation, 62 m.mol urease/min @ 72 hours from inoculation, 64 m.mol urease/min @ 168 hours from inoculation, and 55 m.mol urease/min @ 240 hours from inoculation). However, the black gram medium consistently increased its urease activity over time. This observation aligns with the findings of Cordero et al. (2019) that the urease activity increases with storage time. These observations suggest that both soybean and black gram media have provided more sustained conditions for favorable urease production.

4.2 Integration of BMA in BCS stabilization

4.2.1 Optimization of feed composition

An optimization process was carried out for the feed composition of bacteria. The aim was to enhance the urease activity of the medium while considering both the performance of the bacteria and the cost economics associated with the production of essential nutrients. The experiments were planned using a CCD, resulting in 20 experiments in total (Table 4.1). The effects of three factors, namely black gram (protein source), yeast extract (vitamin source), and dextrose (carbon source), on the urease activity were evaluated using the CCD. The experiments were conducted following the sequence order the Design Expert software provided.

Table 4.1 Factor codes and levels in CCD for urease activity

Factor	Name	Units	Minimum (-α)	Low (-1)	Mean (0)	High (+1)	Maximum (+α)
A	Protein	g/L	0.00	5.00	12.51	20.00	25.11
B	Vitamin	g/L	0.00	0.75	1.88	3.00	3.77
C	Carbon	g/L	0.00	0.13	0.3126	0.50	0.6278

The statistical fit of the data to the different standard models (linear, 2-factorial, quadratic) was evaluated using the coefficient of determination (R^2), adjusted-R^2, predicted-R^2, and the signal-to-noise ratio. R^2 represents the proportion of the variance in the dependent variable (urease activity) that can be explained by the independent variables (protein, vitamin, and carbon doses) in the regression model. A high R^2 value indicates a better fit of the model to the data. Predicted-R^2 adjusts for overfitting and provides a more realistic estimate of the model's performance on new data. Adjusted-R^2 further adjusts for the number of predictors in the model and penalizes the addition of unnecessary predictors. It provides a more accurate measure of the model's performance.

The signal-to-noise ratio (S/N ratio) is another important measure to assess the model's performance. A higher S/N ratio indicates a stronger signal (desired information) than noise (unwanted variations or errors). A high S/N ratio implies that the model can effectively capture the underlying patterns and relationships in the data. In general, an S/N ratio of more than 4 is considered desirable. Also, models with R^2 greater than 0.95 are generally considered to fit the experimental data properly. The difference between adjusted-R^2 and predicted-R^2 is expected to be less than 0.2.

The residuals for each model were analyzed, and the root mean squared error (RMSE) was calculated. RMSE estimates the standard deviation of the prediction errors and represents the average magnitude of the differences between predicted and actual values. A lower RMSE indicates better model performance and closer predictions of the actual values.

Based on the fit statistics and RMSE analysis, the quadratic model was selected as the preferred model to represent the urease activity as a function of the protein, vitamin, and carbon doses. The quadratic model exhibited a high R^2 value of 0.9513, indicating an excellent fit for the experimental responses. The adjusted-R^2 value of 0.9075 demonstrated the adequacy of the model, and the difference from the predicted-R^2 value (0.7581) was less than 0.2, suggesting the robustness of the model (Table 4.2). The model's adequacy precision, which measures the signal-to-noise ratio, was calculated to be 18.844, indicating a strong signal relative to noise. Additionally, the RMSE for the quadratic model was found to be the lowest among the compared models, further

supporting its superior predictive accuracy. Hence, the quadratic model was deemed appropriate for representing the relationship between the urease activity and the protein, vitamin, and carbon doses. A pictorial representation of the predicted data by the three models can be seen in Figure 4.5.

Table 4.2 Comparison of standard models for urease activity

Model	R^2	Adjusted-R^2	Predicted-R^2	S/N	Root mean squared error
Linear	0.803	0.766	0.659	13.992	3.961
2-Factorial	0.912	0.872	0.799	19.171	2.637
Quadratic	0.951	0.907	0.758	18.844	1.970

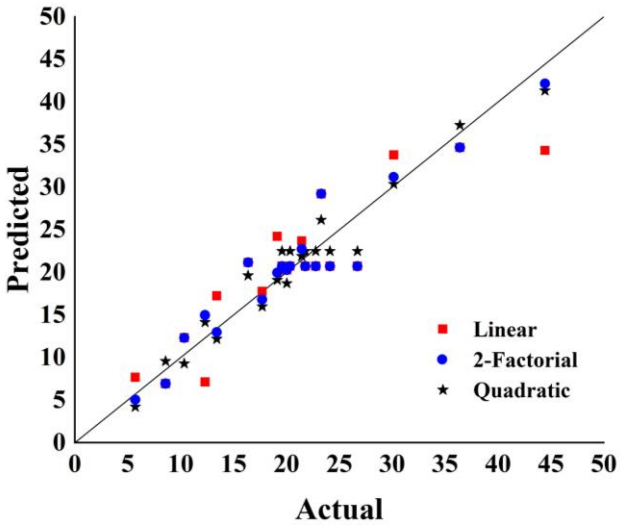

Figure 4.5 Actual vs Predicted values of urease activity according to the different models

The coded polynomial equation, Equation 4.1, represents the relationship between the urease activity of the medium and the coded values of the protein (A), vitamin (B), and carbon (C) quantities.

$$Urease\ activity = 22.49 + 5.06A + 8.27B - 0.25C + 2.61AB - 3.44AC - 1.79BC - 1.72A^2 + 0.31B^2 - 1.19C^2 \quad \text{(Equation 4.1)}$$

To determine the significance of each term in the equation, a multivariate analysis of variance (ANOVA) was conducted (Table 4.3). The assumptions of the model's adequacy were tested to ensure its validity. It was confirmed that the data followed a normal distribution, the variance was consistent, and the data were independent of time

relativity (Shokoohi et al. 2020). The residuals representing the differences between the predicted and actual values were analyzed for any patterns. It was found that there was no discernible pattern in the residuals, further supporting the consistency of the variables. The F statistic, which measures the ratio of explained variance to unexplained variance, was calculated to assess the significance of the quadratic model. In this case, the F statistic was determined to be 21.77, and the associated p-value was less than 0.001. This indicates that the quadratic model is statistically significant and that the obtained F value is unlikely to be due to noise.

The lack of fit is an important factor to consider in the design of the experiment. In this case, the lack of fit was evaluated and found to have a value of 1.28. A lack of fit value of this magnitude implies that the lack of fit is insignificant relative to the pure error. The associated probability, 39.74%, indicates that there is a chance of 39.74% that a lack of fit F-value this large could occur due to noise.

Table 4.3 ANOVA analysis for quadratic model on urease activity

Source	Sum of squares	Degree of freedom	Mean square	F-value	p-value
Model	1515.76	9	168.42	21.71	< 0.0001
A	348.64	1	348.64	44.93	< 0.0001
B	930.74	1	930.74	119.95	< 0.0001
C	0.8828	1	0.8828	0.1138	0.7429
AB	54.60	1	54.60	7.04	0.0242
AC	94.53	1	94.53	12.18	0.0058
BC	25.56	1	25.56	3.29	0.0996
A^2	41.87	1	41.87	5.40	0.0426
B^2	1.35	1	1.35	0.1741	0.6853
C^2	20.08	1	20.08	2.59	0.1387
Residual	77.59	10	7.76		
Lack of Fit	43.52	5	8.70	1.28	0.3974
Pure Error	34.07	5	6.81		
Cor Total	1593.35	19			

Overall, based on the results of the multivariate ANOVA, it can be concluded that the quadratic model is statistically significant for representing the relationship between the urease activity and the protein, vitamin, and carbon quantities in the medium. The lack of fit is considered insignificant, further supporting the adequacy of the model. Based

on the significance analysis using p-values, the terms A, B, AB, AC, and A^2 are significant in the urease activity model.

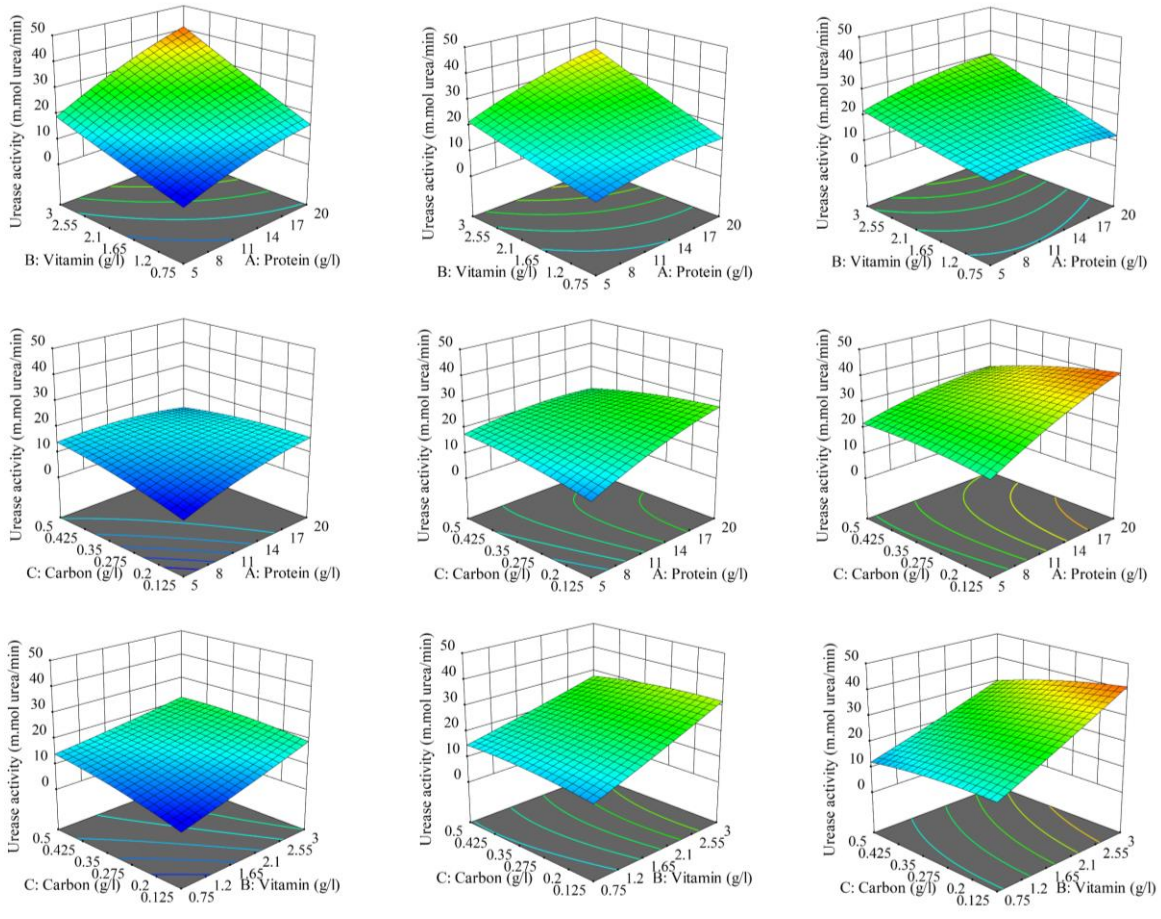

Figure 4.6 Response surfaces of urease activity

Based on Table 4.3, it is evident that the quantities of protein and vitamins play a vital role in determining the urease activity in the medium. In contrast, the carbon dose has a relatively lesser impact. To further understand the interactions among the variables and their effects on urease activity, three-dimensional figures were developed (Figure 4.6). In these figures, each factor was held constant at the low, center, and high levels, while the other two factors were varied. Visualizing these plots shows how the urease activity changes when two of the three components in the nutrient medium are altered.

Furthermore, it was noted that the actual and predicted values of urease activity from the quadratic model showed good agreement. From the model analysis, it was observed that the protein content had the highest impact on urease activity. This observation

suggests that protein concentration in the medium significantly influences the enzyme's activity. An optimal combination of 23.47 g/L of black gram, 3.45 g/L of yeast extract, and 0.03 g/L of dextrose was derived from the optimization of the model for achieving a maximum urease activity of 54 m.mol urease/min.

4.2.2 Leachate extraction and heavy metal analysis

The results of the ICP-OES analysis showed that the leachates from the mBMA contained significantly lower concentrations of heavy metals than those from untreated BMA (Figure 4.7). The reduction in metal concentrations in the leachates was attributed to coprecipitation with calcium carbonate, which involves the incorporation of heavy metal ions into the crystal structure of calcium carbonate, effectively immobilizing the metals and preventing them from leaching into the environment.

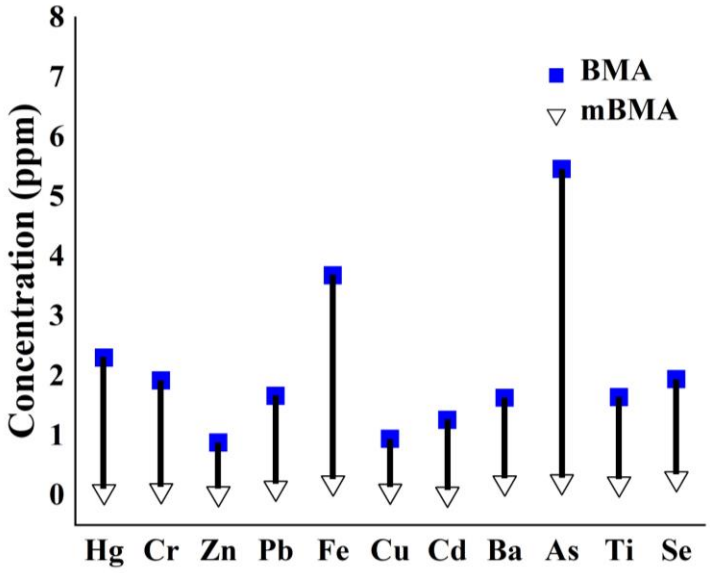

Figure 4.7 Heavy metals in leachates of BMA and mBMA

The immobilization efficiency of each metal was calculated based on the percentage reduction in concentration. The results indicated high immobilization efficiencies, with the reduction in concentration ranging from 86% to 98%. The leachates from the mBMA exhibited a reduction of 97% in Hg, 96% in Cr, 97% in Zn, 93% in Pb, 94% in Fe, 93% in Cu, 98% in Cd, 87% in Ba, 96% in As, 88% in Ti, and 86% in Se concentrations. The obtained results are consistent with the findings of Cuaxinque-Flores et al. (2020). Zhang et al. (2019) also reported the effectiveness of

coprecipitation with calcium carbonate in reducing heavy metal leaching from various waste materials.

4.2.3 Characterization of mBMA

(i) X-ray fluorescence

The composition of the mBMA, as determined by XRF analysis, shows a significant presence of calcium oxide (CaO), silica oxide (SiO_2), and aluminum oxide (Al_2O_3). Approximately 38% of the ash comprises calcium oxide, 11% silica oxide, and about 3% aluminum oxide (Table 4.4). The high content of calcium oxide suggests that the mBMA has the potential to function as an excellent cementitious material. Calcium oxide, also known as lime or quicklime, is a key component in cement production and is responsible for its binding properties. Therefore, mBMA could exhibit cement-like properties when mixed with appropriate additives.

Additionally, about 11% of the ash's chloride content represents chloride ions released during calcium release from calcium chloride. It is important to note that the chloride ions may also be naturally present in the biomedical waste, contributing to the overall chloride content.

Table 4.4 Chemical oxide composition of mBMA

Element	SiO_2	Al_2O_3	Fe_2O_3	CaO	MgO	Na_2O	K_2O	P_2O_5	Cl	SO_3	Cr_2O_3	ZnO
(%)	11	2.23	0.56	37.6	2.29	2.14	0.85	0.82	11.4	6.22	0.04	0.7

(ii) X-ray diffraction

The X'pert Highscore Plus software was used to analyze the diffraction pattern of mBMA, and the results indicated the presence of several components. The analysis determined that calcite accounted for 85% of the composition, making it the most abundant mineral. Anhydrite, another significant component, was identified at a concentration of 12%. Additionally, sodium chloride, as halite, constituted 3% of the composition.

These structures were identified based on reference patterns, unique identifiers used to match experimental diffraction data with known crystal structures. The specific reference patterns used for this analysis were: 96-901-6023; 96-900-9668; 96-901-

5391; 96-900-9669; 96-900-7688; 96-210-0190; 00-005-0586; 96-500-0041; 96-154-7348; 96-154-7351; 96-210-0993; 96-900-0966; 96-900-0096; 96-154-7349; 96-900-7690; 96-702-2028; 96-154-7350; 00-005-0628; 96-900-8679; 96-900-4097. The highest intensity peak observed in the diffraction pattern occurred at 29.38 °, corresponding to the presence of calcite in the mBMA (Figure 4.8). In addition, the peaks at 23.03 °, 25.47 °, 31.34 °, 35.98 °, 39.41 °, 43.15 °, 45.44 °, 48.48 °, and 57.40 ° correspond to calcite. By comparing the findings of the current analysis with those of previous studies, a greater confidence level can be established regarding the presence and proportions of these minerals in the mBMA. The consistency of the XRD analysis results with previous studies conducted by Anastasiadou et al. (2012), Astrup et al. (2016), and Vivek et al. (2019) further strengthen the validity of the findings. This finding supports the hypothesis that calcite is formed in BMA due to biomineralization.

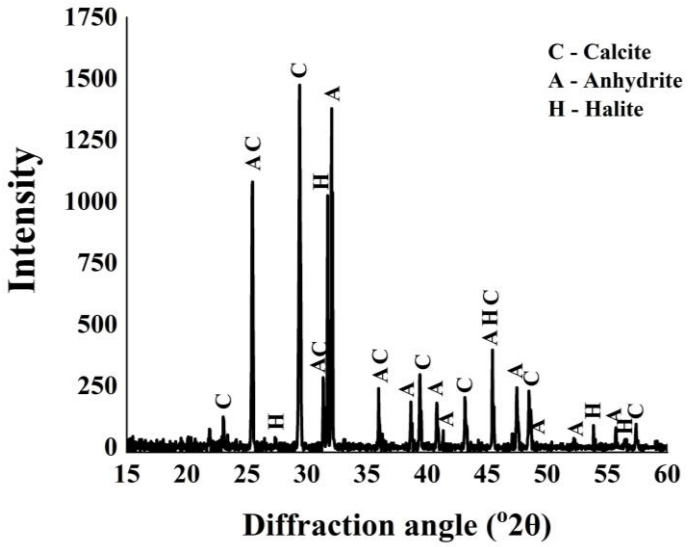

Figure 4.8 XRD profile of mBMA

(iii) Field emission gun scanning electron microscopy

To investigate the microstructural changes caused by biomineralization, SEM images of mBMA were captured at the magnifications of 500 times (Figure 4.9 (a)), 5000 times (Figure 4.9 (b)), and 15000 times (Figure 4.9 (c)). Upon examining the SEM images, it is observed that a dense material was present between the ash particles. Similar formations of calcium carbonate precipitates have been previously reported by Joshi et al. (2019) and Sharma et al. (2021). Furthermore, EDS analysis was performed on the

BMA (Figure 4.9 (d)). The results revealed that calcium (Ca) was the prominent element in the ash. Approximately 41% of the deposit by weight in the mBMA was identified as calcium. This finding suggests a stoichiometric balance of Ca^{2+} in forming calcium carbonate ($CaCO_3$).

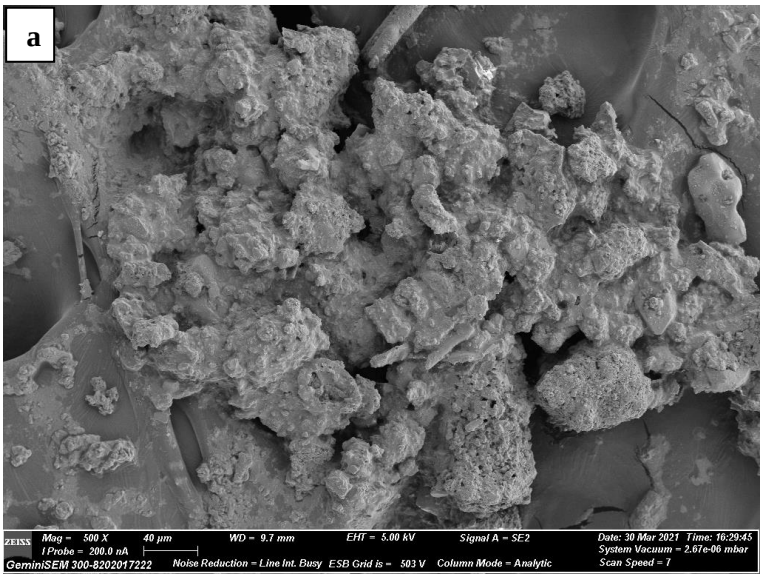

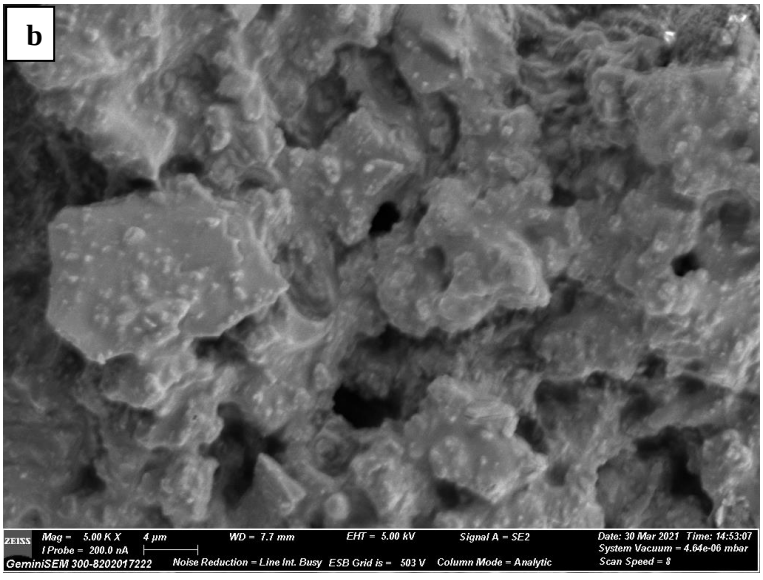

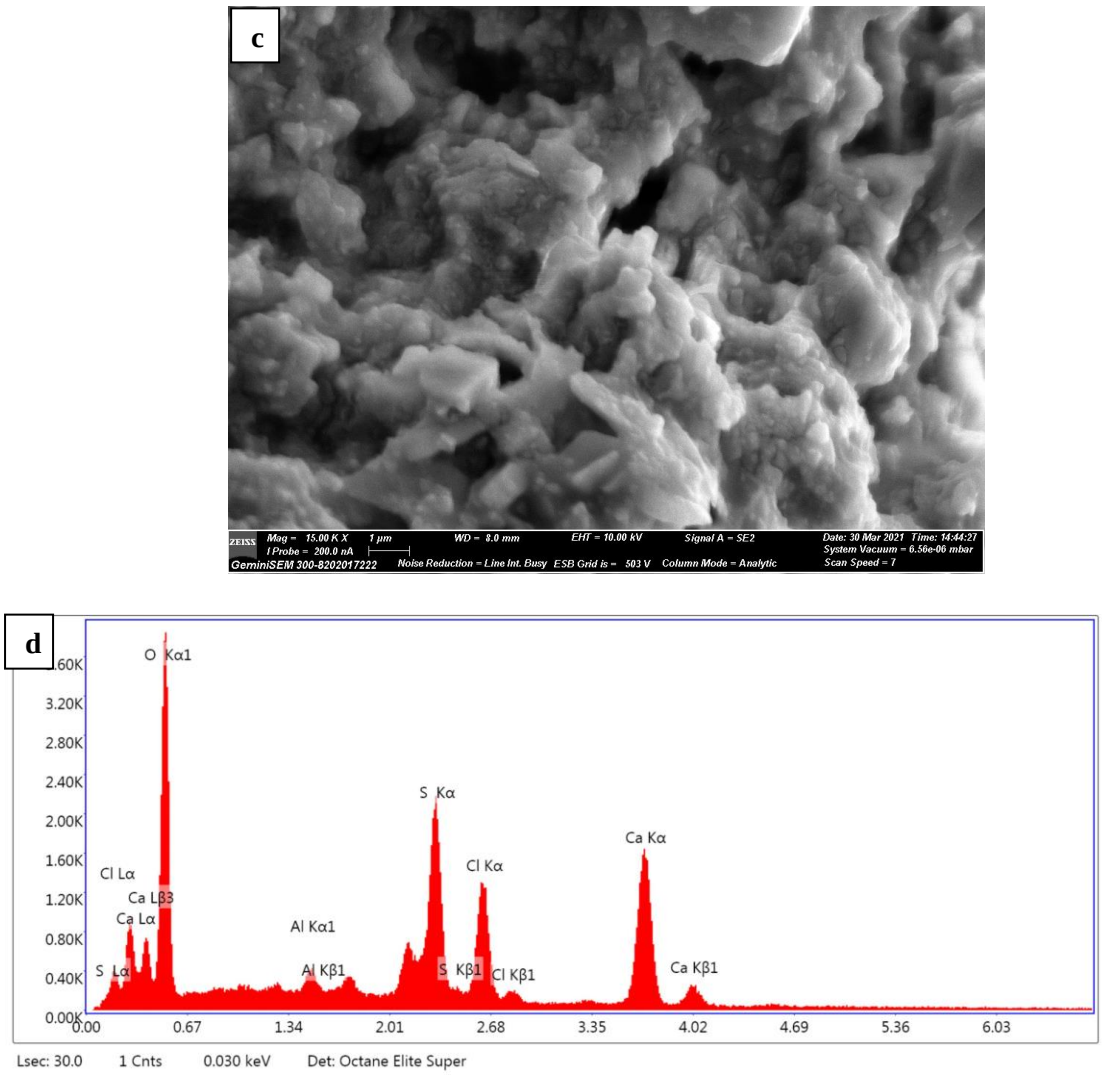

Figure 4.9 SEM-EDS of mBMA

(iv) Fourier Transform Infrared Spectroscopy

The FTIR analysis of the mBMA revealed several absorption bands that indicate the presence of carbonates (Figure 4.10). These bands are observed at specific wavenumbers and correspond to different vibrational modes of the carbonate ions. The absorption band at 711.6 cm^{-1} represents the in-plane deformation caused by OCO bending. This mode is associated with the bending motion of the carbonate ion, where the oxygen atoms move closer together or farther apart while the carbon remains stationary. The absorption band at 873.6 cm^{-1} indicates inadequate plane deformation of carbonates. This mode involves the bending and stretching of the carbonate group in a way that disrupts the ideal planar structure of the carbonate ion. The absorption band at 1420.3 cm^{-1} corresponds to the asymmetric CO stretch. This mode involves the

stretching motion of the carbonate ion, where the carbon and oxygen atoms move in opposite directions.

In addition to these strong absorption bands, weak absorption bands are observed at 1798.3 cm^{-1}, 2512.8 cm^{-1}, and 2875.3 cm^{-1}, suggesting carbonates in the BMA. The band at 1798.3 cm^{-1} is associated with the stretching vibration of the carbonate group, while the bands at 2512.8 cm^{-1} and 2875.3 cm^{-1} are related to the combination of carbonate stretching and organic functional groups. These observations align with the findings of Sharma et al. (2021), Bruckman and Wriessnig (2013). Jozanikohan and Abarghooei (2022) have reported similar vibrational modes and wavenumbers for carbonates. Overall, the FTIR analysis provided strong evidence of carbonates in the mBMA.

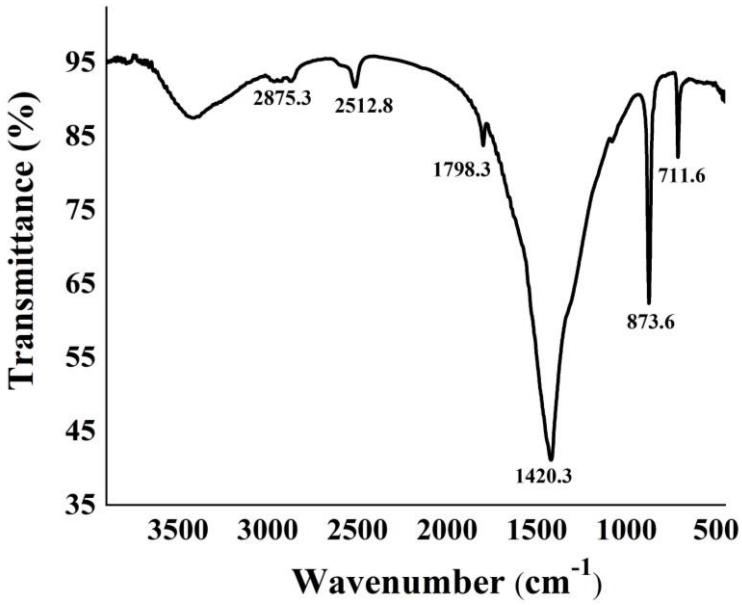

Figure 4.10 FTIR of mBMA

(v) Thermogravimetric analysis

The TGA of the mBMA sample, as depicted in Figure 4.11, provides valuable insights into its thermal behavior. Initially, a weight drop is observed in the sample, which can be attributed to dehydration, lasting until it reaches a temperature of 100°C. At around 270°C, a notable depression is observed in the thermogram, accompanied by a nearly

10% reduction in sample weight. This weight loss exhibits a maximum depletion rate of 54µg/minute and is accompanied by an endothermic peak of -0.5µV. The occurrence of this depression is attributed to the thermal decomposition of anhydrite present in the sample. Further analysis reveals that the weight of the sample continues to decrease due to the thermal degradation of the organic matter found in the ash. This decomposition of surplus nutrients intended for bacteria contributes to the ongoing reduction in sample weight. Jroundi et al. (2014), Šovljanski et al. (2021), and Vavva et al. (2020) reported weight loss in a similar thermal region and justified the degradation of organic matter. Additionally, within the characteristic thermal range for calcium carbonate decomposition, which spans from 570 °C to 660 °C, a steep depression is observed in the thermogram. In this temperature zone, the sample weight experiences a reduction exceeding 10 % with a maximum rate of 40 µg/minute observed at 640 °C. This weight loss can be attributed to the decomposition of calcium carbonate that formed in the ash during the biomineralization process (Li et al. 2019; Pan et al. 2019).

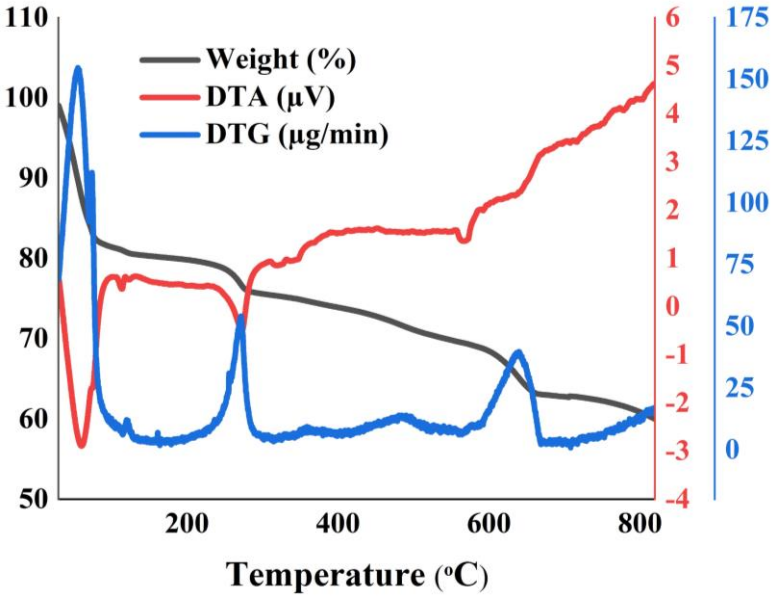

Figure 4.11 TG profile of mBMA

4.2.4 Soil Testing

(i) Atterberg Limits

BCS's liquid limit (LL) and plastic limit (PL) were determined as 53% and 25 %, respectively. When 10% of the BCS was replaced with mBMA, the LL and PL values changed to 49 % and 28 %, respectively. Increasing the percentage of mBMA by another 10 % resulted in LL and PL values of 48 % and 32 %. Further, adding 10 % of mBMA led to LL and PL values of 47 % and 33 %. When the replacement reached 40% of the soil with mBMA, the LL and PL values were observed as 47 % and 34 %, respectively. Figure 4.12 illustrates that with each stage of mBMA replacement, there was a decrease in LL and an increase in PL, ultimately improving the soil's toughness. This improvement can be attributed to the contribution of ash particles in enhancing yield strength and impeding crack development.

Moreover, it indicates that the soil remains semi-solid until higher soil moisture levels are reached. A similar pattern of reducing LL and increasing PL was observed by Amadi (2014) when BCS was stabilized with cement kiln dust. Gautam et al. (2021) observed that the soil's LL reduced, and the PL increased with increasing incinerator ash and lime content. However, Shukla and Parihar (2016) reported that this pattern was valid until 6 % micro-fine slag was added to the soil. Singh and Kalita (2021) observed a decreasing pattern of PL with increasing bagasse ash in the soil. Initially, when ash was mixed in the soil, LL and PL reduced; beyond 15 %, LL and PL increased drastically. It was reported that once the bagasse ash occupied all the pores in the soil, further addition of the bagasse ash led to the formation of cenospheres which made the soil require more water to reach LL and PL. Yohanna et al. (2022) reported that adding sisal fiber beyond 1 % reduced the LL, increasing soil stiffness and improving workability. Also, the PL was initially reduced with low fiber and gradually increased with the fiber content in the soil.

The plasticity index (PI), calculated as the difference between LL and PL, was 27 % for BCS. It reduced to 22 % for m10, 16 % for m20, 13 % for m30, and 13 % for m40, respectively. As indicated by the narrowing of the plasticity index, the soil's compressibility decreases with the increased content of mBMA. Tiwari et al. (2021) reported a similar observation that adding bottom ash to clayey soil reduces the PI.

Initially, the consistency of the BCS was characterized as very soft. However, with the addition of mBMA, the consistency of the soil reached the level of stiff clay, as classified by the specifications outlined in IS:1498-1970.

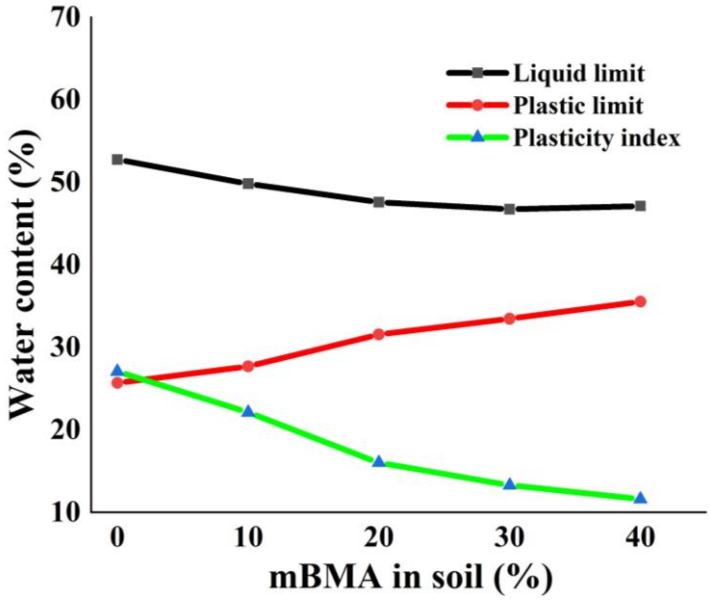

Figure 4.12 Atterberg limits of BCS stabilized with mBMA

(ii) Free swell Index

The untreated BCS has an FSI value of 114 %. Different compositions of BCS, namely m10, m20, m30, and m40, had FSI values of 63 %, 40 %, 36 %, and 17 %, respectively. This gradual decrease in FSI, as shown in Figure 4.13, indicates the inherent non-expansive nature of mBMA when exposed to moisture. Consequently, a higher proportion of mBMA reduces the swelling potential of BCS. This improvement in soil behavior signifies a transition from the critical stage to a more manageable level, categorized as marginal according to the standards set by IS: 1498-1970.

The FSI value of the untreated BCS was determined as 114 %. different compositions of BCS, namely m10, m20, m30, and m40, were, 63%, 40%, 36%, and 17% respectively. This gradual decrease in FSI (Figure 4.13) corresponds to the inherent non-expansive characteristics of mBMA when exposed to moisture. Consequently, an increased proportion of mBMA reduces the swelling potential of BCS. This improvement in soil behavior signifies a transition from the critical stage to a more manageable level, categorized as marginal based on the standards set by IS: 1498-1970.

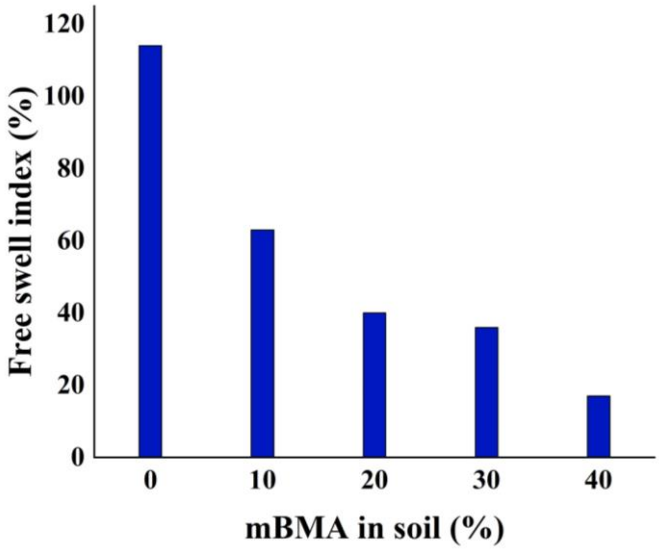

Figure 4.13 FSI of BCS stabilized with mBMA

Saride and Datta (2016) attributed the reduction in the FSI to flocculation and the reduction in the water affinity of the soil. Reddy et al. (2018) observed a similar reducing pattern of FSI with high lime content in the soil. Singh and Kalita (2021) reported an identical relationship between FSI and bagasse ash content in the soil. Gautam et al. (2021) stated that mixing the soil with lime and municipal solid waste incinerated ash reduced the FSI of the soil by 100 %.

(iii) Standard Proctor test

When the BCS undergoes a standard compaction effort at the OMC, it can achieve MDD. Dry density is a relative indicator of strength, permeability, and compressibility. The highest dry density values were obtained at different moisture contents: 21.7 %, 21.9 %, 22.7 %, 24.9 %, and 26.1 % corresponded to 1.596 g/cm³, 1.547 g/cm³, 1.522 g/cm³, 1.490 g/cm³, and 1.458 g/cm³ for BCS, m10, m20, m30, and m40, respectively.

The specific gravity of mBMA (2.48) is slightly lower than that of BCS (2.56), indicating a decrease in maximum dry density with adding mBMA. As the proportion of mBMA in the mixture increased, the overall mixture became lighter (Figure 4.14). The optimal moisture content also shifted towards higher values as the fraction of mBMA increased. Consequently, the soil became more workable over a broader range

of moisture, and variations in moisture content in the field had a relatively lesser impact on soil density.

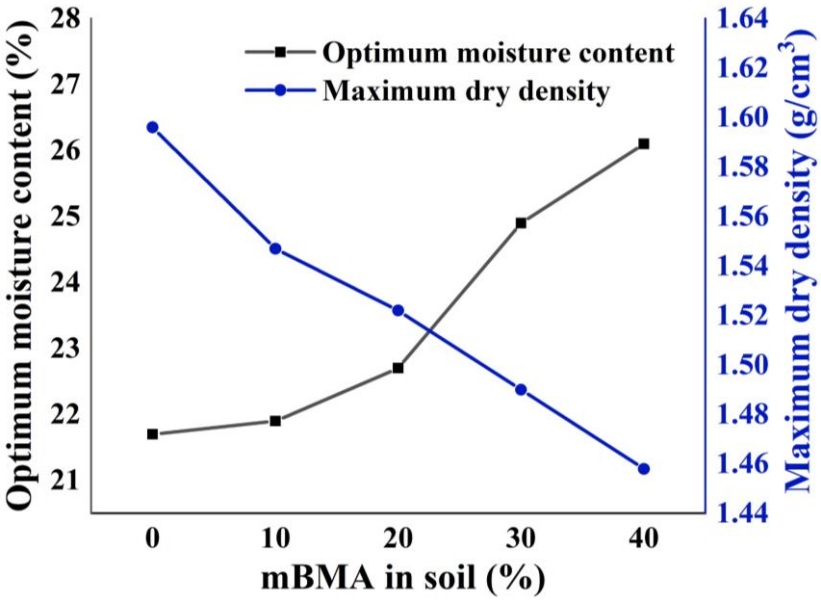

Figure 4.14 OMC and MDD of BCS stabilized with mBMA

This trend of increasing OMC and decreasing MDD aligns with observations made in soil stabilization using fly ash. According to Saride and Datta (2016), the increase in the OMC is caused by the higher fines content and the resulting expansion of the specific surface area. Additionally, the inclusion of fly ash, which possesses a lower specific gravity, results in a decrease in MDD. Ramesh and Manjunatha (2020) reported a similar observation with the inclusion of rice husk ash in the soil. Randhawa et al. (2021) too observed a rising profile for OMC corresponding to the increase in lime content in the soil. However, along with OMC, MDD also had an increasing pattern with higher lime content.

(iv) Unconfined compression test

The samples were prepared at densities obtained from the standard proctor test curves corresponding to each mix's OMC. The mean average values of three specimens were considered as the UCS (Figure 4.15). The untreated soil exhibited a UCS of 34.6 kPa, while the UCS values for m10, m20, m30, and m40 were determined as 64.3 kPa, 98.4

kPa, 146.9 kPa, and 111.6 kPa, respectively. The increase in the UCS is due to the combined effect of BMA and biomineralization.

According to Ramesh and Manjunatha (2020), the addition of lime and rice husk ash led to an increase in the UCS of the soil. This increase was attributed to two factors: soil agglomeration and an increase in the internal friction angle. Soil agglomeration refers to the process of particles binding together, which can enhance the strength of the soil. The increase in the internal friction angle indicates an improvement in the soil's ability to resist shear forces, contributing to increased strength. Kulanthaivel et al. (2020) reported a two-fold increase in soil UCS through biomineralization. Biomineralization involves the process of microbial-induced calcium carbonate precipitation within the soil. The formation of calcium carbonate crystals helps to bind the soil particles together, thereby improving its strength and stiffness. The precipitation of calcium carbonate minerals within the soil matrix increased the interparticle bonding, leading to a substantial increase in UCS. These observations align with the findings reported by Wani and Mir (2020) and Arpajirakul et al. (2021).

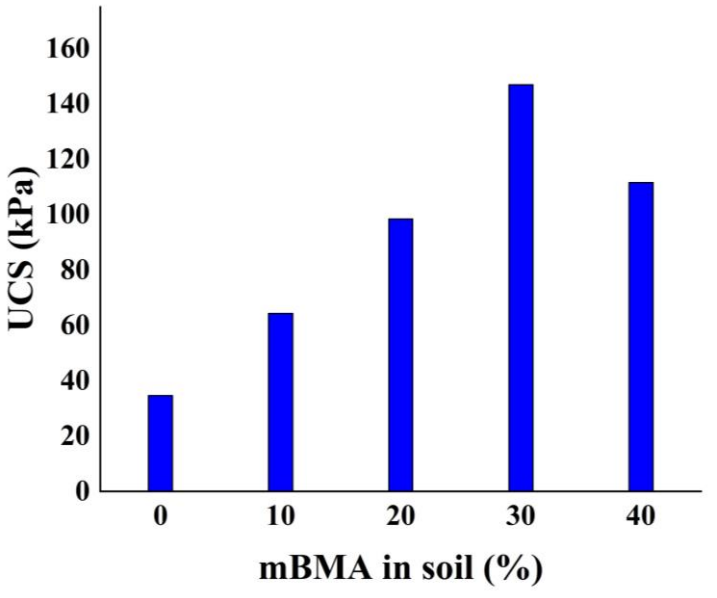

Figure 4.15 UCS of BCS stabilized with mBMA

Failure angles were measured using the tested specimens to gain insight into the friction angle. The failure envelope of the BCS was observed at 49°. Upon adding 10% mBMA

to the BCS, the failure envelope was observed at 51°. Similarly, the failure envelopes for m20, m30, and m40 were observed at 53°, 54°, and 57°, respectively.

4.3 Integration of FCA in BCS stabilization

This section describes the experimental results, characterization tests, and analogies to using FCA for soil stabilization in synergy with biomineralization. The indigenous bacteria were initially modeled for optimal urease activity and optical density. Soil bacteria were used to bioprecipitate calcium carbonate in the stabilized soil composite. The effect of each factor on the strength of the stabilized soil composite was modeled using a CCD. Heavy metal analysis was performed on the highest strength of the leachates extracted from the soil composite

4.3.1 Medium optimization for indigenous bacteria in FCA

After inoculation and 12 hours of continuous stirring at 150 rpm and 37 °C, the bacterial growth was monitored in a series of 20 experiments using the combinations of factors and levels presented in Table 4.5.

Table 4.5 Factor codes and levels in CCD for urease activity and optical density

Factor	Name	Units	Minimum (-α)	Low (-1)	Mean (0)	High (+1)	Maximum (+α)
A	Protein	g/L	0.00	5.00	12.50	20.00	25.11
B	Vitamin	g/L	0.00	0.75	1.88	3.00	3.77
C	Carbon	g/L	0.00	0.13	0.3125	0.50	0.6278

It was found that the growth varied across different experimental runs. Specifically, the 7^{th} test (-1, -1, -1) exhibited the least bacterial growth, while the 20^{th} experiment (+1, +1, -1) displayed the highest bacterial growth. These observations suggest a notable variation in bacterial growth under the given conditions. The urease activity of the bacteria was assessed in the same series of experiments.

$$Optical\ Density = 1.630 + 0.173A + 0.133B + 0.019C - 0.065AB - 0.103AC - 0.118BC - 0.061A^2 - 0.063B^2 - 0.001C^2 \quad \text{(Equation 4.2)}$$

$$Urease\ Activity = 18.180 + 3.760A + 4.220B - 0.574C - 1.040AB - 1.180AC + 0.688BC + 0.961A^2 - 0.284B^2 + 0.164C^2 \quad \text{(Equation 4.3)}$$

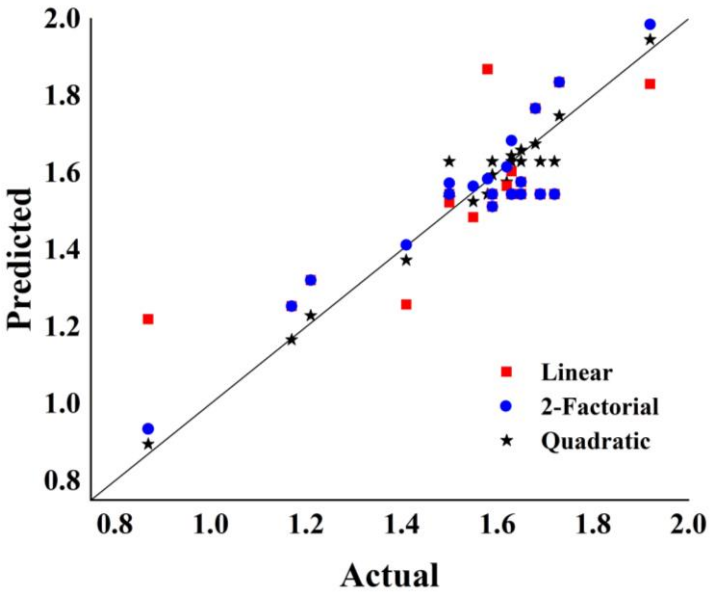

Figure 4.16 Actual vs Predicted values of optical density according to the different models

It was found that the 16th experimental run displayed the maximum urease activity (+α, 0, 0), while the 7th run (-1, -1, -1) exhibited the least urease activity. Preliminary observations indicate that the protein dosage strongly correlates with bacterial growth and urease activity. It is observed that media containing higher quantities of protein sources resulted in better bacterial growth and increased urease activity. According to the fit statistics, the quadratic model is considered most suitable to represent the optical density (Table 4.6) and urease activity (Table 4.7) in terms of the medium's protein, vitamin, and carbon dosages. Figure 16 and Figure 17 presents the comparison of different models to fit the data corresponding to optical density and urease activity, respectively.

Table 4.6 Comparison of standard models for optical density

Model	R^2	Adjusted-R^2	Predicted-R^2	S/N	Root mean squared error
Linear	0.639	0.571	0.382	9.553	0.136
2-Factorial	0.862	0.798	0.699	17.049	0.084
Quadratic	0.962	0.927	0.882	23.734	0.044

Table 4.7 Comparison of standard models for urease activity

Model	R^2	Adjusted-R^2	Predicted-R^2	S/N	Root mean squared error
Linear	0.875	0.851	0.798	19.268	1.776
2-Factorial	0.922	0.886	0.861	16.61	1.403
Quadratic	0.953	0.910	0.857	15.852	1.091

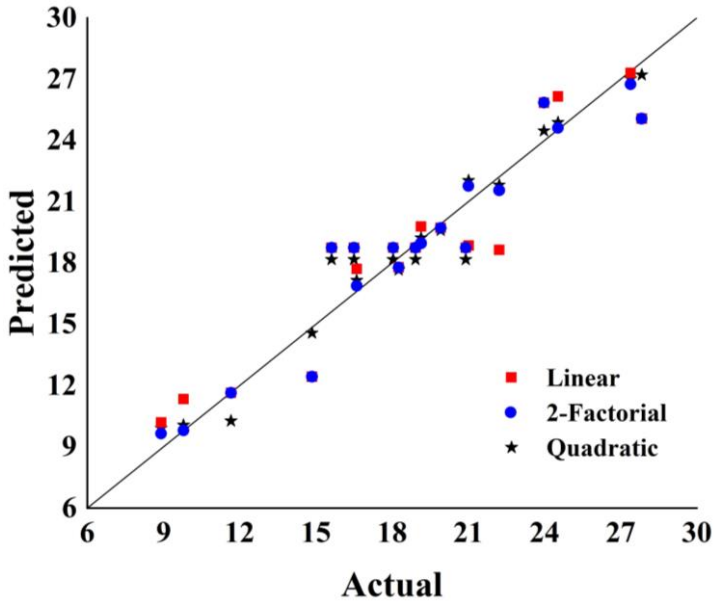

Figure 4.17 Actual vs Predicted values of urease activity according to the different models

Table 4.8 ANOVA analysis for quadratic model on optical density

Source	Sum of squares	Degree of freedom	Mean square	F-value	p-value
Model	0.9837	9	0.1093	27.87	< 0.0001
A	0.4084	1	0.4084	104.15	< 0.0001
B	0.24	1	0.24	61.2	< 0.0001
C	0.005	1	0.005	1.27	0.2859
AB	0.0338	1	0.0338	8.62	0.0149
AC	0.0841	1	0.0841	21.43	0.0009
BC	0.1105	1	0.1105	28.16	0.0003
A^2	0.0536	1	0.0536	13.67	0.0041
B^2	0.0567	1	0.0567	14.47	0.0035
C^2	0	1	0	0.0028	0.9585
Residual	0.0392	10	0.0039		
Lack of Fit	0.0086	5	0.0017	0.2817	0.9047
Pure Error	0.0306	5	0.0061		
Cor Total	1.02	19			

Table 4.8 and Table 4.9 show that the terms C and C^2 are insignificant, corresponding to their high p-values in optical density and urease activity models. This observation suggests that the protein and vitamin dosage plays a crucial role in influencing the growth and enzymatic activity of the bacteria. The optimization of the data for maximum optical density and urease activity revealed 20 g/L soybean, 3 g/L yeast extract and 0.125 g/L of dextrose as the ideal combination. This combination produced optical density of 1.946 and urease activity of 27 m.mol urease/min. The 3-dimensional responses predicted by the model are presented in the Figure 4.18 for optical density and Figure 4.19 for urease activity.

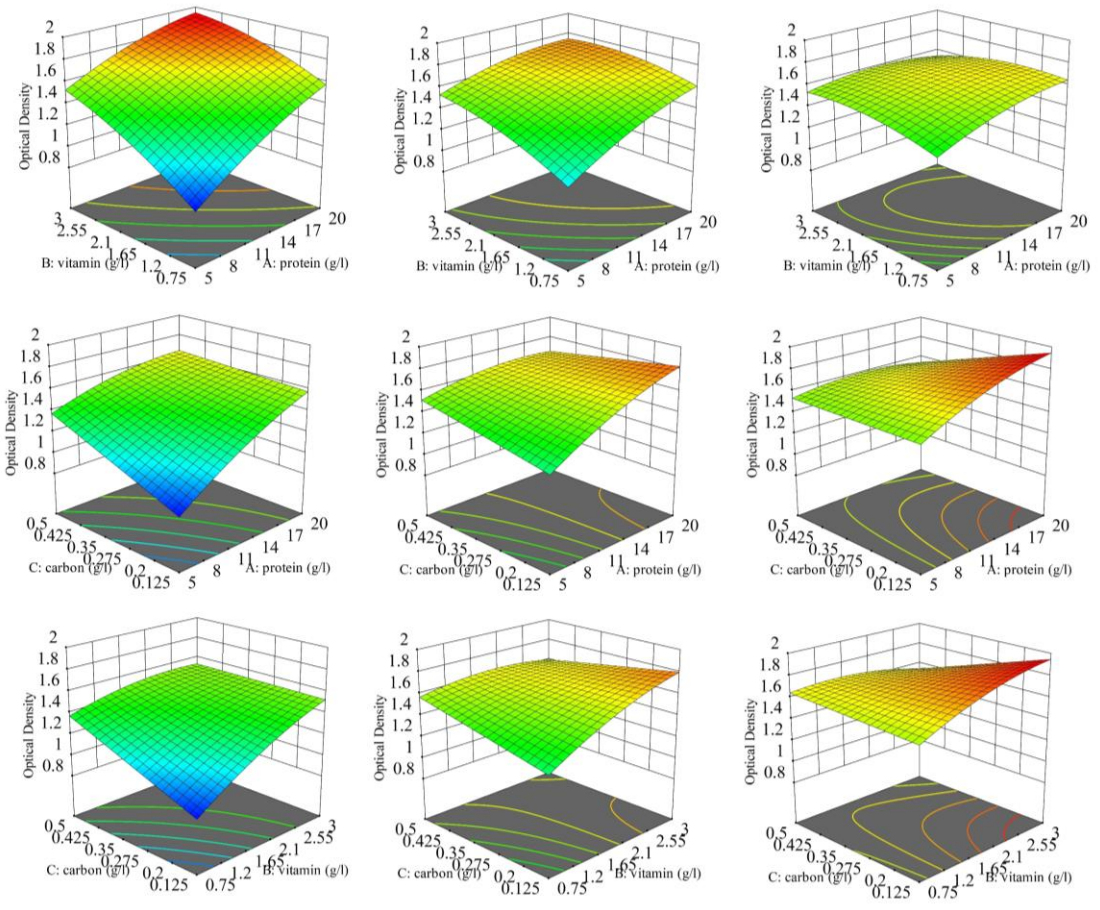

Figure 4.18 Three-dimensional response surfaces from the quadratic model on optical density

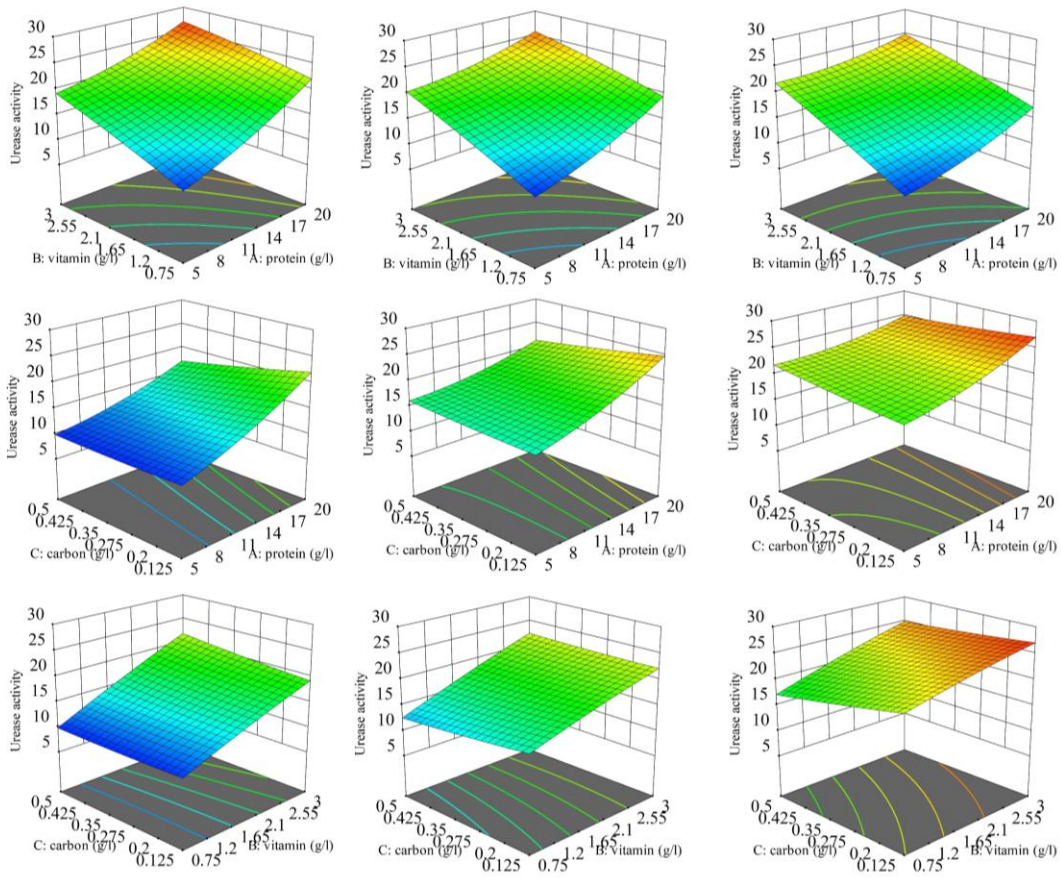

Figure 4.19 Three-dimensional response surfaces from the quadratic model on urease activity

Table 4.9 ANOVA analysis for quadratic model on urease activity

Source	Sum of squares	Degree of freedom	Mean square	F-value	p-value
Model	480.131	9	53.348	22.40	< 0.0001
A	192.774	1	192.774	80.93	< 0.0001
B	243.610	1	243.610	102.27	< 0.0001
C	4.495	1	4.495	1.89	0.1996
AB	8.736	1	8.736	3.67	0.0845
AC	11.186	1	11.186	4.70	0.0554
BC	3.781	1	3.781	1.59	0.2363
A^2	13.302	1	13.302	5.58	0.0397
B^2	1.160	1	1.160	0.49	0.5011
C^2	0.385	1	0.385	0.16	0.696
Residual	23.82	10	2.38		
Lack of Fit	5.937	5	1.187	0.33	0.8742
Pure Error	17.88	5	3.58		
Cor Total	503.95	19			

4.3.2 Soil preparation and scheme of experiments

The soil was directly blended with the FCA and the materials required for biomineralization. Unconfined compression tests were conducted on thirty samples in the sequence given by the CCD, and the results are presented in Figure 4.20.

It illustrates that the fifth combination produced the highest compressive strength of 350 kPa with factors at levels +1, +1, +1, and -1, respectively (Table 4.10). It is henceforth referred to as TC5. It is a ten-fold increase from 35kPa for untreated BCS. The combination in the 19th experiment resulted in 62 kPa where the factors are at the levels -α, 0, 0, 0. The correlation between factors and the response measures how changes in the factors affect the response. From the initial observations, it is understood that the FCA content had the highest correlation of 0.909 with the UCS. Optical density also had a minor but positive correlation of 0.153 with the UCS.

Table 4.10 Factor codes and levels in CCD for urease activity

Factor	Name	Units	Minimum (-α)	Low (-1)	Mean (0)	High (+1)	Maximum (+α)
A	FCA replaced	%	10.00	20.00	30.00	40.00	50.00
B	Optical density	-	0.395	0.67	0.902	1.13	1.41
C	Calcium chloride	g	0.25	0.50	0.75	1.00	1.25
D	Urea	g	0.00	0.50	1.00	1.50	2.00

Table 4.11 Comparison of standard models for urease activity

Model	R^2	Adjusted-R^2	Predicted-R^2	S/N	Root mean squared error
Linear	0.862	0.839	0.786	24.429	25.781
2-Factorial	0.948	0.921	0.890	23.541	15.72
Quadratic	0.983	0.968	0.923	32.394	8.961

Changes in calcium concentration have a negligible effect on the UCS as seen from the correlation value of -0.027. However, changes in the urea concentration had a significant negative correlation of -0.106 with the UCS. The quadratic model provides

a superior fit to the data in comparison to the linear and two-factorial models (Table 4.11). The results were used to develop a model evaluated by ANOVA (Table 4.12). Using the experimental data, the UCS of the soil composite was illustrated by the coded polynomial equation (Equation 4.4).

$$UCS = 215.76 + 69.98A + 10.85B - 2.09C - 8.42D + 19.50AB - 8.75AC - 7.00AD + 0.45BC + 7.48BD + 11.25CD - 5.77A^2 - 2.59B^2 - 6.02C^2 + 8.98D^2$$

(Equation 4.4)

The quadratic model exhibits a p-value below 0.001 and an F-value of 62.99, signifying its significance. The likelihood of the F-value occurring due to noise is less than 0.01%. Moreover, the model reveals a negligible lack of fit of 1.42, indicating that the fitted model adequately describes the data and no additional terms are necessary for improvement.

Table 4.12 ANOVA analysis for quadratic model on UCS

Source	Sum of Squares	Degree of freedom	Mean Square	F-value	p-value
Model	1.416E+05	14	10116.73	62.99	< 0.0001
A	1.175E+05	1	1.175E+05	731.31	< 0.0001
B	3429.00	1	3429.00	21.35	0.0003
C	105.12	1	105.12	0.6545	0.4311
D	1699.79	1	1699.79	10.58	0.0053
AB	7396.00	1	7396.00	46.05	< 0.0001
AC	1225.00	1	1225.00	7.63	0.0145
AD	784.00	1	784.00	4.88	0.0431
BC	4.00	1	4.00	0.0249	0.8767
BD	1089.00	1	1089.00	6.78	0.0199
CD	2025.00	1	2025.00	12.61	0.0029
A^2	913.44	1	913.44	5.69	0.0307
B^2	271.44	1	271.44	1.69	0.2132
C^2	994.30	1	994.30	6.19	0.0251
D^2	2211.44	1	2211.44	13.77	0.0021
Residual	2409.08	15	160.61		
Lack of Fit	1781.08	10	178.11	1.42	0.3673
Pure Error	628.00	5	125.60		
Cor Total	1.440E+05	29			

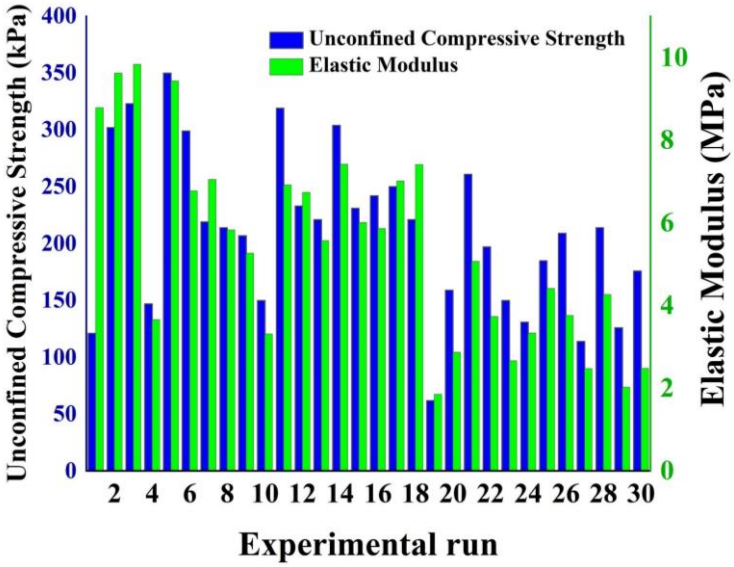

Figure 4.20 UCS and elastic modulus of stabilized BCS

The statistically significant terms in the model, with p-values less than 0.05, include A, B, D, AB, AC, AD, BD, CD, A^2, C^2, and D^2. Therefore, all the factors considered in developing this model have an impact on the UCS. While the linear term C, representing the concentration of calcium chloride, is deemed insignificant, its interaction with FCA and urea significantly affects the UCS. With the exception of bacterial density, all factors contribute to the curvature of the response surface, as evidenced by the significance of the quadratic terms in the model. Hence, it can be inferred that both FCA and biomineralization play a role in enhancing the UCS of soil. The model exhibited a coefficient of determination of 0.9833, suggesting that over 95% of the experimental responses were exceptionally well-fitted to the model. Furthermore, the adjusted R^2 value of 0.9677 confirms the model's adequacy, with a difference of less than 0.2 from the predicted R^2 (0.9225), underscoring its robustness. The model's signal-to-noise ratio of 32.394 indicates that the signal is not attributable to noise. Also, it was observed that the model's actual and predicted values of UCS were in good agreement (Figure 4.21).

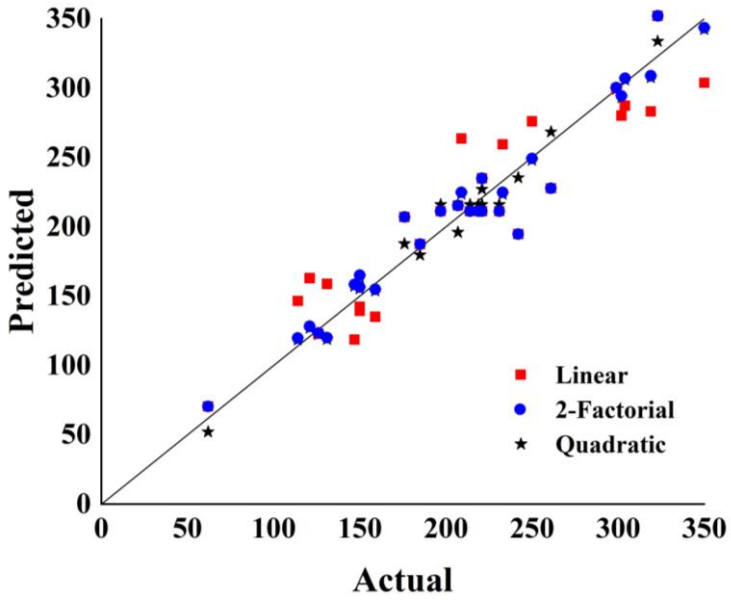

Figure 4.21 Actual vs Predicted values of optical density according to the different models

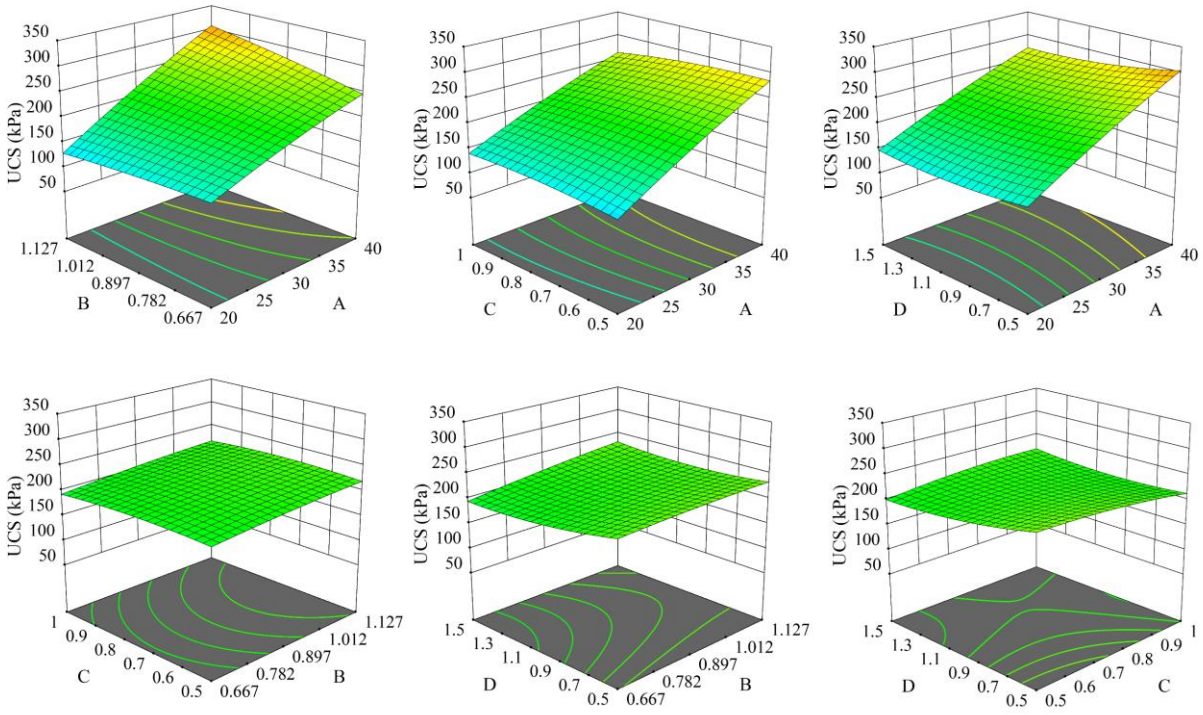

Figure 4.22 Three-dimensional response surfaces from the quadratic model on UCS

Responses are predicted from the model and three-dimensional surfaces were developed to understand the interaction of the variables on UCS (Figure 4.22). In each figure, two factors were held constant at the center level and the interactive effect on the other two on UCS is displayed. The plots depict how UCS varies by changing two of the combination's four factors.

4.3.3 Leachate extraction and heavy metal analysis

The concentrations of heavy metals obtained from the extracts and leachates were documented in Table 4.13. The results reveal that heavy metals easily disperse into water when present in the FCA. However, the concentration of heavy metals in the leachate of TC5 is significantly low compared to the extraction sample, indicating that the TC5 sample effectively immobilizes Cr (99 %), Fe (98 %), Zn (99 %), Pb (100 %), Ni (95 %), Cd (100 %), Cu (97 %), Ti (100 %), Hg (100 %), and As (100 %).

Table 4.13 Concentration of heavy metals

Sample / Element	FCA		TC5	
	H_2SO_4 extract	Water leachate	H_2SO_4 extract	Water leachate
Chromium	386.78	360.54	181.92	2.86
Iron	345.02	297.58	402.36	4.21
Zinc	886.29	674.25	527.97	2.73
Lead	12.45	12.22	5.56	ND
Nickel	1.92	1.53	1.8	0.07
Cadmium	0.38	0.26	0.25	ND
Copper	0.78	0.64	0.48	0.02
Titanium	5.42	3.21	1.1	ND
Mercury	0.10	0.08	0.01	ND
Arsenic	0.40	0.40	0.46	ND

ND – Not Detected

The pH values of the BCS and FCA were measured to be 7.4 and 8.9, respectively. The alkaline conditions in FCA promote bioprecipitation, facilitating the fixation of heavy metals by calcium carbonate. As a result, heavy metals only escape from TC5 in strongly acidic environments. Therefore, biomineralization effectively addresses the issue of heavy metal leaching from FCA, making it suitable for stabilizing BCS.

Previous studies have demonstrated that heavy metals can be co-precipitated with calcium carbonate (Ali et al. 2022; Khadim et al. 2019; Peng et al. 2023).

4.3.4 Characterization studies

(i) X-ray diffraction

TC5, FCA, and BCS diffraction patterns from the diffractometer were recorded and analyzed using X'pert Highscore Plus software (Figure 4.23). The minerals present in the samples were identified by comparing the positions of high-intensity peaks and their corresponding Bragg angles with the structures in the International Centre for Diffraction Data (ICDD) database.

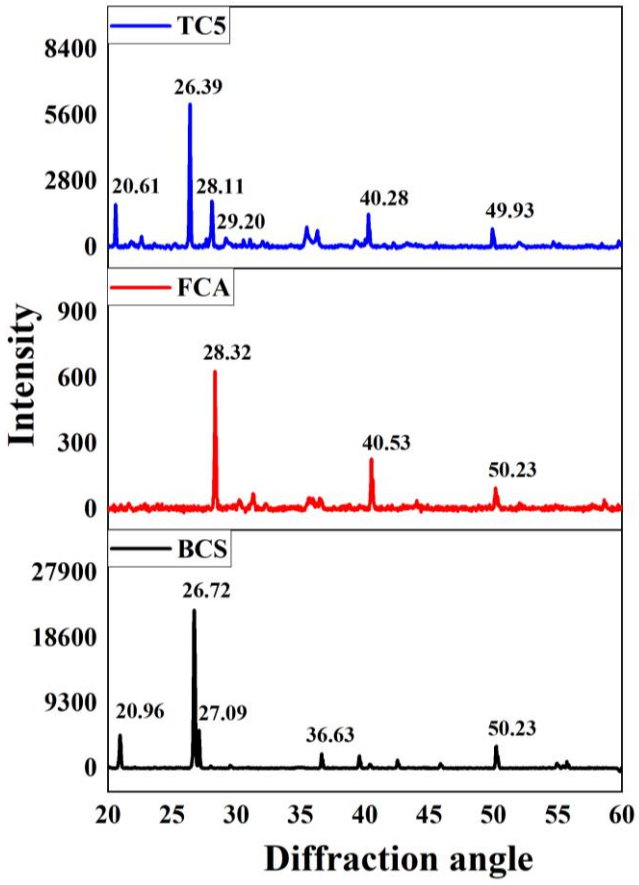

Figure 4.23 X-ray diffraction pattern of BCS, FCA, and the target sample with maximum UCS

The diffraction pattern of BCS exhibited high-intensity peaks at diffraction angles 20.96°, 26.72°, 36.63°, 39.58°, 40.41°, 42.53°, 45.92°, and 50.24°. The peak at 26.72

º displayed the highest intensity and matched the diffraction pattern of quartz (SiO_2) with the reference pattern 96-152-6861. The crystal system was identified as hexagonal. In the FCA diffraction pattern, high-intensity peaks were observed at 28.32 º, 40.54 º, and 50.23 º. These peaks closely resembled the diffraction pattern of sylvite (KCl) with the reference pattern 96-900-8652.

The diffraction pattern of the representative TC5 sample contained the peaks of both BCS and FCA. TC5 also exhibited peaks corresponding to calcite, sylvite, and quartz. Peaks at 20.61 º, 26.39 º, 28.08 º, 29.20 º, 31.08 º, 36.29 º, 39.21 º, 42.20 º, 43.16 º, 49.92 º, and 55.17 º closely matched the diffraction pattern of calcite with the reference pattern 96-900-0969. This confirms the occurrence of calcite resulting from biomineralization. Previous studies on calcium carbonate biomineralization have also observed similar peak positions (Eltarahony et al. 2021; Ideo and Miyazaki 2022).

(ii) Field emission gun scanning electron microscopy

Secondary electron signals were used to capture images of the BCS, FCA, and TC5 samples. The image capture process involved a working distance of 3.2mm for BCS and TC5 samples and 9mm for FCA. All images were taken at a magnification of 10,000 times. The image of BCS, as shown in Figure 4.24 (a), revealed an irregular and flaky surface. This surface morphology is characteristic of clayey soils and is consistent with previous findings by Wani et al. (2021) and Wani and Mir (2021). In contrast, the microstructure of the FCA sample, depicted in Figure 4.24 (b), predominantly consisted of spherical particles of various sizes. The dark regions in the image are likely attributed to the gaps between these particles.

The image of the TC5 sample revealed the presence of rhombohedral crystals alongside the spherical particles of FCA on the flaky surface of the clayey soil (Figure 4.24 (c)). This combination suggests the formation of calcite bioprecipitates. Similar formations of bioprecipitates align with earlier studies on biomineralization (Eltarahony et al. 2021; Nasser et al. 2022; Omoregie et al. 2022; Ortega-Villamagua et al. 2020). Moreover, the spherical particles of FCA were found to be deposited over the flaky surfaces of the clayey soil, forming bridges through the calcium carbonate that was formed during the bioprecipitation. This observation indicates a dense structure in the

TC5 sample, resulting from the interaction between the clayey soil, FCA particles, and the bioprecipitated calcium carbonate.

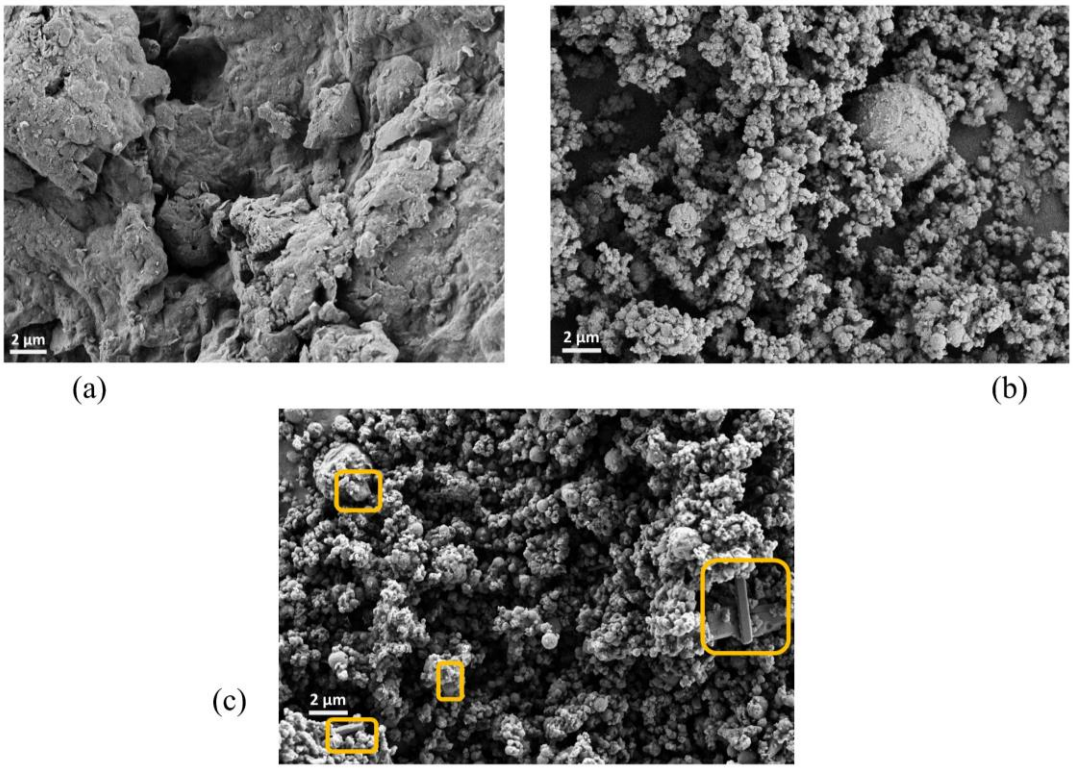

Figure 4.24 FEGSEM images of (a) BCS, (b) FCA and (c) TC5

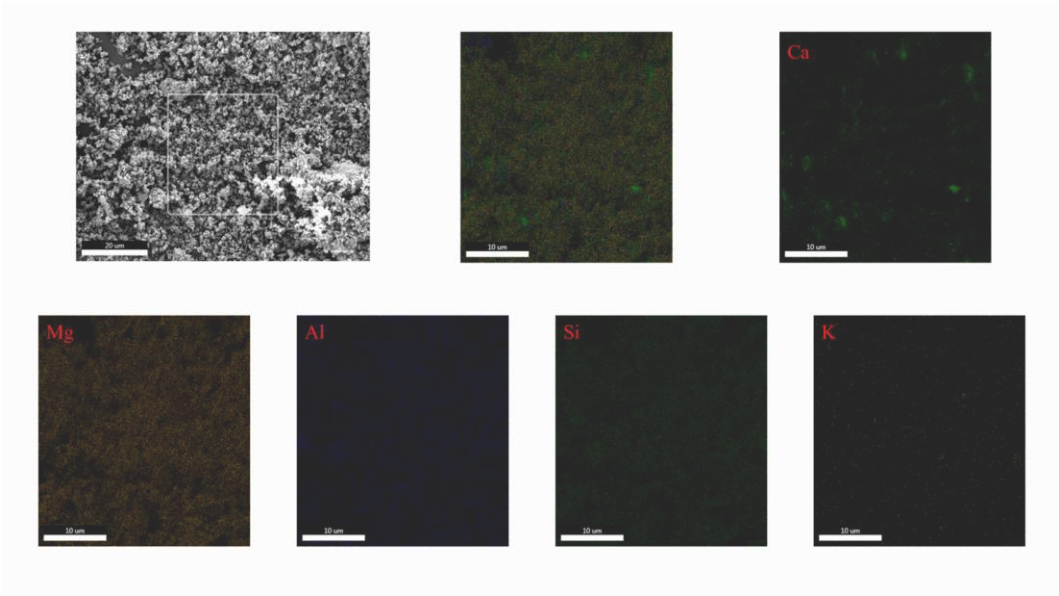

Figure 4.25 Elemental mapping distribution of TC5 sample

Furthermore, an elemental mapping analysis conducted using energy-dispersive X-ray analysis revealed a uniform distribution of Si, Al, K, and Mg throughout the sample (Figure 4.25). However, significant amounts of Ca were observed only in a few specific locations. This observation aligns with the concept of biomineralization of calcium carbonate around ureolytic bacteria, indicating that the presence of ureolytic bacteria influences calcium distribution.

(iii) Fourier Transform Infrared Spectroscopy

This section of the results compares the infrared pattern of the TC5 sample to the patterns of clayey soil and FCA, as shown in Figure 4.26. The analysis reveals that the infrared pattern of the TC5 sample contains peaks that are characteristic of both the soil and the FCA. Specifically, a peak at 993 cm^{-1} in TC5 indicates an asymmetric stretching and bending vibration of Si-O-Si, which is associated with forming C-S-H (calcium-silicate-hydrate) gel (Wang et al. 2021).

Additionally, a peak at 1457 cm^{-1} in TC5 is identified as a characteristic absorption band for calcium carbonate. This peak corresponds to the asymmetric stretching of the carbonate group. The development of calcium carbonate through biomineralization aligns with Elzwawy et al. (2022) and Mocanu et al. (2019), who have studied the vibrational signatures of calcium carbonate. Notably, the characteristic absorption band at 1457 cm^{-1} is not observed in the FTIR spectra of the clayey soil or the FCA, indicating that the development of calcium carbonate is specific to the TC5 sample.

Furthermore, an absorption band at 1633 cm^{-1} in the TC5 sample is attributed to the H-O-H stretch. This information is derived from the study conducted by Cardoso et al. (2018). Overall, the comparisons between the infrared pattern of the TC5 sample and the reference studies provide evidence of the presence of C-S-H gel and calcium carbonate formation through biomineralization. These findings contribute to understanding the composition and properties of the TC5 sample.

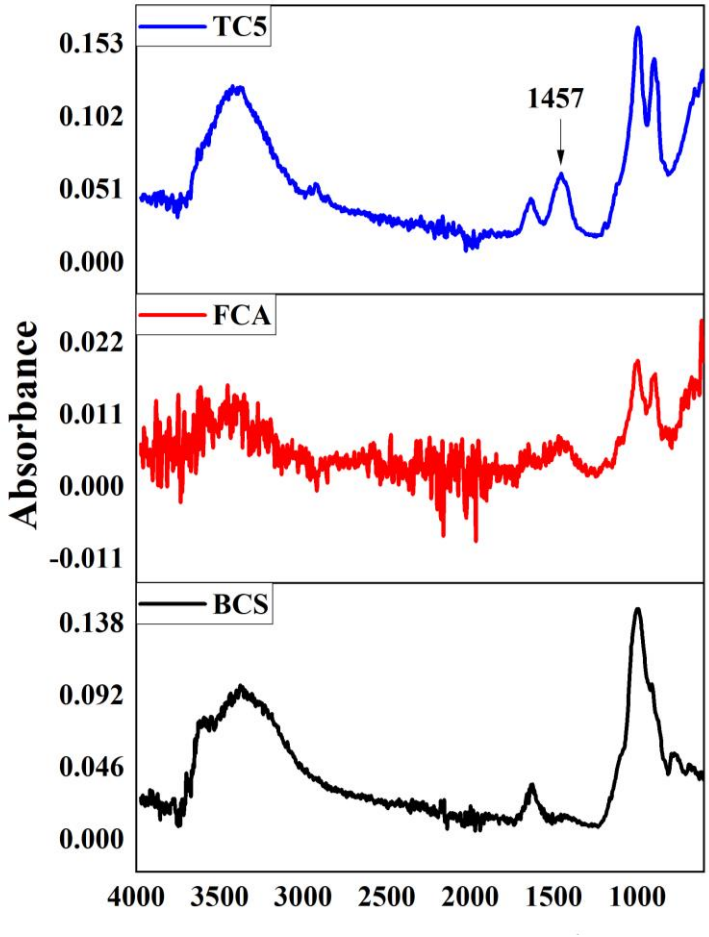

Figure 4.26 FTIR spectrum of BCS, FCA and TC5 sample

(iv) Thermogravimetric analysis

A minor weight change was observed during the thermal analysis of BCS. Around 7% weight loss occurred within the temperature range of 270 °C. This weight loss can be attributed to removing of moisture or volatile organic compounds in the sample. Beyond 270 °C, BCS did not experience substantial weight change. This observation indicates that BCS exhibits relatively stable behavior in terms of weight change during the analyzed temperature range (Figure 4.27 (a)).

In the case of FCA, the thermal analysis graph displayed three distinct steps of weight change. Initially, during the temperature rise up to 200 °C, there was a 5 % reduction in weight. This weight loss can be attributed to the loss of water molecules associated with hydration products in the FCA sample. The second weight loss step was observed between 300 °C and 600 °C, constituting approximately 7 % of the sample's weight.

This weight loss corresponds to the decomposition of C-S-H (calcium-silicate-hydrate) gel, a significant FCA component. Finally, the third step of weight loss occurred beyond 800 °C, accounting for approximately 15% of the sample's weight. This weight loss at higher temperatures indicates the decomposition of other components present in FCA (Figure 4.27 (b)).

In the case of the TC5 sample, a major step of weight loss was observed within a temperature range of 590 °C to 810 °C (Figure 4.27 (c)). During this range, the sample's weight was reduced by 18 %. This significant weight loss can be attributed to the decomposition of calcium carbonate. The presence of calcium carbonate crystals in the TC5 sample, formed during bioprecipitation, is indicated by this decomposition behavior. These observations align with the findings reported by Wani et al. (2021) and Wani and Mir (2021).

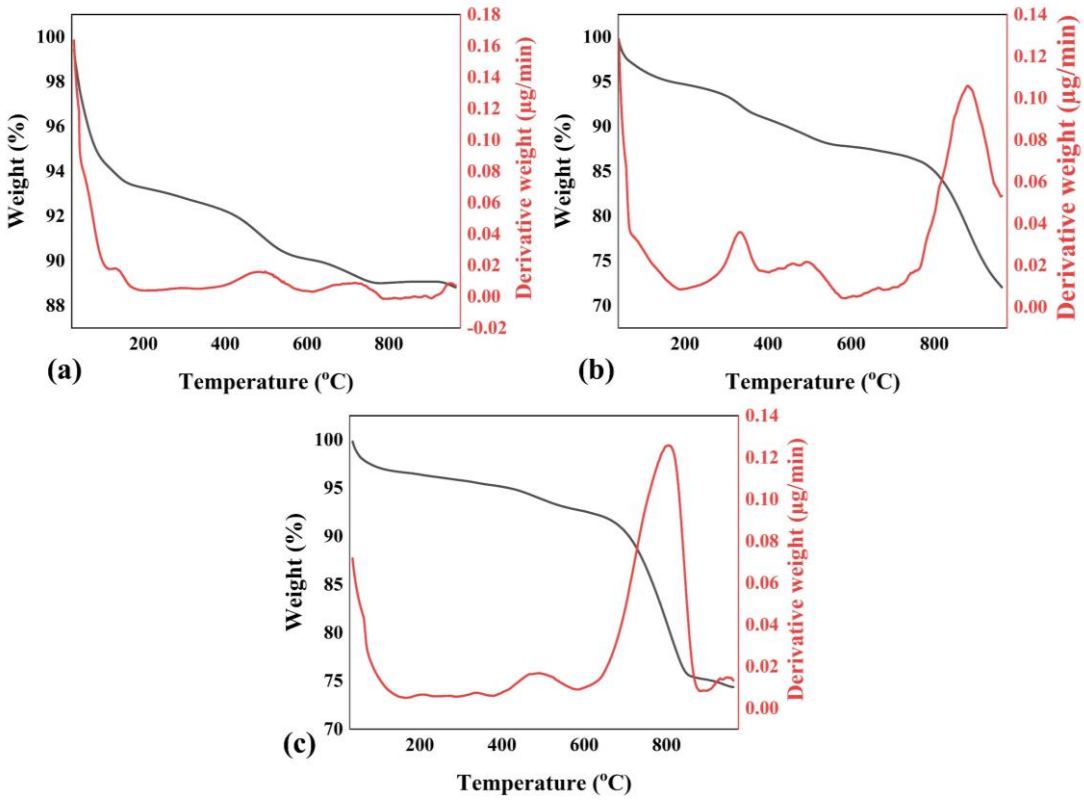

Figure 4.27 Thermogravimetric profiles of (a) BCS, (b) FCA and, (c) TC5 samples

CHAPTER 5
CONCLUSIONS

This chapter presents the conclusions derived from the experimental work carried out to achieve the objectives. It includes evaluating microbial growth in waste ashes, identifying the optimal protein source for bacterial urease production, optimizing the composition of the nutrient medium to enhance biomineralization, and analyzing the combined effect of biomineralization with BMA and FCA on the geotechnical properties and characteristics of BCS. A three-stage experimental methodology has been implemented to address these objectives. The key findings of this study are outlined below:

(i) Isolation of indigenous bacteria and selection of suitable protein source

- Biomedical ash and ferrochrome ash contained urease-positive bacteria. The 16SrRNA analysis determined *Lysinibacillus sphaericus* in ferrochrome ash and *Bacillus cereus* in biomedical ash.
- The nutritional medium containing blackgram sustained its pH between 7.4 & 8.2. Soybean demonstrated the highest urease activity of 22 m.mol urease/min (0^{th} hour), 35 m.mol urease/min (24^{th} hour), 55 m.mol urease/min (48^{th} hour, 62 m.mol urease/min (72^{nd} hour), 64 m.mol urease/min (168^{th} hour), and 55 m.mol urease/min (240^{th} hour). However, not much difference was observed while comparing the protein sources regarding optical density. Hence among chickpeas, peanuts, blackgram, garbanzo beans, and soybean as the protein source, blackgram and soybean exhibited the most favorable conditions for bacterial growth suitable for biomineralization.

(ii) Incorporation of mineralized biomedical ash in black cotton soil

- The optimal nutritional combination was 23.47 g/L black gram, 3.45 g/L yeast extract, and 0.03 g/L dextrose for the highest urease activity of 54 m.mol urease/min. The quantitative dosage of proteins and vitamins is crucial for urease activity.

- The leachates from the mBMA exhibited a reduction of Hg (97 %), Cr (96 %), Zn (97 %), Pb (93 %), Fe (94 %), Cu (93 %), Cd (98 %), Ba (87 %), As (96 %), Ti (88 %), and Se (86 %) concentrations compared to the leachates from BMA.
- Attempts on soil stabilization experiments resulted in partial soil replacement (10 %, 20 %, 30 %, and 40 %) with mBMA. At 40 % soil replacement by mBMA, the soil's LL decreased from 53 % to 47 %, PL increased from 25 % to 34 %, and the PI reduced from 27 % to 13 %. The FSI of the soil reduced from 114 % to 17%. OMC increased from 22 % to 26 %, and the corresponding MDD reduced from 1.596 g/cm^3 to 1.458 g/cm^3.
- Replacing 30% BCS by mBMA enhanced the UCS from 35 kPa to the maximum of 147 kPa compared to other percentages (10 %, 20 %, and 40 %) replacement by weight.
- X-ray diffraction detected calcite (23.03 ^{o}, 29.38 ^{o}, 25.47 ^{o}, 31.34 ^{o}, 35.98 ^{o}, 39.41 ^{o}, 43.15 ^{o}, 45.44 ^{o}, 48.48 ^{o}, and 57.40 ^{o}) in mBMA. FESEM images of mBMA revealed dense matter connecting the ash particles, expected to be the calcite formed during the biomineralization. FTIR absorption bands corresponding to carbonates at 711.6 cm^{-1}, 873.6 cm^{-1}, 1420.3 cm^{-1}, 1798.3 cm^{-1}, 2512.8 cm^{-1}, and 2875.3 cm^{-1} support the occurrence of biomineralization. A 10 % weight reduction in the characteristic thermal decomposition range (570 °C to 660 °C) for calcium carbonate further ascertained the biomineralization.

(iii) Integration of biomineralization in soil stabilization using ferrochrome ash

- The optimized combination of 20 g/L soybean, 3 g/L yeast extract, and 0.125 g/L dextrose determined the optical density as 1.946 and urease activity of 27 m.mol urease/min, respectively.
- The concentration of heavy metals in the leachate of TC5 reduced with efficiencies of 95 % (Ni), 97 % (Cu), 98 % (Fe), 99 % (Cr and Zn), and 100 % (Pb, Cd, Ti, Hg, and As).
- The highest compressive strength of 350 kPa was achieved when replacing 40% of BCS with FCA, using bacteria with an optical density of 1.12, a calcium chloride dose of 0.5 g, and a urea dose of 0.5 g. FSI reduced from 114 % for BCS to 12 % for TC5.

- The interaction between ferrochrome ash, bacterial density, calcium chloride, and urea concentrations on unconfined compressive strength was explored using a quadratic model, revealing that ferrochrome ash had the most substantial influence among the factors examined.
- A combination with 40 % FCA, a bacterial optical density of 1.12, 0.5 g urea, and 0.5 g calcium chloride increased the unconfined compressive strength of BCS from 35 kPa to 350 kPa. The FSI of TC5 (12 %) is exceptionally lower than BCS (114 %).
- The XRD of TC5 (20.61 ^{o}, 26.39 ^{o}, 28.08 ^{o}, 29.20 ^{o}, 31.08 ^{o}, 36.29 ^{o}, 39.21 ^{o}, 42.20 ^{o}, 43.16 ^{o}, 49.92 ^{o}, and 55.17 ^{o}) contained peaks of calcite in addition to FCA (28.32 ^{o}, 40.54 ^{o}, and 50.23 ^{o}) and BCS (20.96 ^{o}, 26.72 ^{o}, 36.63 ^{o}, 39.58 ^{o}, 40.41 ^{o}, 42.53 ^{o}, 45.92 ^{o}, and 50.24 ^{o}). The SEM image contained rhombohedral crystals of calcium carbonate and the spherical particles of the FCA on the flaky surface of the clayey soil. The peak observed at 1457 cm^{-1} in the FTIR profile is a characteristic absorption band for calcium carbonate, which is present neither in the spectra of BCS nor in FCA. Other bands at 993 cm^{-1} and 1633 cm^{-1} represent the C-S-H formation. TGA of TC5 detected 18 % weight loss in the range of 590 ^{o}C and 810 ^{o}C, representing the decomposition of calcium carbonate formed during biomineralization.

Biomineralization is a safe process for immobilizing heavy metals from waste materials. Its integration in waste ash-based soil stabilization with both BMA and FCA restricted the heavy metal dispersion and enhanced the soil's consistency, UCS, and reduced plasticity.

SCOPE FOR FUTURE STUDY

The present investigation can be extended to:

1. different waste ashes and stabilizing different soils
2. different food sources for bacteria using dairy/agro waste

REFERENCES

Abo-El-Enein, S. A., Ali, A. H., Talkhan, F. N. and Abdel-Gawwad, H. A. (2013). "Application of microbial biocementation to improve the physico-mechanical properties of cement mortar." *HBRC Journal*, 9(1), 36–40.

Achal, V., Mukerjee, A. and Sudhakara Reddy, M. (2013). "Biogenic treatment improves the durability and remediates the cracks of concrete structures." *Constr Build Mater*, 48, 1–5.

Achal, V., Mukherjee, A., Basu, P. C. and Reddy, M. S. (2009). "Lactose mother liquor as an alternative nutrient source for microbial concrete production by Sporosarcina pasteurii." *J Ind Microbiol Biotechnol*, 36(3), 433–438.

Acharya, P. K., Kumar Patro, S. and Patro, S. K. (2016). "Flexural behaviour of ferrochrome ash concrete beams." *The Indian Concr J*, 90, 1–8.

Acharya, P. K. and Patro, S. K. (2015). "Effect of lime and ferrochrome ash (FA) as partial replacement of cement on strength, ultrasonic pulse velocity and permeability of concrete." *Constr Build Mater*, 94, 448–457.

Acharya, P. K. and Patro, S. K. (2016a). "Strength, sorption and abrasion characteristics of concrete using ferrochrome ash (FCA) and lime as partial replacement of cement." *Cem Concr Compos*, 74, 16–25.

Acharya, P. K. and Patro, S. K. (2016b). "Use of ferrochrome ash (FCA) and lime dust in concrete preparation." *J Clean Prod*, 131, 237–246.

Acharya, P. K. and Patro, S. K. (2023). "Evaluation of environmental disturbance indicator using functional performance and life cycle assessment of ferrochrome waste concrete." *J Build Eng*, 65, 105788.

Adepoju-Bello. (2012). "Analysis of some selected toxic metals in registered herbal products manufactured in Nigeria." *Afr J Biotechnol*, 11(26), 6918–6922.

Ajorloo, M., Ghodrat, M., Scott, J. and Strezov, V. (2022). "Heavy metals removal/stabilization from municipal solid waste incineration fly ash: a review and recent trends." *J Mater Cycles Waste Manag*, 24(5), 1693–1717.

Akram, S., Najam, R., Rizwani, G. H. and Abbas, S. A. (2015). “Determination of heavy metal contents by atomic absorption spectroscopy (AAS) in some medicinal plants from Pakistani and Malaysian origin.” *Pak J Pharm Sci*, 28(5), 1781–1787.

Ali, A., Li, M., Su, J., Li, Y., Wang, Z., Bai, Y., Ali, E. F. and Shaheen, S. M. (2022). “Brevundimonas diminuta isolated from mines polluted soil immobilized cadmium (Cd2+) and zinc (Zn2+) through calcium carbonate precipitation: Microscopic and spectroscopic investigations.” *Sci Total Environ*, 813, 152668.

Amadi, A. A. (2014). “Enhancing durability of quarry fines modified black cotton soil subgrade with cement kiln dust stabilization.” *Transp Geotech*, 1(1), 55–61.

Amini, A. B., Koucheh, M. F., Babakhani, S., Kafil, H. S. and Fahmi, A. (2022). “Improvement of Mortar Samples Using the Bacterial Suspension Cultured in the Industrial Corn Steep Liquor Media.” *Ind Biotechnol*, 18(3), 162–167.

Amini Kiasari, M., Pakbaz, M. S. and Ghezelbash, G. R. (2019). “Comparison of Effects of Different Nutrients on Stimulating Indigenous Soil Bacteria for Biocementation.” *J Mater Civ Eng*, 31(6), 04019067.

Anand, K., Goyal, S. and Reddy, M. S. (2023). “Development of field applicable remediation procedure using bio-cementitious grout for concrete cracks in variable orientations.” *J Build Eng*, 67, 106024.

Anastasiadou, K., Christopoulos, K., Mousios, E. and Gidarakos, E. (2012). “Solidification/stabilization of fly and bottom ash from medical waste incineration facility.” *J Hazard Mater*, 207–208, 165–170.

Arpajirakul, S., Pungrasmi, W. and Likitlersuang, S. (2021). “Efficiency of microbially-induced calcite precipitation in natural clays for ground improvement.” *Constr Build Mater*, 282, 122722.

Astrup, T., Muntoni, A., Polettini, A., Pomi, R., Gerven, T. van and Zomeren, A. van. (2016). “Treatment and Reuse of Incineration Bottom Ash.” *Environ Mater Waste: Resour Recovery Pollut Prevent*, Elsevier Inc., 607–645.

Bai, H., Liu, D., Zheng, W., Ma, L., Yang, S., Cao, J., Lu, X., Wang, H. and Mehta, N. (2021). "Microbially-induced calcium carbonate precipitation by a halophilic ureolytic bacterium and its potential for remediation of heavy metal-contaminated saline environments." *Int Biodeterior Biodegrad*, 165, 105311.

Baloochi, H., Aponte, D. and Barra, M. (2020). "Soil stabilization using waste paper fly ash: Precautions for its correct use." *Appl Sci*, 10(23), 8750.

Behzadipour, H. and Sadrekarimi, A. (2021). "Biochar-assisted bio-cementation of a sand using native bacteria." *Bull Eng Geol Env*, 80(6), 4967–4984.

Belie, N. De and Wang, J. (2015). "Bacteria-based repair and self-healing of concrete." *J Sustain Cem Based Mater*, 5(1), 35–56.

Benassi, L., Pasquali, M., Zanoletti, A., Dalipi, R., Borgese, L., Depero, L. E., Vassura, I., Quina, M. J. and Bontempi, E. (2016). "Chemical Stabilization of Municipal Solid Waste Incineration Fly Ash without Any Commercial Chemicals: First Pilot-Plant Scaling Up." *ACS Sustain Chem Eng*, 4(10), 5561–5569.

Benassi, L., Zanoletti, A., Depero, L. E. and Bontempi, E. (2019). "Sewage sludge ash recovery as valuable raw material for chemical stabilization of leachable heavy metals." *J Environ Manag*, 245, 464–470.

Bhattacharya, A., Naik, S. N. and Khare, S. K. (2018). "Harnessing the bio-mineralization ability of urease producing Serratia marcescens and Enterobacter cloacae EMB19 for remediation of heavy metal cadmium (II)." *J Environ Manag*, 215, 143–152.

Bilal, M., Singh, N. and Rasool, T. (2022). "A model supported biomedical waste for the enhancement of mechanical properties of concrete." *Model Earth Syst Environ*, 8(2), 2075–2082.

Biswas, N., Puppala, A. J., Chakraborty, S. and Khan, Md. A. (2021). "Utilization of Silica-Based Admixture to Improve the Durability of Lime-Treated Expansive Soil." *IFCEE 2021*, 233–242.

Brasileiro, P. P. F., Silva, R. C. F. S. Da, Rocha E Silva, F. C. P., Brandão, Y. B., Sarubbo, L. A. and Benachour, M. (2020). "Biomineralization of calcium carbonate by bacillus cereus for self-healing biocement." *Chem Eng Trans*, 79, 97–102.

Briga-Sá, A., Silva, R. A., Gaibor, N., Neiva, V., Leitão, D. and Miranda, T. (2022). "Mechanical Characterization of Masonry Built with iCEBs of Granite Residual Soils with Cement–Lime Stabilization." *Build*, 12(9), 1419.

Bruckman, V. J. and Wriessnig, K. (2013). "Improved soil carbonate determination by FT-IR and X-ray analysis." *Environ Chem Lett*, 11(1), 65–70.

Bulut, U., Ozverdi, A. and Erdem, M. (2009). "Leaching behavior of pollutants in ferrochrome arc furnace dust and its stabilization/solidification using ferrous sulphate and Portland cement." *J Hazard Mater*, 162(2–3), 893–898.

Cai, Q., Xu, M., Ma, J., Zhang, X., Yang, G., Long, L., Chen, C., Wu, J., Song, C. and Xiao, Y. (2023). "Improvement of cadmium immobilization in contaminated paddy soil by using ureolytic bacteria and rice straw." *Sci Total Environ*, 874, 162594.

Cardoso, R., Pires, I., Duarte, S. O. D. and Monteiro, G. A. (2018). "Effects of clay's chemical interactions on biocementation." *Appl Clay Sci*, 156, 96–103.

Castillo, J., Alom, J., Gomez-Arias, A., Cebekhulu, S., Matu, A., Cason, E. and Valverde, A. (2023). "Bacterial communities shift and influence in an acid mine drainage treatment using barium carbonate disperse alkaline substrate system." *Sci Total Environ*, 885, 163526.

Central Pollution Control Board. (2018). Annual Report on Biomedical Waste Management as per Biomedical Waste Management Rules , 2016 For the year 2018.

Charpe, A. U. and Latkar, M. V. (2020). "Effect of biocementation using soil bacteria to augment the mechanical properties of cementitious materials." *Mater Today Proc*, 21, 1218–1222.

Charpe, A. U., Latkar, M. V. and Chakrabarti, T. (2017). "Microbially assisted cementation – A biotechnological approach to improve mechanical properties of cement." *Constr Build Mater*, 135, 472–476.

Chaurasia, L., Bisht, V., Singh, L. P. and Gupta, S. (2019). “A novel approach of biomineralization for improving micro and macro-properties of concrete.” *Constr Build Mater*, 195, 340–351.

Chen, J., Li, M., Mao, T., Fu, C., Lin, X., Li, X. and Yan, J. (2022a). “Effects of curing pathways and thermal-treatment temperatures on the solidification of heavy metal in fly ash by CaCO3 oligomers polymerization.” *J Clean Prod*, 362, 132526.

Chen, L., Wang, L., Zhang, Y., Ruan, S., Mechtcherine, V. and Tsang, D. C. W. (2022b). “Roles of biochar in cement-based stabilization/solidification of municipal solid waste incineration fly ash.” *Chem Eng J*, 430, 132972.

Chen, L., Wang, Y.-S., Wang, L., Zhang, Y., Li, J., Tong, L., Hu, Q., Dai, J.-G. and Tsang, D. C. W. (2021). “Stabilisation/solidification of municipal solid waste incineration fly ash by phosphate-enhanced calcium aluminate cement.” *J Hazard Mater*, 408, 124404.

Chen, W., Kirkelund, G. M., Jensen, P. E. and Ottosen, L. M. (2017a). “Comparison of different MSWI fly ash treatment processes on the thermal behavior of As, Cr, Pb and Zn in the ash.” *Waste Manag*, 68, 240–251.

Chen, X. and Achal, V. (2019). “Biostimulation of carbonate precipitation process in soil for copper immobilization.” *J Hazard Mater*, 368, 705–713.

Chen, X., Guo, H. and Cheng, X. (2017b). “Heavy metal immobilisation and particle cementation of tailings by biomineralisation.” *Environ Geotech*, 5(2), 107–113.

Cheshomi, A., Mansouri, S. and Amoozegar, M. A. (2018). “Improving the Shear Strength of Quartz Sand using the Microbial Method.” *Geomicrobiol J*, 35(9), 749–756.

Chethan, B. A. and Ravi Shankar, A. U. (2021). “Strength and Durability Characteristics of Cement and Class F Fly Ash-Treated Black Cotton Soil.” *Indian Geotech J*, 51(5), 1121–1133.

Chetty, K., Xie, S., Song, Y., McCarthy, T., Garbe, U., Li, X. and Jiang, G. (2021). "Self-healing bioconcrete based on non-axenic granules: A potential solution for concrete wastewater infrastructure." *J Water Process Eng*, 42, 102139.

Choi, S. G., Wang, K., Wen, Z. and Chu, J. (2017). "Mortar crack repair using microbial induced calcite precipitation method." *Cem Concr Compos*, 83, 209–221.

Comadran-Casas, C., Schaschke, C. J., Akunna, J. C. and Jorat, M. E. (2022). "Cow urine as a source of nutrients for Microbial-Induced Calcite Precipitation in sandy soil." *J Environ Manag*, 304, 114307.

Cordero, I., Snell, H. and Bardgett, RD. (2019). "High throughput method for measuring urease activity in soil." *Soil Biol Biochem*, 134, 72–77.

Crannell, B. S., Eighmy, T. T., Krzanowski, J. E., Eusden, J. D., Shaw, E. L. and Francis, C. A. (2000). "Heavy metal stabilization in municipal solid waste combustion bottom ash using soluble phosphate." *Waste Manag*, 20(2–3), 135–148.

Cuaxinque-Flores, G., Aguirre-Noyola, J. L., Hernández-Flores, G., Martínez-Romero, E., Romero-Ramírez, Y. and Talavera-Mendoza, O. (2020). "Bioimmobilization of toxic metals by precipitation of carbonates using Sporosarcina luteola: An in vitro study and application to sulfide-bearing tailings." *Sci Total Environ*, 724, 138124.

Cuzman, O. A., Rescic, S., Richter, K., Wittig, L. and Tiano, P. (2015). "Sporosarcina pasteurii use in extreme alkaline conditions for recycling solid industrial wastes." *J Biotechnol*, 214, 49–56.

Darsi, B. P., Molugaram, K. and Madiraju, S. V. H. (2021). "Subgrade Black Cotton Soil Stabilization Using Ground Granulated Blast-Furnace Slag (GGBS) and Lime, an Inorganic Mineral." *Environ Sci Proc*, 6, 15.

Dinesh, A., Indhumathi, S. and Pichumani, M. (2021). "Performance Assessment of Copper Slag and Sawdust Ash in Stabilization of Black Cotton Soil." *Adv Sustain Constr Mater*, S. Biswas, S. Metya, S. Kumar, and P. Samui, eds., Singapore: Springer Singapore, 124, 213–227.

Disi, Z. Al, Attia, E., Ahmad, M. I. and Zouari, N. (2022). “Immobilization of heavy metals by microbially induced carbonate precipitation using hydrocarbon-degrading ureolytic bacteria.” *Biotechnol Rep*, 35, e00747.

Do, H., Wang, Y., Long, Z., Ketehouli, T., Li, X., Zhao, Z. and Li, M. (2020). “A psychrotolerant Ni-resistant Bacillus cereus D2 induces carbonate precipitation of nickel at low temperature.” *Ecotoxicol Environ Saf*, 198, 110672.

Dourado, H., Mori, M., Hwa, T. and Lercher, M. J. (2021). “On the optimality of the enzyme–substrate relationship in bacteria.” *PLoS Biol*, 19(10), e3001416.

Eltarahony, M., Kamal, A., Zaki, S. and Abd-El-Haleem, D. (2021). “Heavy metals bioremediation and water softening using ureolytic strains Metschnikowia pulcherrima and Raoultella planticola.” *J Chem Technol Biotechnol*, 96(11), 3152–3165.

Elzwawy, A., Mansour, A. M., Magar, H. S., Hammad, A. B. A., Hassan, R. Y. A. and Nahrawy, A. M. el. (2022). “Exploring the structural and electrochemical sensing of wide bandgap calcium phosphate/CuxFe3-xO4 core-shell nanoceramics for H2O2 detection.” *Mater Today Commun*, 33, 104574.

Ersan, Y. C. (2019). “Overlooked Strategies in Exploitation of Microorganisms in the Field of Building Materials.” *Ecolog Wisdom Inspir Restor Eng*, Springer Singapore, 19–45.

Erşan, Y. Ç., Silva, F. B. Da, Boon, N., Verstraete, W. and Belie, N. De. (2015). “Screening of bacteria and concrete compatible protection materials.” *Constr Build Mater*, 88, 196–203.

Fahimizadeh, M., Abeyratne, A. D., Mae, L. S., Raman Singh, R. K. and Pasbakhsh, P. (2020). “Biological self-healing of cement paste and mortar by non-ureolytic bacteria encapsulated in alginate hydrogel capsules.” *Materials*, 13(17), 3711.

Fan, C., Wang, B. and Zhang, T. (2018). “Review on cement stabilization/solidification of municipal solid waste incineration fly ash.” *Adv Mater Sci Eng*, 2018, 5120649.

Fang, C., He, J., Achal, V. and Plaza, G. (2019). “Tofu Wastewater as Efficient Nutritional Source in Biocementation for Improved Mechanical Strength of Cement Mortars.” *Geomicrobiol J,* 36(6), 515–521.

Fondjo, A. A., Theron, E. and Ray, R. P. (2021). “Stabilization of Expansive Soils Using Mechanical and Chemical Methods: A Comprehensive Review.” *Civ Eng Archit,* 9(5), 1289–1294.

García-Díaz, I., Gázquez, M. J., Bolivar, J. P. and López, F. A. (2016). “Characterization and Valorization of Norm Wastes for Construction Materials.” *Manag Hazard Wastes,* H. E.-D. M. Saleh and R. O. A. Rahman, eds., Rijeka: IntechOpen, 50644.

Gautam, K. K., Sharma, R. K. and Sharma, A. (2021). “Effect of Municipal Solid Waste Incinerator Ash and Lime on Strength Characteristics of Black Cotton Soil.” *Sustain Develop Thr Eng Innov,* H. Singh, P.P. Singh Cheema and P. Garg, eds., Springer, Singapore, 113, 115–123.

Girma, M. and Asteray, B. (2022). “Fresh, Mechanical, and Microstructural Properties Investigation on the Combined Effect of Biomedical Waste Incinerator Ash and Bagasse Ash for High-Strength Concrete.” *Adv Mater Sci Eng*, 2022, 5685372.

Goodarzi, A. R., Akbari, H. R. and Salimi, M. (2016). “Enhanced stabilization of highly expansive clays by mixing cement and silica fume.” *Appl Clay Sci*, 132–133, 675–684.

Grabiec, A. M., Starzyk, J., Stefaniak, K., Wierzbicki, J. and Zawal, D. (2017). “On possibility of improvement of compacted silty soils using biodeposition method.” *Constr Build Mater,* 138(43), 134–140.

He, J., Chen, X., Zhang, Q. and Achal, V. (2019). “More effective immobilization of divalent lead than hexavalent chromium through carbonate mineralization by Staphylococcus epidermidis HJ2.” *Int Biodeterior Biodegradation,* 140, 67–71.

Heera, S., Kunal and Rajor, A. (2014). “Bacterial Treatment and Metal Characterization of Biomedical Waste Ash.” *J Waste Manag,* 2014, 956316.

Hu, H., Tang, C. S., Shen, Z., Pan, X., Gu, K., Fan, X., Lv, C., Mu, W. and Shi, B. (2023). "Enhancing lead immobilization by biochar: Creation of 'surface barrier' via bio-treatment." *Chemosphere*, 327, 138477.

Hu, Y., Zhang, P., Li, J. and Chen, D. (2015). "Stabilization and separation of heavy metals in incineration fly ash during the hydrothermal treatment process." *J Hazard Mater*, 299, 149–157.

Ideo, K. and Miyazaki, H. (2022). "Growth of calcium carbonate crystal on various substrates from a saturated calcium carbonate solution utilizing difference in solubility." *J Ceram Soc Jpn*, 130(4), 281–285.

Ikeagwuani, C. C., Obeta, I. N. and Agunwamba, J. C. (2019). "Stabilization of black cotton soil subgrade using sawdust ash and lime." *Soils Found*, 59(1), 162–175.

Intarasoontron, J., Pungrasmi, W., Nuaklong, P., Jongvivatsakul, P. and Likitlersuang, S. (2021). "Comparing performances of MICP bacterial vegetative cell and microencapsulated bacterial spore methods on concrete crack healing." *Constr Build Mater*, 302, 124227.

Jalilvand, N., Akhgar, A., Alikhani, H. A., Rahmani, H. A. and Rejali, F. (2020). "Removal of Heavy Metals Zinc, Lead, and Cadmium by Biomineralization of Urease-Producing Bacteria Isolated from Iranian Mine Calcareous Soils." *J Soil Sci Plant Nutr*, 20(1), 206–219.

Jiang, N. J., Liu, R., Du, Y. J. and Bi, Y. Z. (2019). "Microbial induced carbonate precipitation for immobilizing Pb contaminants: Toxic effects on bacterial activity and immobilization efficiency." *Sci Total Environ*, 672, 722–731.

Joshi, S., Goyal, S., Mukherjee, A. and Reddy, M. S. (2019). "Protection of concrete structures under sulfate environments by using calcifying bacteria." *Constr Build Mater*, 209, 156–166.

Joshi, S., Goyal, S. and Reddy, M. S. (2018). "Corn steep liquor as a nutritional source for biocementation and its impact on concrete structural properties." *J Ind Microbiol Biotechnol*, 45(8), 657–667.

Jozanikohan, G. and Abarghooei, M. N. (2022). “The Fourier transform infrared spectroscopy (FTIR) analysis for the clay mineralogy studies in a clastic reservoir.” *J Pet Explor Prod Technol*, 12(8), 2093–2106.

Jroundi, F., Gonzalez-Muñoz, M. T., Garcia-Bueno, A. and Rodriguez-Navarro, C. (2014). “Consolidation of archaeological gypsum plaster by bacterial biomineralization of calcium carbonate.” *Acta Biomater*, 10(9), 3844–3854.

Kahani, M., Kalantary, F., Soudi, M. R., Pakdel, L. and Aghaalizadeh, S. (2020). “Optimization of cost effective culture medium for Sporosarcina pasteurii as biocementing agent using response surface methodology: Up cycling dairy waste and seawater.” *J Clean Prod*, 253, 120022.

Kalantary, F. and Kahani, M. (2018). “Optimization of the biological soil improvement procedure.” *Int J Environ Sci Technol*, 16, 4231–4240.

Kang, C. H. and So, J. S. (2016). “Heavy metal and antibiotic resistance of ureolytic bacteria and their immobilization of heavy metals.” *Ecol Eng*, 97, 304–312.

Karatai, T. R., Kaluli, J. W., Kabubo, C. and Thiong’o, G. (2017). “Soil Stabilization Using Rice Husk Ash and Natural Lime as an Alternative to Cutting and Filling in Road Construction.” *J Constr Eng Manag*, 143(5), 04016127.

Katare, K. N., Samaiya, N. K. and IyerMurthy, Y. (2022). “Strength and durability properties of concrete using incinerated biomedical waste ash.” *Environ Eng Res*, 28(2), 220024.

Kaur, H., Siddique, R. and Rajor, A. (2019). “Influence of incinerated biomedical waste ash on the properties of concrete.” *Constr Build Mater*, 226, 428–441.

Kaur, H., Siddique, R. and Rajor, A. (2021). “Removal of alkalinity and metal toxicity from incinerated biomedical waste ash by using Bacillus halodurans.” *Bioremediat J*, 26(1), 1–19.

Kaur, N. P., Majhi, S., Dhami, N. K. and Mukherjee, A. (2020). “Healing fine cracks in concrete with bacterial cement for an advanced non-destructive monitoring.” *Constr Build Mater*, 242, 118151.

Khadim, H. J., Ammar, S. H. and Ebrahim, S. E. (2019). “Biomineralization based remediation of cadmium and nickel contaminated wastewater by ureolytic bacteria isolated from barn horses soil.” *Environ Technol Innov*, 14, 100315.

Khaleghi, M. and Rowshanzamir, M. A. (2019). “Biologic improvement of a sandy soil using single and mixed cultures: A comparison study.” *Soil Tillage Res*, 186, 112–119.

Kim, H. M., Choi, T. Y., Park, M. J. and Jeong, D. W. (2022). “Heavy metal removal using an advanced removal method to obtain recyclable paper incineration ash.” *Sci Rep*, 12(1), 1–11.

Kim, J. H. and Lee, J. Y. (2019). “An optimum condition of MICP indigenous bacteria with contaminated wastes of heavy metal.” *J Mater Cycles Waste Manag*, 21(2), 239–247.

Koch, A. L. (1988). “Why can’t a cell grow infinitely fast?” *Can J Microbiol*, 34(4), 421–426.

Kulanthaivel, P., Soundara, B. and Das, A. (2020). “Performance Study on Stabilization of Fine Grained Clay Soils Using Calcium Source Producing Microbes.” *KSCE J Civ Eng*, 24(9), 2631–2642.

Kumar, B. A. V. R., Keshav, L., Sivanantham, P. A., Arokiaraj, G. G. V., Rahman, D. R. Z., Kumar, P. M. and Somashekar, D. (2022). “Comprehensive Characterization of Ferrochrome Slag and Ferrochrome Ash as Sustainable Materials in Construction.” *J Nanomater*, 2022, 8571055.

Kumar B, C., Yaragal, S. C. and Das, B. B. (2020). “Ferrochrome ash – Its usage potential in alkali activated slag mortars.” *J Clean Prod*, 257, 120577.

Li, M., Fang, C., Kawasaki, S., Huang, M. and Achal, V. (2019). “Bio-consolidation of cracks in masonry cement mortars by Acinetobacter sp. SC4 isolated from a karst cave.” *Int Biodeterior Biodegrad*, 141, 94–100.

Li, M., Zhu, X., Mukherjee, A., Huang, M. and Achal, V. (2017). “Biomineralization in metakaolin modified cement mortar to improve its strength with lowered cement content.” *J Hazard Mater*, 329, 178–184.

Li, W., Fishman, A. and Achal, V. (2021). “Ureolytic bacteria from electronic waste area, their biological robustness against potentially toxic elements and underlying mechanisms.” *J Environ Manage*, 289, 112517.

Li, W., Yang, Y. and Achal, V. (2022). “Biochemical composite material using corncob powder as a carrier material for ureolytic bacteria in soil cadmium immobilization.” *Sci Total Environ*, 802, 149802.

Li, X., Chen, Q., Zhou, Y., Tyrer, M. and Yu, Y. (2014). “Stabilization of heavy metals in MSWI fly ash using silica fume.” *Waste Management*, 34(12), 2494–2504.

Liang, D. H. and Hu, Y. (2021). “Application of a heavy metal-resistant Achromobacter sp. for the simultaneous immobilization of cadmium and degradation of sulfamethoxazole from wastewater.” *J Hazard Mater*, 402, 124032.

Liang, S., Chen, J., Niu, J., Gong, X. and Feng, D. (2019). “Using recycled calcium sources to solidify sandy soil through microbial induced carbonate precipitation.” *Mar Georesour Geotechnol*, 38(4), 393–399.

Liao, Z., Wu, S., Xie, H., Chen, F., Yang, Y. and Zhu, R. (2023). “Effect of phosphate on cadmium immobilized by microbial-induced carbonate precipitation: Mobilization or immobilization?” *J Hazard Mater*, 443, Part B, 130242.

Liu, J., Ali, A., Su, J., Wu, Z., Zhang, R. and Xiong, R. (2021a). “Simultaneous removal of calcium, fluoride, nickel, and nitrate using microbial induced calcium precipitation in a biological immobilization reactor.” *J Hazard Mater*, 416, 125776.

Liu, L., Liu, H., Xiao, Y., Chu, J., Xiao, P. and Wang, Y. (2018). “Biocementation of calcareous sand using soluble calcium derived from calcareous sand.” *Bull Eng Geol Environ*, 77(4), 1781–1791.

Liu, P., Zhang, Y., Tang, Q. and Shi, S. (2021b). “Bioremediation of metal-contaminated soils by microbially-induced carbonate precipitation and its effects on ecotoxicity and long-term stability.” *Biochem Eng J*, 166.

Lu, C., Li, Z., Wang, J., Zheng, Y. and Cheng, L. (2023). “An approach of repairing concrete vertical cracks using microbially induced carbonate precipitation driven by ion diffusion.” *J Build Eng*, 73, 106798.

Lv, L. and Zhou, W. (2016). “Meso-2, 3-dimercaptosuccinic acid as a novel chemical agent to stabilize heavy metals in MSWI fly ash.” *Int Conf Energy Environ Protect (ICEEP 2016)*, 274–279.

Ma, W., Fang, Y., Chen, D., Chen, G., Xu, Y., Sheng, H. and Zhou, Z. (2017). “Volatilization and leaching behavior of heavy metals in MSW incineration fly ash in a DC arc plasma furnace.” *Fuel*, 210, 145–153.

Maitra, A. and Dill, K. A. (2015). “Bacterial growth laws reflect the evolutionary importance of energy efficiency.” *Proc Natl Acad Sci U S A*, 112(2), 406–411.

Maity, J. P., Chen, G. S., Huang, Y. H., Sun, A. C. and Chen, C. Y. (2019). “Ecofriendly Heavy Metal Stabilization: Microbial Induced Mineral Precipitation (MIMP) and Biomineralization for Heavy Metals within the Contaminated Soil by Indigenous Bacteria.” *Geomicrobiol J*, 36(7), 612–623.

Manzoor, J. and Sharma, M. (2019). “Impact of Biomedical Waste on Environment and Human Health.” *Environ Claims J*, 31(4), 311–334.

Matalkah, F. (2023). “Recycling of hazardous medical waste ash toward cleaner utilization in concrete mixtures.” *J Clean Prod*, 400, 136736.

Min, Y., Wang, Z., Su, J., Ali, A., Huang, T. and Yang, W. (2023). “Simultaneous removal of ammonia nitrogen, recovery of phosphate, and immobilization of nickel in a polyester fiber with shell powder and iron carbon spheres bioreactor: Optimization and pathways mechanism.” *Environ Res*, 224, 115476.

Mir, B. A. (2015). “Some studies on the effect of fly ash and lime on physical and mechanical properties of expansive clay.” *Int J Civ Eng*, 13(3).

Mir, B. A. and Sridharan, A. (2017). “Mechanical behaviour of fly-ash-treated expansive soil.” *Proc Inst Civ Eng - Ground Improv*, 172(1), 12–24.

Mishra, J., Das, S. K., Krishna, R. S., Nanda, B., Patro, S. K. and Mustakim, S. M. (2020). "Synthesis and characterization of a new class of geopolymer binder utilizing ferrochrome ash (FCA) for sustainable industrial waste management." *Mater Today Proc*, 33, 5001–5006.

Mishra, J., Nanda, B., Patro, S. K., Das, S. K. and Mustakim, S. M. (2022a). "Influence of ferrochrome ash on mechanical and microstructure properties of ambient cured fly ash-based geopolymer concrete." *J Mater Cycles Waste Manag*, 24(3), 1095–1108.

Mishra, J., Nanda, B., Patro, S. K., Das, S. K. and Mustakim, S. M. (2022b). "Strength and Microstructural Characterization of Ferrochrome Ash- and Ground Granulated Blast Furnace Slag-Based Geopolymer Concrete." *J Sustain Metall*, 8(1), 156–169.

Mocanu, A. C., Stan, G. E., Maidaniuc, A., Miculescu, M., Antoniac, I. V., Ciocoiu, R. C., Voicu, Ş. I., Mitran, V., Cîmpean, A. and Miculescu, F. (2019). "Naturally-derived biphasic calcium phosphates through increased phosphorus-based reagent amounts for biomedical applications." *Materials*, 12(3), 381.

Mohanty, T., Majhi, S., Saha, P. and Das, B. (2019). "Combined Effect of Fly-Ash and Ferrochrome Ash as Partial Replacement of Cement on Mechanical Properties of Concrete." *E3S Web of Conf*, 93, 02008.

Montoya, B. M., Safavizadeh, S. and Gabr, M. A. (2019). "Enhancement of Coal Ash Compressibility Parameters Using Microbial-Induced Carbonate Precipitation." *J Geotech Geoenviron Eng*, 145(5), 1–14.

Mu, Y., Saffarzadeh, A. and Shimaoka, T. (2016). "Feasibility of Using Natural Fishbone Apatite on Removal of Pb from Municipal Solid Waste Incineration (MSWI) Fly Ash." *Procedia Environ Sci*, 31, 345–350.

Mu, Y., Saffarzadeh, A. and Shimaoka, T. (2018). "Influence of ignition of waste fishbone on enhancing heavy metal stabilization in municipal solid waste incineration (MSWI) fly ash." *J Clean Prod*, 189, 396–405.

Mujah, D., Cheng, L. and Shahin, M. A. (2019). "Microstructural and geomechanical study on biocemented sand for optimization of MICP process." *J Mater Civ Eng*, 31(4), 1–10.

Mwandira, W., Nakashima, K. and Kawasaki, S. (2017). “Bioremediation of lead-contaminated mine waste by Pararhodobacter sp. based on the microbially induced calcium carbonate precipitation technique and its effects on strength of coarse and fine grained sand.” *Ecol Eng*, 109, 57–64.

Mwandira, W., Nakashima, K., Kawasaki, S., Ito, M., Sato, T., Igarashi, T., Banda, K., Chirwa, M., Nyambe, I., Nakayama, S. and Ishizuka, M. (2019a). “Efficacy of biocementation of lead mine waste from the Kabwe Mine site evaluated using Pararhodobacter sp.” *Environ Sci Pollut Res*, 26(15), 15653–15664.

Mwandira, W., Nakashima, K., Kawasaki, S., Ito, M., Sato, T., Igarashi, T., Chirwa, M., Banda, K., Nyambe, I., Nakayama, S., Nakata, H. and Ishizuka, M. (2019b). “Solidification of sand by Pb(II)-tolerant bacteria for capping mine waste to control metallic dust: Case of the abandoned Kabwe Mine, Zambia.” *Chemosphere*, 228, 17–25.

Nag, M., Saffarzadeh, A. and Shimaoka, T. (2022). “Feasibility of Natural Zeolite for Heavy Metal Stabilization in Municipal Solid Waste Incineration Fly Ash: A Novel Approach.” *J Geosci Environ Prot*, 10(07), 70–86.

Nam, I. H., Roh, S. B., Park, M. J., Chon, C. M., Kim, J. G., Jeong, S. W., Song, H. and Yoon, M. H. (2016). “Immobilization of heavy metal contaminated mine wastes using Canavalia ensiformis extract.” *Catena*, 136, 53–58.

Nasser, A. A., Sorour, N. M., Saafan, M. A. and Abbas, R. N. (2022). “Microbially-Induced-Calcite-Precipitation (MICP): A biotechnological approach to enhance the durability of concrete using Bacillus pasteurii and Bacillus sphaericus.” *Heliyon*, 8(7), e09879.

Nataraja, M. C., Chakravarthy H. G, N., Shivaprasad, R. and Naganna, S. R. (2023). “Self-compacting concrete incorporating incinerated biomedical waste ash: a performance assessment.” *J Eng Appl Sci*, 70(1), 1–16.

Navagire, O. P., Sharma, S. K. and Rambabu, D. (2022). “Stabilization of black cotton soil with coal bottom ash.” *Mater Today Proc*, 52, 979–985.

Nikseresht, F., Landi, A., Sayyad, G., Ghezelbash, G. R. and Schulin, R. (2020). "Sugarecane molasse and vinasse added as microbial growth substrates increase calcium carbonate content, surface stability and resistance against wind erosion of desert soils." *J Environ Manage*, 268, 110639.

Niu, Q., Li, C., Liu, Z., Li, Y., Meng, S., He, X., Liu, X., Wang, W., He, M., Yang, X., Liu, Q. and Liu, L. (2022). "Solidification of uranium mill tailings by MBS-MICP and environmental implications." *Nucl Eng Technol*, 54(10), 3631–3640.

Noolu, V., Mallikarjuna Rao, G., Sudheer Kumar Reddy, B. and Chavali, R. V. P. (2021). "Strength and durability characteristics of GGBS geopolymer stabilized black cotton soil." *Mater Today Proc*, 43, 2373–2376.

Okada, T. and Tomikawa, H. (2016). "Efficiencies of metal separation and recovery in ash-melting of municipal solid waste under non-oxidative atmospheres with different reducing abilities." *J Environ Manage*, 166, 147–155.

Omoregie, A. I., Muda, K. and Ngu, L. H. (2022). "Dairy manure pellets and palm oil mill effluent as alternative nutrient sources in cultivating Sporosarcina pasteurii for calcium carbonate bioprecipitation." *Lett Appl Microbiol*, 74(5), 671–683.

Omur, T., Miyan, N., Kabay, N., Birol, B. and Oktay, D. (2023). "Characterization of ferrochrome ash and blast furnace slag based alkali-activated paste and mortar." *Constr Build Mater*, 363, 129805.

Ortega-Villamagua, E., Gudiño-Gomezjurado, M. and Palma-Cando, A. (2020). "Microbiologically Induced Carbonate Precipitation in Heritage Materials." *Molecules*, 25(23), 5499.

Oza, J. B. and Gundaliya, P. J. (2013). "Study of black cotton soil characteristics with cement waste dust and lime." *Procedia Eng*, Elsevier Ltd, 51, 110–118.

Pan, X., Shi, C., Farzadnia, N., Hu, X. and Zheng, J. (2019). "Properties and microstructure of CO 2 surface treated cement mortars with subsequent lime-saturated water curing." *Cem Concr Compos*, 99, 89–99.

Pandey, S. and Singh, S. (2021). “Performance evaluation of black cotton soil with waste, fibers and minerals.” *Mater Today Proc*, 48, 1539–1544.

Pateriya, A. S., Robert, D. J., Dharavath, K. and Soni, S. K. (2022). “Stabilization of marble wastes using cement and nano materials for subgrade applications.” *Constr Build Mater*, 326, 126865.

Peng, C., Zhao, X., Ji, X., Wu, J., Liang, W., Song, H., Zhang, W. and Wang, X. (2023). “Mixed bacteria passivation for the remediation of arsenic, lead, and cadmium: Medium optimization and mechanisms.” *Process Safety and Environmental Protection*, 170, 720–727.

Peng, D., Qiao, S., Luo, Y., Ma, H., Zhang, L., Hou, S., Wu, B. and Xu, H. (2020). “Performance of microbial induced carbonate precipitation for immobilizing Cd in water and soil.” *J Hazard Mater*, 400, 123116.

Qian, X., Fang, C., Huang, M. and Achal, V. (2017). “Characterization of fungal-mediated carbonate precipitation in the biomineralization of chromate and lead from an aqueous solution and soil.” *J Clean Prod*, 164, 198–208.

Qiao, S., Zeng, G., Wang, X., Dai, C., Sheng, M., Chen, Q., Xu, F. and Xu, H. (2021). “Multiple heavy metals immobilization based on microbially induced carbonate precipitation by ureolytic bacteria and the precipitation patterns exploration.” *Chemosphere*, 274, 129661.

Rajasekar, A., Moy, C. K. S. and Wilkinson, S. (2017). “MICP and Advances towards Eco-Friendly and Economical Applications.” *IOP Conf Ser Earth Environ Sci*, 78, 012016.

Ramesh, H. N. and Manjunatha, B. V. (2020). “Justification of strength properties of microstructural changes in the black cotton soil stabilized with rice husk ash and carbide lime in the presence of sodium salts.” *SN Appl Sci*, 2(3), 1–12.

Randhawa, K. S., Chauhan, R. and Kumar, R. (2021). “An investigation on the effect of lime addition on UCS of Indian black cotton soil.” *Mater Today Proc*, Elsevier BV, 797–803.

Reddy, S. S., Prasad, A. C. S. V. and Krishna, N. V. (2018). “Lime-stabilized black cotton soil and brick powder mixture as subbase material.” *Adv Civ Eng*, 2018, 5834685.

Ruth F. Schulte. (2020). “Mineral Commodity Summaries.” <https://pubs.usgs.gov/periodicals/mcs2020/mcs2020-chromium.pdf>.

Saha, S., Mohanty, T. and Saha, P. (2021). “Mechanical Properties of Fly Ash and Ferrochrome Ash-Based Geopolymer Concrete Using Recycled Aggregate.” *Recent Dev Sustain Infrastruct*, B. Das, S. Barbhuiya, R. Gupta, and P. Saha, eds., Springer Singapore, 75, 417–426.

Saride, S. and Dutta, T. T. (2016). “Effect of Fly-Ash Stabilization on Stiffness Modulus Degradation of Expansive Clays.” *J Mater Civ Eng*, 28(12), 04016166.

Sarkar, M., Maiti, M., Xu, S. and Mandal, S. (2023). “Bio-concrete: Unveiling self-healing properties beyond crack-sealing.” *J Build Eng*, 74, 106888.

Schwantes-Cezario, N., Porto, M. F., Sandoval, G. F. B., Nogueira, G. F. N., Couto, A. F. and Toralles, B. M. (2019). “Effects of Bacillus subtilis biocementation on the mechanical properties of mortars.” *IBRACON Struct Mater J*, 12(1), 31–38.

Sharaky, A. M., Mohamed, N. S., Elmashad, M. E. and Shredah, N. M. (2018). “Application of microbial biocementation to improve the physico-mechanical properties of sandy soil.” *Constr Build Mater*, 190, 861–869.

Sharma, M., Behera, P., Saha, S., Mohanty, T. and Saha, P. (2022). “Effect of silica fume and red mud on mechanical properties of ferrochrome ash based concrete.” *Mater Today Proc*, 60, 55–61.

Sharma, M., Satyam, N. and Reddy, K. R. (2021). “Investigation of various gram-positive bacteria for MICP in Narmada Sand, India.” *Int J Geotech Eng*, 15(2), 220–234.

Sheng, M., Peng, D., Luo, S., Ni, T., Luo, H., Zhang, R., Wen, Y. and Xu, H. (2022). “Micro-dynamic process of cadmium removal by microbial induced carbonate precipitation.” *Environ Pollut*, 308, 119585.

Shokoohi, R., Nematollahi, D., Samarghandi, M. R., Azarian, G. and Latifi, Z. (2020). "Optimization of three-dimensional electrochemical process for degradation of methylene blue from aqueous environments using central composite design." *Environ Technol Innov*, 18, 100711.

Shukla, R. P. and Parihar, N. S. (2016). "Stabilization of Black Cotton Soil Using Micro-fine Slag." *J Inst Eng (India): Series A*, 97(3), 299–306.

Silva, F. B. da, Belie, N. De, Boon, N. and Verstraete, W. (2015). "Production of non-axenic ureolytic spores for self-healing concrete applications." *Constr Build Mater*, 93, 1034–1041.

Singh, N. K. and Kalita, A. (2021). "Use of Bagasse Ash and Coconut Fiber in Stabilization of Black Cotton Soil." *Adv Sustain Constr Mater*, S. Biswas, S. Metya, S. Kumar, and P. Samui, eds., Singapore: Springer Singapore, 124, 351–360.

Singh, S. (2020). "Experimental investigation on black cotton soil altered thru cement kiln dust and terrazyme." *Mater Today Proc*, 37(Part 2), 3661–3664.

Sobiecka, E., Obraniak, A. and Antizar-Ladislao, B. (2014). "Influence of mixture ratio and pH to solidification/stabilization process of hospital solid waste incineration ash in Portland cement." *Chemosphere*, 111, 18–23.

Sohail, M. G., Disi, Z. Al, Zouari, N., Nuaimi, N. Al, Kahraman, R., Gencturk, B., Rodrigues, D. F. and Yildirim, Y. (2022). "Bio self-healing concrete using MICP by an indigenous Bacillus cereus strain isolated from Qatari soil." *Constr Build Mater*, 328, 126943.

Sohal, B., Ahmad Bhat, S. and Vig, A. P. (2021). "Vermiremediation and comparative exploration of physicochemical, growth parameters, nutrients and heavy metals content of biomedical waste ash via ecosystem engineers Eisenia fetida." *Ecotoxicol Environ Saf*, 227, 112891.

Song, H., Kumar, A. and Zhang, Y. (2022a). "Microbial-induced carbonate precipitation prevents Cd2+ migration through the soil profile." *Sci Total Environ*, 844, 157167.

Song, M., Lan, T., Meng, Y., Ju, T., Chen, Z., Shen, P., Du, Y., Deng, Y., Han, S. and Jiang, J. (2022b). "Effect of microbially induced calcium carbonate precipitation treatment on the solidification and stabilization of municipal solid waste incineration fly ash (MSWI FA) - Based materials incorporated with metakaolin." *Chemosphere*, 308, 136089.

Šovljanski, O., Pezo, L., Stanojev, J., Bajac, B., Kovač, S., Tóth, E., Ristić, I., Tomić, A., Ranitović, A., Cvetković, D. and Markov, S. (2021). "Comprehensive profiling of microbiologically induced caco3 precipitation by ureolytic bacillus isolates from alkaline soils." *Microorganisms*, 9(8), 1–20.

Su, Y., Yang, J., Liu, D., Zhen, S., Lin, N. and Zhou, Y. (2016). "Effects of municipal solid waste incineration fly ash on solidification/stabilization of Cd and Pb by magnesium potassium phosphate cement." *J Environ Chem Eng*, 4(1), 259–265.

Sukandar, Padmi, T., Tanaka, M. and Aoyama, I. (2009). "Chemical stabilization of medical waste fly ash using chelating agent and phosphates: Heavy metals and ecotoxicity evaluation." *Waste Manag*, 29(7), 2065–2070.

Sun, C., Ge, W., Zhang, Y., Wang, L., Xia, Y., Lin, X., Huang, Q., Lu, S., Tsang, D. C. W. and Yan, J. (2023). "Designing low-carbon cement-free binders for stabilization/solidification of MSWI fly ash." *J Environ Manage*, 339, 117938.

Suresh Kumar, A., Muthukannan, M., Arunkumar, K., Chithambar Ganesh, A. and Kanniga Devi, R. (2022). "Utilisation of waste glass powder to improve the performance of hazardous incinerated biomedical waste ash geopolymer concrete." *Innov Infrastruct Solut*, 7, 93.

Suresh Kumar, A., Muthukannan, M. and Sri Krishna, I. (2020). "Optimisation of bio medical waste ash in GGBS based of geopolymer concrete." *IOP Conf Ser Mater Sci Eng*, 012163.

Tan, J., Wang, X., Zhang, M., Meng, D., Hu, Y., Li, Y., Song, S., Wu, L., Sánchez, R. M. T., Farías, M. E. and Xia, L. (2023). "Chlorella sorokiniana FK-montmorillonite interaction enhanced remediation of heavy metals in tailings." *Sci Total Environ*, 876, 163208.

Tan, J., Yi, H., Zhang, Z., Meng, D., Li, Y., Xia, L., Song, S., Wu, L., Sáncheze, R. M. T. and Farías, M. E. (2022). "Montmorillonite facilitated Pb(II) biomineralization by Chlorella sorokiniana FK in soil." *J Hazard Mater*, 423, Part A, 127007.

Tayebani, B. and Mostofinejad, D. (2019). "Penetrability, Corrosion Potential, and Electrical Resistivity of Bacterial Concrete." *J Mater Civ Eng*, 31(3), 04019002.

Tchounwou, P. B., Yedjou, C. G., Patlolla, A. K. and Sutton, D. J. (2012). "Heavy Metal Toxicity and the Environment." *Mol Clin Environ Toxicol*, 101, 133–164.

Teng, F., Sie, Y. C. and Ouedraogo, C. (2021). "Strength improvement in silty clay by microbial-induced calcite precipitation." *Bull Eng Geol Environ*, 80(8), 6359–6371.

Thakur, A. K., Ojha, C. S. P., Grischek, T., Ray, C. S. C. and Saandhu, C. (2010). "Water Quality Improvement through river bank filtration in extreme environmental conditions". *J Indian Water Works Assoc*, 43(2), 106-115.

Tiwari, N., Satyam, N. and Sharma, M. (2021). "Micro-mechanical performance evaluation of expansive soil biotreated with indigenous bacteria using MICP method." *Sci Rep*, 11(1), 1–12.

Tzanakos, K., Mimilidou, A., Anastasiadou, K., Stratakis, A. and Gidarakos, E. (2014). "Solidification/stabilization of ash from medical waste incineration into geopolymers." *Waste Manag*, 34(10), 1823–1828.

Vavva, C., Lymperopoulou, T., Magoulas, K. and Voutsas, E. (2020). "Chemical Stabilization of Fly Ash from Medical Waste Incinerators." *Environ Process*, 7(2), 421–441.

Vavva, C., Voutsas, E. and Magoulas, K. (2017). "Process development for chemical stabilization of fly ash from municipal solid waste incineration." *Chem Eng Res Des*, 125, 57–71.

Vijayan, D. S., Devarajan, P., Kumar, S. R., Kumar, A. V., Kumar, R. S. and Rahman, S. H. (2023). "An investigational study on Pre and post-stabilization behaviour of Lime stabilized Expansive soil admixed with palm kernel ash." *IOP Conf Ser Earth Environ Sci*, 1130(1), 012032.

Vivek, J. M., Singh, R., Sutar, R. S. and Asolekar, S. R. (2019). "Characterization and Disposal of Ashes from Biomedical Waste Incinerator." *Adv Waste Manag*, Springer, Singapore, 421–435.

Wang, L., Zhang, Y., Chen, L., Guo, B., Tan, Y., Sasaki, K. and Tsang, D. C. W. (2022a). "Designing novel magnesium oxysulfate cement for stabilization/solidification of municipal solid waste incineration fly ash." *J Hazard Mater*, 423, 127025.

Wang, M., Wu, S., Guo, J., Liao, Z., Yang, Y., Chen, F. and Zhu, R. (2021a). "Immobilization and migration of arsenic during the conversion of microbially induced calcium carbonate to hydroxylapatite." *J Hazard Mater*, 412, 125261.

Wang, M., Wu, S., Guo, J., Liao, Z., Yang, Y., Chen, F. and Zhu, R. (2022b). "Enhanced immobilization of uranium(VI) during the conversion of microbially induced calcite to hydroxylapatite." *J Hazard Mater*, 434, 128936.

Wang, M., Wu, S., Guo, J., Zhang, X., Yang, Y., Chen, F. and Zhu, R. (2019). "Immobilization of cadmium by hydroxyapatite converted from microbial precipitated calcite." *J Hazard Mater*, 366, 684–693.

Wang, X., Ni, W., Li, J., Zhang, S. and Li, K. (2021b). "Study on mineral compositions of direct carbonated steel slag by QXRD, TG, FTIR, and XPS." *Energies*, 14(15), 14154489.

Wani, K. M. N. S. and Mir, B. A. (2020a). "Unconfined Compressive Strength Testing of Bio-cemented Weak Soils: A Comparative Upscale Laboratory Testing." *Arab J Sci Eng*, 45(10), 8145–8157.

Wani, K. M. N. S. and Mir, B. A. (2020b). "A Laboratory-Scale Study on the Bio-cementation Potential of Distinct River Sediments Infused with Microbes." *Transp Infrastruct Geotechnol*, 8(1), 162–185.

Wani, K. M. N. S. and Mir, B. A. (2021). "Effect of Microbial Stabilization on the Unconfined Compressive Strength and Bearing Capacity of Weak Soils." *Transp Infrastruct Geotechnol*, 8(1), 59–87.

Wani, K. M. N. S., Mir, B. A. and Sheikh, I. R. (2021). “Biological processes in the stabilization of weak river sediments: an innovative approach.” *Innov Infrastruct Solut*, 6(3), 164.

Wilkinson, S. and Rajasekar, A. (2019). “An Electron Microscope Study of Biomineralisation for Geotechnical Engineering Purposes.” *IAEG/AEG Annu Meet Proc*, Springer International Publishing, San Francisco, California, 6, 83–88.

World Health Organization (WHO). (2017). Report on health-care waste management status in countries of the South-East Asia Region.

Xiang, J., Qiu, J., Wang, F., Li, Z. and Gu, X. (2022). “Utilization of bioactivated incineration bottom ash in cement binder for mortar harmless treatment and performance improvement.” *J Build Eng*, 57, 104980.

Xiao, J. Z., Wei, Y. Q., Cai, H., Wang, Z. W., Yang, T., Wang, Q. H. and Wu, S. F. (2020). “Microbial-Induced Carbonate Precipitation for Strengthening Soft Clay.” *Adv Mater Sci Eng*, 2020, 8140724.

Xie, Y. X., Cheng, W. C., Wang, L., Xue, Z. F., Rahman, M. M. and Hu, W. (2023). “Immobilizing copper in loess soil using microbial-induced carbonate precipitation: Insights from test tube experiments and one-dimensional soil columns.” *J Hazard Mater*, 444, Part A, 130417.

Xu, Z., Liang, Z., Shao, H. and Zhao, Q. (2023). “Heavy metal stabilization in MSWI fly ash using an additive-assisted microwave hydrothermal method.” *J Ind Eng Chem*, 117, 352–360.

Xue, Z. F., Cheng, W. C., Wang, L., Qin, P. and Zhang, B. (2022). “Revealing degradation and enhancement mechanisms affecting copper (Cu) immobilization using microbial-induced carbonate precipitation (MICP).” *J Environ Chem Eng*, 10(5), 108479.

Xue, Z. F., Cheng, W. C., Xie, Y. X., Wang, L., Hu, W. and Zhang, B. (2023). “Investigating immobilization efficiency of Pb in solution and loess soil using bio-inspired carbonate precipitation.” *Environ Pollut*, 322, 121218.

Yang, J., Pan, X., Zhao, C., Mou, S., Achal, V., Al-Misned, F. A., Mortuza, M. G. and Gadd, G. M. (2016). “Bioimmobilization of heavy metals in acidic copper mine tailings soil.” *Geomicrobiol J*, 33(3–4), 261–266.

Yang, Y., Chu, J., Cao, B., Liu, H. and Cheng, L. (2020). “Biocementation of soil using non-sterile enriched urease-producing bacteria from activated sludge.” *J Clean Prod* , 262, 121315.

Yi, Y., Gu, L., Liu, S. and Puppala, A. J. (2015). “Carbide slag–activated ground granulated blastfurnace slag for soft clay stabilization.” *Can Geotech J*, 52(5), 656–663.

Yin, Z., Lekalpure, R. L. and Ndiema, K. M. (2022). “Experimental Study of Black Cotton Soil Stabilization with Natural Lime and Pozzolans in Pavement Subgrade Construction.” *Coatings*, 12(1), 12010103.

Yohanna, P., Johnson, P., Victor, B. P., Badamasi, A., Mije, F. G., Ako, T. and Bassey Bassey, A. (2022). “Evaluation of Geotechnical Properties of Black Cotton Soil Reinforced with Sisal Fibre for Waste Containment Application.” *Eng Sci Technol*, 3(2), 151–168.

Yoosathaporn, S., Tiangburanatham, P., Bovonsombut, S., Chaipanich, A. and Pathom-aree, W. (2016). “A cost effective cultivation medium for biocalcification of Bacillus pasteurii KCTC 3558 and its effect on cement cubes properties.” *Microbiol Res*, 186–187, 132–138.

Yu, J., Qiao, Y., Jin, L., Ma, C., Paterson, N. and Sun, L. (2015). “Removal of toxic and alkali/alkaline earth metals during co-thermal treatment of two types of MSWI fly ashes in China.” *Waste Manag*, 46, 287–297.

Yu, X., Qian, C. and Jiang, J. (2019). “Desert sand cemented by bio-magnesium ammonium phosphate cement and its microscopic properties.” *Constr Build Mater*, 200, 116–123.

Zeng, G., Qiao, S., Wang, X., Sheng, M., Wei, M., Chen, Q., Xu, H. and Xu, F. (2021). “Immobilization of cadmium by Burkholderia sp. QY14 through modified microbially induced phosphate precipitation.” *J Hazard Mater*, 412, 125156.

Zeng, Y., Chen, Z., Lyu, Q., Cheng, Y., Huan, C., Jiang, X., Yan, Z. and Tan, Z. (2023). "Microbiologically induced calcite precipitation for in situ stabilization of heavy metals contributes to land application of sewage sludge." *J Hazard Mater*, 441, 129866.

Zeng, Y., Chen, Z., Lyu, Q., Wang, X., Du, Y., Huan, C., Liu, Y. and Yan, Z. (2022). "Mechanism of microbiologically induced calcite precipitation for cadmium mineralization." *Sci Total Environ*, 852, 158465.

Zha, F., Chen, S., Kang, B., Xu, L., Shen, Y. and Wang, R. (2022). "Synergistic solidification of lead-contaminated soil by magnesium oxide and microorganisms." *Chemosphere*, 308, 136422.

Zhang, J., Kumari, D., Fang, C. and Achal, V. (2019a). "Combining the microbial calcite precipitation process with biochar in order to improve nickel remediation." *Appl Geochem*, 103, 68–71.

Zhang, J., Su, P. and Li, L. (2022a). "Bioremediation of stainless steel pickling sludge through microbially induced carbonate precipitation." *Chemosphere*, 298, 134213.

Zhang, K., Xue, Y., Xu, H. and Yao, Y. (2019b). "Lead removal by phosphate solubilizing bacteria isolated from soil through biomineralization." *Chemosphere*, 272–279.

Zhang, L. V., Suleiman, A. R., Mehdizadeh Allaf, M., Marani, A., Tuyan, M. and Nehdi, M. L. (2022b). "Crack self-healing in alkali-activated slag composites incorporating immobilized bacteria." *Constr Build Mater*, 326, 79–108.

Zhang, R., Wu, K., Jiang, Z. and Wang, J. (2022c). "Bacterially induced CaCO3 precipitation for the enhancement of quality of coal gangue." *Constr Build Mater*, 319, 126102.

Zhao, J., Csetenyi, L. and Gadd, G. M. (2022). "Fungal-induced CaCO3 and SrCO3 precipitation: a potential strategy for bioprotection of concrete." *Sci Total Environ*, 816, 151501.

Zhu, J., Hao, Q., Chen, J., Hu, M., Tu, T. and Jiang, C. (2020). “Distribution characteristics and comparison of chemical stabilization ways of heavy metals from MSW incineration fly ashes.” *Waste Manag*, 113, 488–496.

Zhu, X., Li, W., Zhan, L., Huang, M., Zhang, Q. and Achal, V. (2016). “The large-scale process of microbial carbonate precipitation for nickel remediation from an industrial soil.” *Environ Pollut*, 219, 149–155.

List of Publications based on Ph.D. Research Work

S. No.	Title of the paper	Authors	Name of the Journal/ Conference/ Symposium, Vol., No., Pages	Month & Year of Publication
1	Effect of Bioprecipitation and Ferrochrome Ash Stabilization on the Strength of Black Cotton Soil DOI: https://doi.org/10.1007/s40710-023-00632-z	Mahindra Kothuri, C P Devatha	Environmental Processes, Vol. 10, No. 18	April 2023
2	Statistical modeling of bacterial culture medium composition affecting mineralization in ferrochrome ash	Mahindra Kothuri, C P Devatha	3rd Euro-Mediterranean Conference For Environmental Integration (EMCEI 2021), Paper: 348	June 2021
3	An Experimental Investigation on Microbial Growth in Ferrochrome Ash and Their Suitability for Calcium Carbonate Precipitation.	Mahindra Kothuri, C P Devatha	3rd International Conference on Waste Management- (RECYCLE 2020), Paper: 172	February 2020

KOTHURI MAHINDRA
H.No:144, Vasavinagar,
Kandukur, Andhra Pradesh – 523105.
9492301702, 8247092073
mahindrakothuri@gmail.com
LinkedIn, Researchgate, Orcid

Career Objective:

I aspire to obtain a position where I can apply my expertise and strong passion for leveraging my skills to benefit myself, my organization, and society as a whole.

Education:

- SSC, Mahindra Academy, April 2008 [82.67%]
- Intermediate, MPC, Sri Chaitanya Junior College, March 2010 [91.90%]
- B.Tech, Civil Engineering, N.B.K.R. Institute of Science & Technology, Vikrama Simhapuri University, May 2014 [82.05%]
- M.Tech, Environmental Engineering, Visvesvaraya National Institute of Technology, May 2016 [CGPA-7.29]
- Ph.D., Environmental Engineering, National Institute of Technology Karnataka, June 2023 (Thesis submitted) [CGPA-8.00]

Ph.D. Thesis:

INVESTIGATION ON SYNERGISTIC EFFECT OF BIOMINERALIZATION AND ASH-BASED SOIL STABILIZATION

Certifications:

- GATE 2021 (Environmental Science and Engineering)
- APSET 2020 (Environmental Science)
- GATE 2018 (Civil Engineering)
- GATE 2014 (Civil Engineering)

Awards:

- M.Tech fellowship – Ministry of Human Resource Development, Government of India (2014-2016)
- Ph.D. fellowship – Ministry of Education, Government of India (2018-2023)

Work Experience:

- Assistant Professor, KL University, Sep 2016 – July 2018

Skills:

I possess a versatile skill set encompassing strong adaptability, communication, problem-solving, and technical abilities, along with a commitment to ethical conduct and disciplined work style.

- Technical exprtise in IC, LCMS, HPLC, ICP-OES, UVVis, SEM, XRD, TG, FTIR analyses.
- Fundamental proficiency in AutoCAD, SPSS, Design Expert, and EPANET softwares.
- Creating and improving documents and visual content using MS Office and Origin Pro packages.

Recent Publications:

- Kothuri, M., & Devatha, C. P. (2023). Effect of Bioprecipitation and Ferrochrome Ash Stabilization on the Strength of Black Cotton Soil. *Environmental Processes*, *10*(2), 1–22. https://doi.org/10.1007/s40710-023-00632-z
- Kothuri, M., Devatha, C.P. (2023). Low-Cost Recovery of Cadmium from Wastewater by Soil Bacteria. In: Mazumder, D. (eds) Sustainable Advanced Technologies for Industrial Pollution Control. ATIPC 2022. Springer Proceedings in Earth and Environmental Sciences. Springer, Cham. https://doi.org/10.1007/978-3-031-37596-5_22